



Master thesis

**Development of a measurement technique to
investigate mixing behavior and gas hold-up
distribution in a multiphase reactor**

Daniel Franz Treffer

Institute of Process and Particle Engineering
Graz University of Technology

Supervision: Univ.-Prof. Dipl.-Ing. Dr .techn. Johannes Khinast

Co-supervision: MSc. Radompon Sungkorn

Copyright © 2011 by Daniel Franz Treffer

All rights reserved. No part of the material protected by this copyright notice may be reproduced or utilized in any form or by any means, electronically or mechanically, including photocopying, recording or by any information storage and retrieval system with written permission from the author.

Deutsche Fassung:

Beschluss der Curricula-Kommission für Bachelor-, Master- und Diplomstudien vom 10.11.2008

Genehmigung des Senates am 1.12.2008

EIDESSTÄTLICHE ERKLÄRUNG

Ich erkläre an Eides statt, dass ich die vorliegende Arbeit selbstständig verfasst, andere als die angegebenen Quellen/Hilfsmittel nicht benutzt, und die den benutzten Quellen wörtlich und inhaltlich entnommene Stellen als solche kenntlich gemacht habe.

Graz, am

.....

(Unterschrift)

Englische Fassung:

STATUTORY DECLARATION

I declare that I have authored this thesis independently, that I have not used other than the declared sources / resources, and that I have explicitly marked all material which has been quoted either literally or by content from the used sources.

.....

date

.....

(signature)

Acknowledgement

First, I would like to thank Prof. Johannes Khinast for his support and the possibility of conducting this thesis.

Next, I would like to express my deepest gratitude to my co supervisor Radompon Sungkorn, who has accompanied me throughout the whole process of the thesis preparation. I am very grateful for his support, inspiring suggestions and his confidence in me.

Special thanks also go to Johann Grubbauer for his excellent work, ideas and advices during the design construction and setup of the laboratory reactor.

Moreover, I would like to thank Friedrich Holzinger for his support during the design of the laboratory reactor.

Finally, my special thanks go to my family and Andrea for their assistance, support and motivation throughout my studies. I dedicate this thesis to them in love and gratefulness.

Index

Acknowledgement	II
Index	III
Abstract	1
Kurzfassung	2
1 Introduction	3
1.1 Literature review	3
1.2 Goal of this work.....	3
1.3 This thesis	4
2 Theory	5
2.1 Conductivity measurement principles.....	5
2.1.1 Mathematical relations between conductivity and resistance.....	5
2.1.2 Temperature dependence of electrical conductivity.....	6
2.2 Liquid hydrodynamics.....	7
2.3 Bubble dynamics.....	8
2.4 Introduction to gas-liquid stirred reactors	10
2.4.1 Impeller types.....	10
2.4.2 Impeller arrangement	11
2.4.3 Gas flow	12
2.4.4 Dimensionless numbers in stirred reactors	13
2.4.5 Flow pattern	14
2.4.6 Flow regimes	15
2.4.7 Regime recognition	16
3 Measurement system	18
3.1 Principle	18
3.2 Signal generation	18
3.3 Probe.....	19
3.4 Signal acquisition and processing.....	21
3.5 Circuit of the measurement system	21
3.6 Data acquisition	22

3.7	Verification with an image analysis technique.....	24
3.7.1	Verification setup	24
3.7.2	Verification	24
3.7.3	Matlab® post processing	25
3.7.4	Calculation of the theoretical contact time	25
3.7.5	Results of the verification	26
4	Test facilities	31
4.1	Laboratory reactor.....	31
4.2	Bubble column – Becker case.....	34
5	Experimental work.....	35
5.1	Bubble column experiments.....	35
5.2	Laboratory stirred reactor experiments.....	36
5.2.1	Gas hold-up experiments	38
5.2.2	Mixing experiments.....	57
5.2.3	Discussion	61
6	Conclusion.....	62
6.1	Summary.....	62
6.2	Outlook	62
7	Lists.....	63
7.1	List of literature	63
7.2	List of figures.....	65
7.3	List of equations	68
7.4	List of tables.....	69
8	Appendix.....	70
8.1	Nomenclature	70
8.1.1	Design drawings	72
8.1.2	Single tip conductivity probe.....	72
8.1.3	Reactor	77
8.2	Hardware	85
8.2.1	M3 - Highspeed camera	85

8.2.2	National Instruments NI 9203 – analog input module.....	85
8.2.3	National Instruments NI 9263 – analog input module.....	85
8.3	Matlab® codes	86
8.3.1	Image analysis post processing	86
8.3.2	Gas hold-up post processing	88
8.3.3	Mixing post processing.....	91

Abstract

Multiphase flow, here referred to as a flow consisting of a continuous and dispersed phase, appear in many industrial processes. Examples for these processes are: absorption in bubble columns, fermentation in bioreactors and floatation in waste water treatment. It is well known that the efficiency of these processes depends on the spatial and bubble size distribution of the dispersed phase.

One of the challenges in these processes is to describe the spatial distribution of the dispersed phase. In this work, a measurement system to obtain the local gas hold-up and mixing time in multiphase reactors has been developed. The measurement system is based on the electrical conductivity principle. It acquires the conductivity with high time resolution. The evolved micro conductivity probe enables the accurate capturing of small bubbles. The gas hold-up and mixing time are calculated with a post processing algorithm.

The developed measurement system has been validated against an image analysis method. The preliminary validation showed that the conductivity measurement overestimates the bubble interaction time. Therefore, a compensation factor has been defined to fine-tuning the measured data from the conductivity measurement system to the image analysis method. Furthermore, a laboratory-scale stirred reactor has been designed and constructed. The measurement system was applied to measure the gas hold-up profile and mixing time in the laboratory-scale reactor.

The measured gas hold-up profiles show good agreement with the observed global gas hold-up. Moreover, the mixing investigations showed a good reproducibility. The outcome of this work is a multifunctional and reliable measurement system to monitor processes related to gas-liquid flows as well as to obtain experimental data for computational fluid dynamics CFD code evaluation.

Kurzfassung

Diese Arbeit beschäftigt sich mit Mehrphasenströmungen, welche aus einer kontinuierlichen flüssigen und einer gasförmigen dispersen Phase bestehen. Solche Strömungen treten in vielen industriellen Prozessen auf, beispielsweise bei Absorption in Blasensäulen, Fermentation in Bioreaktoren und Flotation in der Abwasserreinigung. Grundlegende Einflussfaktoren auf die Effizienz solcher Prozesse sind die Blasengrößenverteilung sowie die räumliche Verteilung der dispersen Phase.

Eine der Herausforderungen in diesen Prozessen ist die Beschreibung der räumlichen Verteilung der dispersen Phase. In dieser Arbeit wurde daher ein Messsystem entwickelt mit dem der lokale Gasphasenanteil und die Mischzeit in einem Mehrphasenreaktor bestimmt werden können. Das Messprinzip basiert auf der elektrischen Leitfähigkeit mit einer hohen zeitlichen Auflösung. In Kombination mit dem entwickelten Mikro-Leitfähigkeitssensor ermöglicht dieses Messprinzip das zuverlässige Erkennen der dispersen Phase. Des Weiteren werden der Gasphasenanteil sowie die Mischzeit mit Hilfe von entwickelten Auswertalgorithmen berechnet.

Das Messsystem wurde mittels Bildanalyse validiert. Die Validierung zeigte, dass die Leitfähigkeitsmessung die Kontaktzeit zwischen Blase und Sensor überschätzt. Daher wurde ein Faktor zur Kompensation der Abweichung definiert. Des Weiteren wurde ein Rührkesselreaktor im Labormaßstab entworfen und aufgebaut. Darin wurden mit dem Messsystem die lokalen Gasphasenanteile und Mischzeiten bestimmt.

Die gemessenen Profile der Gasphasenanteile zeigten eine gute Übereinstimmung mit dem beobachteten globalen Gasphasenanteil. Auch die Untersuchungen der Mischzeiten geben Rückschlüsse auf eine gute Reproduzierbarkeit. Das Ergebnis dieser Arbeit ist somit ein multifunktionales und zuverlässiges Messsystem um Mehrphasenprozesse zu überwachen und experimentelle Daten für die Beurteilung von numerischen Strömungssimulationen zu erhalten.

1 Introduction

Multiphase flow reactors are widely used in process engineering. They are used in processes such as: absorption in bubble columns, fermentation in bioreactors and floatation in waste water treatment. The aim of such a multiphase reactor is the mass transport from one phase to another. An important parameter for the mass transfer is the interfacial area between the phases, which can be derived from the amount of the dispersed phase and its size distribution. It is well known that, the power to distribute the dispersed phase causes enormous energy costs. Therefore, a good distribution with low power input is a desire in engineering of multiphase flow reactors. The difficulty is to describe the spatial distribution within the reactor. Many methods have been developed to measure the distribution. However, each has restrictions such as a low gas hold-up or opacity of the medium. The developed method in this work is based on electrical conductivity, which enables us to measure the gas hold-up distribution and mixing behavior with one system.

1.1 Literature review

Bombac et al.[1] [2] investigated the flow pattern in stirred reactors. They used a resistivity probe to measure the conductivity close to the impeller blades of a Rushton turbine. They determined six different cavity regimes by frequency transformation of the time-domain structural function. They suggested a frequency pattern for each cavity regime. Sanwani et al. [3] investigated the gas hold-up distribution in a 3 [m³] floatation cell with two different methods, namely: electrical conductivity probe and capturing. The measured gas hold-up result obtained by both methods showed good agreement with each other. Jose da Silva [4] developed several measurement techniques for multiphase flow within his dissertation. He measured the conductivity and permittivity of the multiphase flow with a two-tip needle probe. This enabled him to distinguish between each phase within three phase flows. The Research Center Dresden [5] developed a conductivity needle probe for extreme operating conditions up to 300 [°C] and 160 [bar]. The main field of application is basic research concerning multiphase flows in nuclear power plants. Shewale and Pandit [6] studied multiphase multiple impeller reactors. They made visual observations of the flow pattern and mixing time experiments in a stirred reactor with three impellers. The mixing time was determined with a shielded conductivity probe. Shielded conductivity probes are also recommended by Pinelli et al. [7] for mixing experiments in multiphase systems. A shielded probe has a cage above the measurement electrodes. The cage prevents a contact of the dispersed phase with the measurement electrodes. This literature review shows a broad field of application for an electrical conductivity measurement system.

1.2 Goal of this work

The goal of this work was to develop an electrical-conductivity based measurement system to describe the local gas hold-up and mixing behavior of a process involving dispersed multiphase flows. The development included the micro probe design, software development as well as data analysis in Matlab[®] and the validation of the measurement system with image analysis. Furthermore, a test facility to study the flow in multiple impeller gas-liquid reactors was designed and constructed. Gas hold-up profiles and mixing times were

determined for the characteristic flow regimes in a multiphase reactor equipped with three Rushton turbines.

1.3 This thesis

The content of this thesis is divided into six chapters. *Chapter two* discusses the underlying theory to give the reader a basic understanding of each topic treated in this thesis. It begins with the conductivity measurement and explains the gas hold-up and mixing time measurement principles. Next, basic liquid hydrodynamic and bubble dynamics as it appear in multiphase reactors are discussed briefly. After that, an introduction to liquid stirred reactors is given, which explains the necessary terminology. *Chapter three* explains the developed conductivity measurement system. It discusses the functional principle, the micro conductivity probe and the measurement system's hardware. The data acquisition and the graphical user interface GUI developed in Matlab[®] software are explained. In addition, the validation procedure and their analysis finalize this chapter. *Chapter four* explains the used test facilities, the bubble column and the laboratory reactor. *Chapter five* discusses the experimental part of the work. The choice of the experimental conditions are explained and shown in detail for each experiment. The results are represented as gas hold-up profiles and analyzed conductivity curves. *Chapter six* summarizes the results of this thesis and gives an outlook for future work.

2 Theory

2.1 Conductivity measurement principles

By definition, the electrical conductivity is the ability of a material to conduct electrical current. In a multiphase air-water flow system, the gas phase has the electrical conductivity of 3×10^{-5} to 8×10^{-5} [S m^{-1}] [8], while the liquid phase has the electrical conductivity of 5×10^{-4} to 2×10^{-1} [S m^{-1}] [9]. A conductivity measurement system in combination with a special probe design is able to obtain the gas hold-up distribution and mixing time of a multiphase flow. The gas hold-up distribution is a result of several local gas hold-up measurements. The fraction of the gas phase of a volume is defined as the gas hold-up [10]. The mixing time is an empirical parameter which is used to describe the overall behavior in stirred reactors. It is usually determined by a tracer injection which causes a conductivity change in the reactor. The conductivity is recorded and analyzed. The mixing time t_x is defined as interval between tracer injection and the moment when the conductivity reaches a constant level X of the normalized signal change. [7]

The conductivity is measured with a probe inside the multiphase flow, so called “*in situ*” measurement. It can be used to capture the presence and absence of the dispersed phase which is reflected by a change in conductivity. Figure 1 (a) illustrates an ideal local conductivity signal within a multiphase flow. Each signal drop is caused by interaction with a bubble or droplet. It can be noted that this principle should hold within a variety of systems, *i.e.*, liquid-gas and liquid-liquid systems, where an electrical conductivity difference between phases exists. The gas hold-up is defined as a ratio between the cumulative times when the probe is in contact with the dispersed phase and the measurement time. The mixing time is determined by measuring the conductivity of the continuous phase. This principle is illustrated in Figure 1 (b). The conductivity of the continuous phase is changed from the constant level one to the constant level two due to the conductivity as a function of the tracer concentration. The time to reach 90 percent of the signal change to level 2 is defined as mixing time t_{90} .

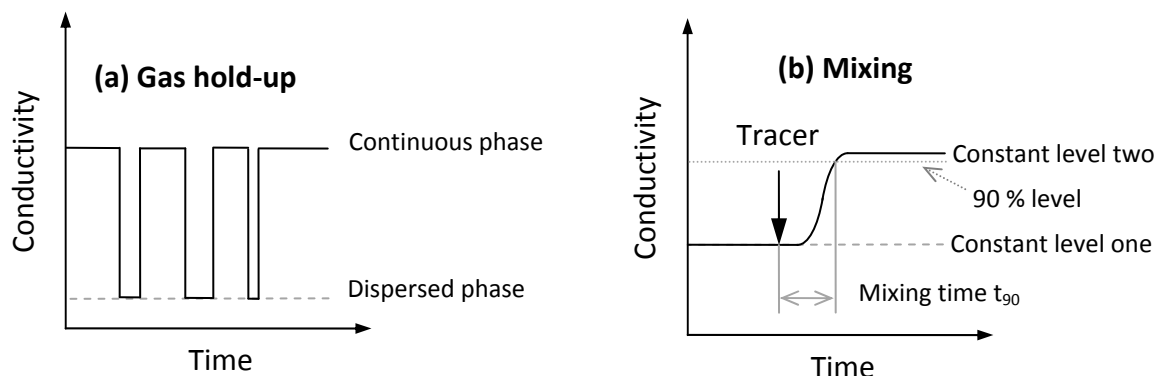


Figure 1: Illustration of the gas hold-up (a) and mixing time (b) measurement principle

2.1.1 Mathematical relations between conductivity and resistance

A calculation of the electrical resistance between two electrodes in liquid is based on Ohm's law which states that the electrical voltage U between two points is proportional to an electrical current I and to the resistance R between them.

The Ohm's law can be written as:

$$U = R \cdot I \quad \text{Equation 1: Ohm's law}$$

The electrical conductivity σ is a measure of a material's ability to conduct electrical current. It is calculated as a reciprocal of the resistance:

$$\sigma = \frac{1}{R} \quad \text{Equation 2: Relation between resistance and conductivity}$$

The conductivity between two electrodes depends on the specific conductivity of the substance σ_{spec} and the geometric design of the measurement probe (see equation 3). The specific conductivity is a material characteristic and the cell constant C depends on the geometric design of the probe.

$$\sigma = \frac{\sigma_{spec}}{C} \quad \text{Equation 3: Conductivity}$$

$$C = \frac{L}{A} \quad \text{Equation 4: Cell constant}$$

The cell constant can be calculated for very simple probe geometries, as shown in figure 2. Cell constants of complex geometries are determined by experiments with reference solutions. The obtained data can be used to estimate the cell constant of a probe using equation 2 and 3.

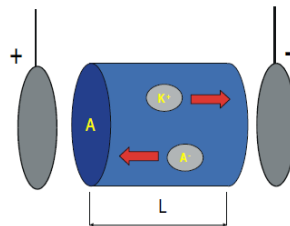


Figure 2: Illustration of a simple probe geometrie[11]

2.1.2 Temperature dependence of electrical conductivity

The electrical conductivity highly depends on the temperature since the ion mobility is also strong temperature dependent. Therefore, in case of a non-constant temperature system, temperature compensation should be applied. For the conductivity in water, a linear compensation is expressed as:

$$\sigma_{spec}(T) = \sigma_{spec}(25^{\circ}C) \cdot [1 + 0.02 \cdot (T - 25)] \quad \text{Equation 5: Temperature compensation for water systems [12]}$$

Equation 5 implies a 2% change in the specific conductivity, when the temperature increases by 1°C. Other temperature compensation correlations can be found in the literature. In this work slow temperature changes are possible within the experiments. A post process temperature compensation algorithm has been developed, which is explained in chapter 5.

2.2 Liquid hydrodynamics

Liquids can be divided based on their rheology into Newtonian and non-Newtonian fluids. Figure 3 shows the relation between shear stress τ and shear rate du/dy . A Newtonian fluid is characterized through a linear relation between shear stress and shear rate. Furthermore, the line for a Newtonian fluid goes always through the origin. On the other hand non-Newtonian fluids (pseudoplastic, dilatant, Bingham fluid) have a non linear relation between shear stress and shear rate, but also go through the origin except from the Bingham fluid. Moreover, the Bingham is characterized through a linear relation, but it has an offset to the origin. The experiments in this work are conducted only with Newtonian fluids, i.e., water and air.

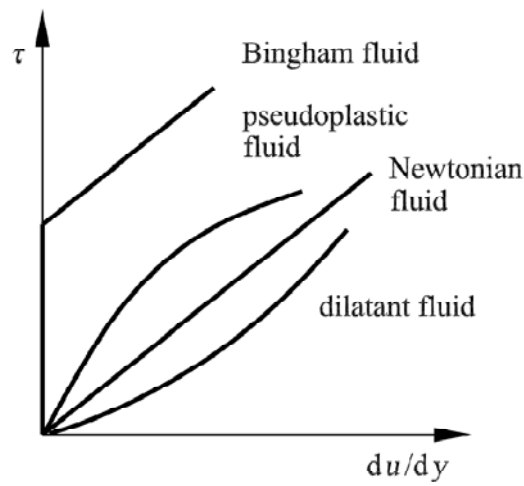


Figure 3: Shear stress for Newtonian and non-Newtonian fluids [13]

In fluid dynamics two main flow types can be distinguished: the laminar flow and the turbulent flow. The Laminar flow is a flow at low velocities, along streamlines and without turbulence or randomness. The turbulent flow is at higher velocities with eddies which cause lateral fluctuations. The criterion (Equation 6) to distinguish laminar and turbulent flow is the Reynolds number. It is a dimensionless number which relates the inertia forces to the viscosity forces.

$$Re = \frac{\rho dv}{\mu}$$

Equation 6: Reynolds number

2.3 Bubble dynamics

A bubble is a coherent region of the dispersed gas phase surrounded by the continuous liquid phase. Figure 4 shows an illustration of a rising bubble. The assumptions for the bubble are: it is a spherical bubble in steady state with stagnant liquid flow. Thus, the forces acting on a bubble are: buoyancy (F_B), gravity (F_G) and drag (F_D) force. An injected bubble with zero velocity will accelerate until the force balance reaches the equilibrium. The velocity at the equilibrium is called terminal velocity. A graph of the terminal velocity depending on the bubble size for an air-water system is shown in Figure 5.

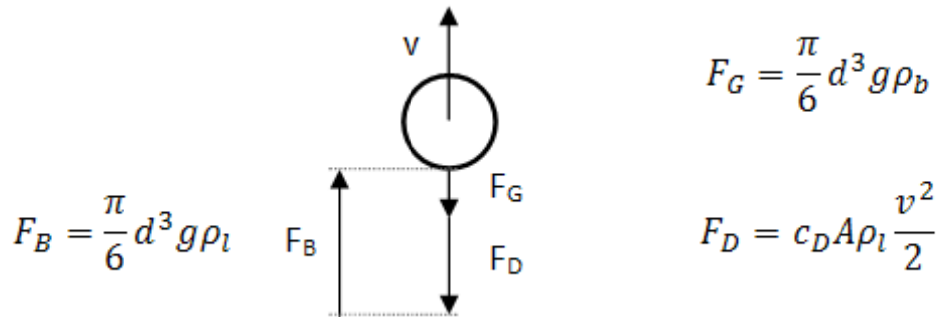


Figure 4: Forces acting on a bubble

A spherical bubble is shown in Figure 4. The bubble shape can change from a sphere to other shapes due to their size and the resulting forces. Three different regimes are stated in the literature [14]. The regimes are named: spherical regime, ellipsoidal regime and spherical-cap regime.

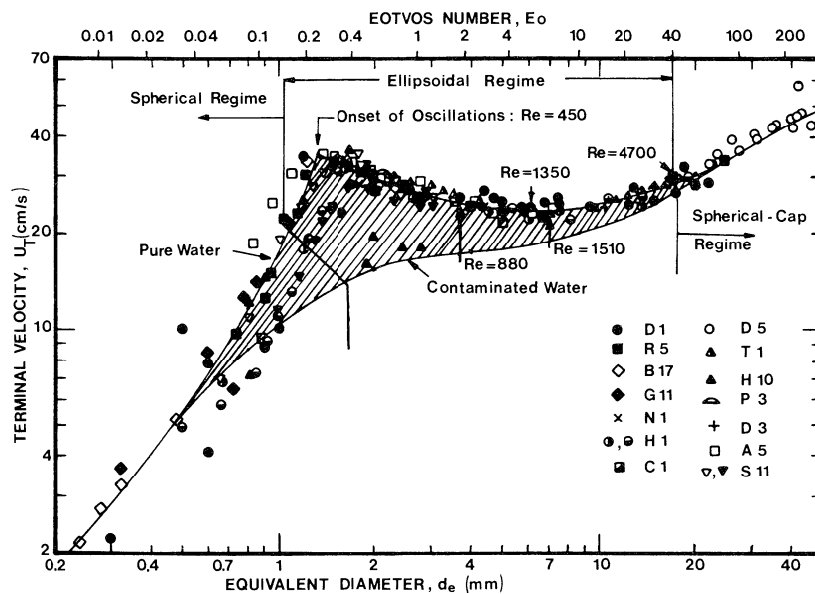


Figure 5: Terminal velocity for an air water system at 20°C [14]

The Reynolds number Re_B of a bubble is calculated with Equation 7. It relates the inertia forces of the bubble to the viscous forces. The equivalent diameter d_e is the diameter of a spherical bubble with equivalent volume as the considering bubble.

$$Re_B = \frac{\rho v d_e}{\mu}$$

Equation 7: Re – Reynolds number of a bubble

The Eötvös number (Equation 8) is used to describe the shape of a rising bubble. It is a relation between buoyancy and surface tension. A low Eö number means that the buoyancy is smaller than the surface tension and results in a spherical bubble. A high Eö number means that the buoyancy is greater than the surface tension and results in a change in the bubble size. The Morton number relates viscous capillary and gravitational forces. Figure 6 shows the bubble shape depending on the Eötvös, Reynolds and Morton number.

$$Eö = \frac{\Delta\rho g d_e^2}{\sigma}$$

Equation 8: Eö – Eötvös number of a bubble

$$M = \frac{g\mu^4\Delta\rho}{\rho^2\sigma^3}$$

Equation 9: M – Morton number of a bubble

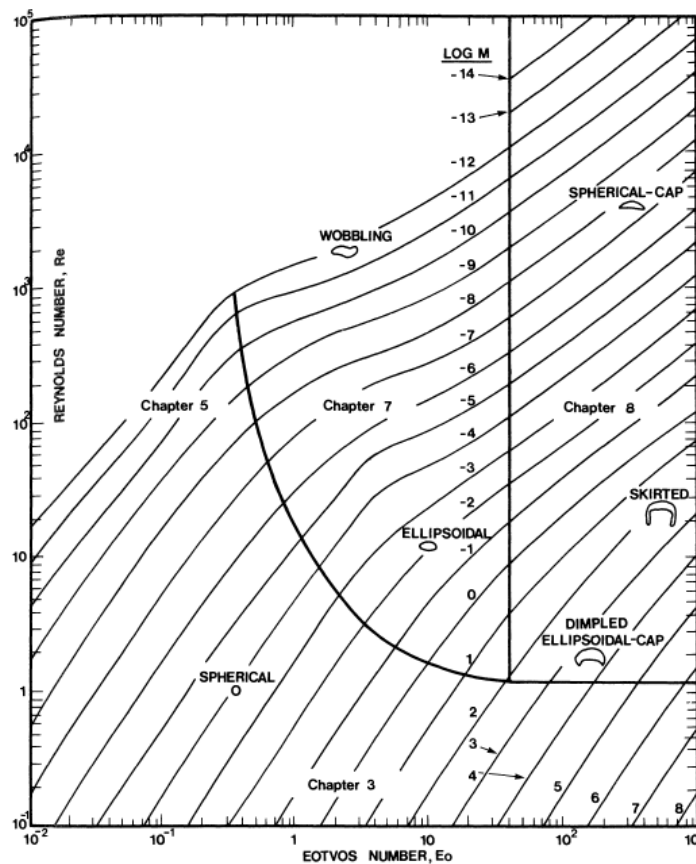


Figure 6: Bubble shape depending on Eö-, Re and M-Number [14]

In industrial multiphase flows the liquid flow field is not stagnant. Therefore, additional forces appear on bubbles such as pressure gradient, shear stress in the liquid phase and subsequently a lift force. In addition, bubbles can breakup due to turbulent eddies or coalescence by collision between bubbles. M.J. Prince and H.W. Blanch [15] described that bubble coalescence occurs in three steps. In the first step the bubbles collide and trap a small amount of liquid in between. Secondly, the trapped liquid drains until the liquid film between the bubbles reaches a critical thickness. Finally, the film ruptures and results in coalescence of the bubbles. Furthermore, they described the bubble breakup by the interaction with turbulent eddies. Eddies with size equal or slightly smaller than the bubble are responsible for the breakup. Larger eddies transport the bubbles and smaller eddies does not contain enough energy to cause a breakup.

2.4 Introduction to gas-liquid stirred reactors

In this thesis, a gas-liquid stirred reactor is referred to a stirred vessel with a gas sparger below the stirrer. Stirred reactors can have one or more impellers. Single impeller reactors are used in smaller tanks whereas multiple impeller systems are used to increase the efficiency of a multiphase process in taller reactors. It can provide a better gas distribution and lower power input compared to single impeller systems. Figure 7 shows a sketch of a multiphase stirred reactor. It has three disc blade impellers, an air sparger and four baffles. The impellers are mounted on a rotating shaft. Furthermore, the baffles prevent solid body rotation as they transform tangential flows to vertical flows and provide top-to-bottom mixing [16]. The clearance (C) and the spacing (S) between the impellers have an important impact on the power consumption and to the flow pattern.

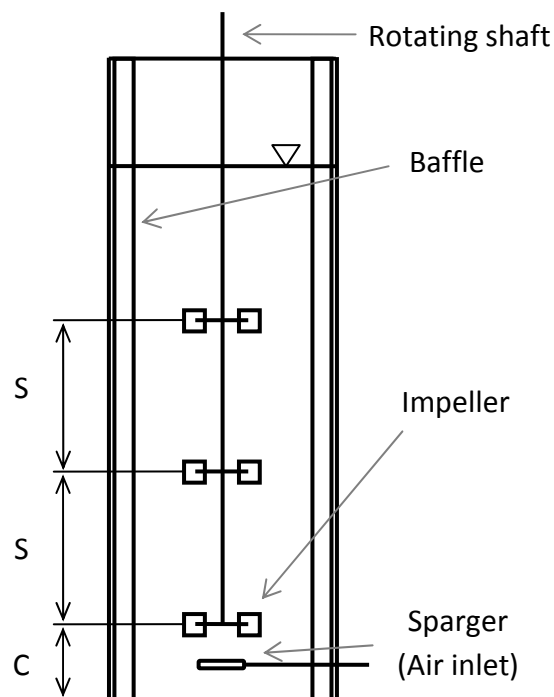


Figure 7: Illustration of multiple impeller multiphase reactor

2.4.1 Impeller types

The impeller induces momentum and therefore velocity to the fluid in the reactor. The liquid flow in the reactor changes in time and space. Consequently, these changes cause shear stress, mixing and dispersion of the gas phase. There are many different impeller types commercially available. Examples for different impellers are illustrated in Figure 8 and Figure 9. They can be classified into four main groups:

- Axial flow impeller
- Radial flow impeller
- Hydrofoil impeller
- High shear impeller

Axial flow impellers are recommended for liquid blending and solid suspensions. An axial flow impeller creates an axial flow stream as illustrated in Figure 10. On the other hand, a

radial flow impeller creates a radial flow stream and is recommended for gas dispersion. In this work the Rushton impeller has been chosen. Figure 9 shows examples for hydrofoil and high shear impellers. A hydrofoil impeller generates an axial flow field with low shear rates whereas high shear impellers generate a radial flow field.

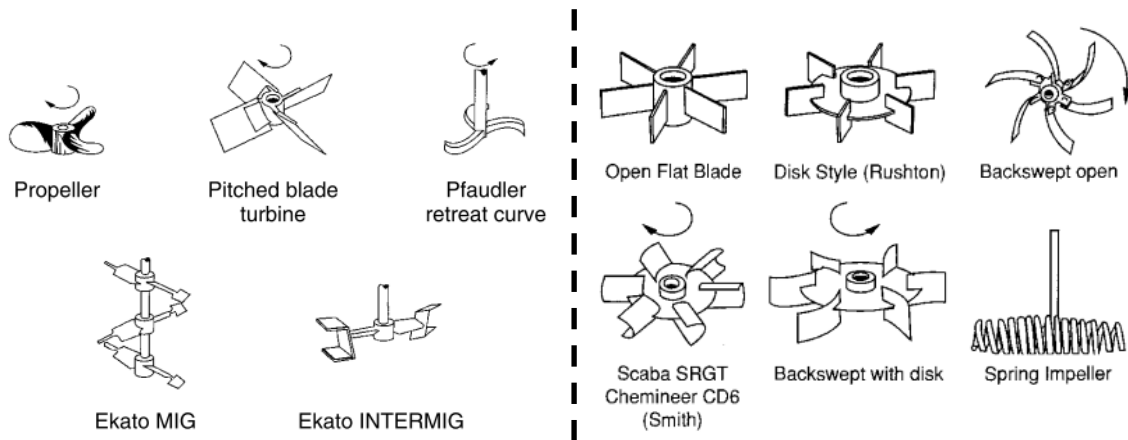


Figure 8: Axial flow impellers (left), radial flow impellers (right) [16]

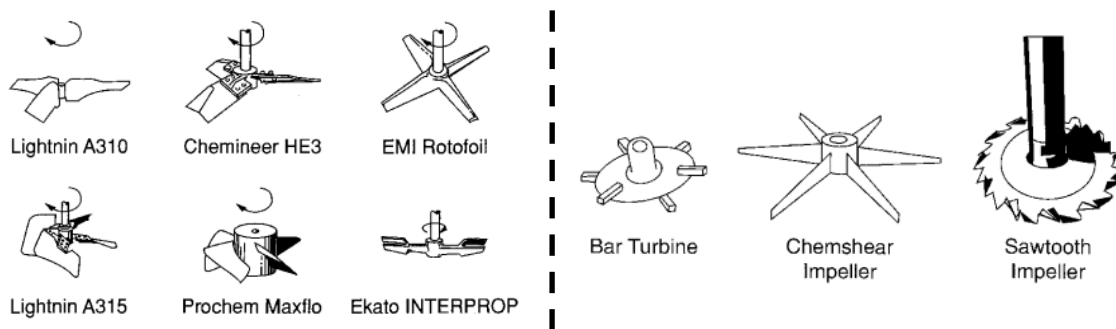


Figure 9: Hydrofoil impeller (left), high shear impeller (right) [16]

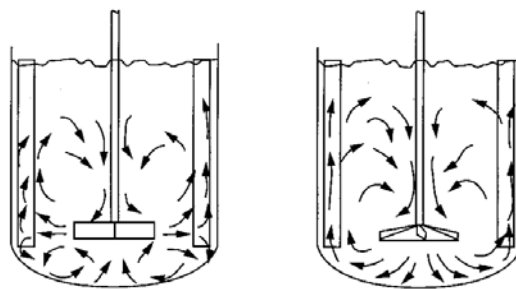


Figure 10: Liquid flow pattern in a stirred reactor; left: radial impeller, right: axial impeller [16]

2.4.2 Impeller arrangement

Figure 11 shows three different flow patterns as a function of the impeller spacing for a dual Rushton impeller reactor. Case (A) shows a reactor setup without spacing between the impellers. The flow pattern is similar to a flow pattern obtained with a single impeller system. Case (B) shows the flow pattern with a spacing of one impeller diameter. The flow patterns of the impellers interact with each other. Case (C) shows the flow pattern obtained with spacing greater than two impeller diameters. Each impeller can develop its characteristic flow pattern. Figure 12 shows the unaerated power input as a function of the impeller spacing. The power input is shown as a ratio between the two impeller system and

single impeller power input. The power consumption of Figure 11 case (A) with zero spacing shows a similar power input as a single impeller system, because the impellers develop one common flow pattern. The power input increases with the impeller spacing until the spacing is bigger than two impeller diameters (Figure 11 case (C)). Then the power input is doubled compared to a single impeller system because each impeller develops now its own flow field.

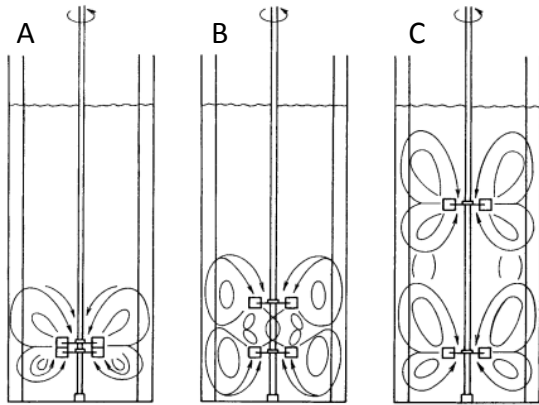


Figure 11: Flow pattern as a function of the impeller spacing [28]

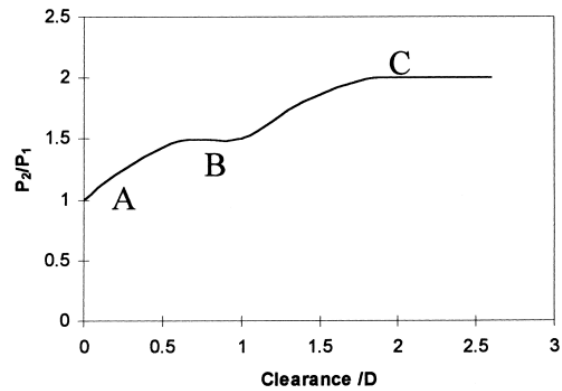


Figure 12: Variation of un-aerated power draw with impeller spacing[28] [29]

2.4.3 Gas flow

The gas flow in stirred reactors can be expressed in several ways. A common way is to express it as a gas flow rate \dot{G} as [m³/h] or [l/s]. Other ways to express the gas flow are: vvm and the superficial gas velocity. The definition of vvm and superficial gas velocity is explained below.

vvm - Gas volume flow per liquid volume per minute

$$vvm = \frac{\dot{G}}{V_R} = \frac{[m^3/min]}{[m^3]}$$

Equation 10: vvm Gas flow

U_s - Superficial gas velocity

The superficial gas velocity is calculated with the gas flow and the cross sectional area of the reactor. It is used to characterize the air flow through the multiphase reactor.

$$U_s = \frac{\dot{G}}{A_R} = \frac{[m]}{[s]}$$

Equation 11: Superficial gas velocity

The superficial gas velocity can be used to roughly approximate three different gas flow regimes inside the reactor [17][18]. In case of low superficial gas velocity, i.e., U_s below 0.02 [m/s], homogeneous gas flow is obtained. The gas bubbles have a narrow size distribution (Figure 13 (a)). At higher superficial gas velocity U_s above 0.03 [m/s] the bubble size distribution becomes bimodal. That means there are small and large bubbles dispersed in the reactor (Figure 13 (d)). The regime between the homogeneous and heterogeneous is called transition regime.

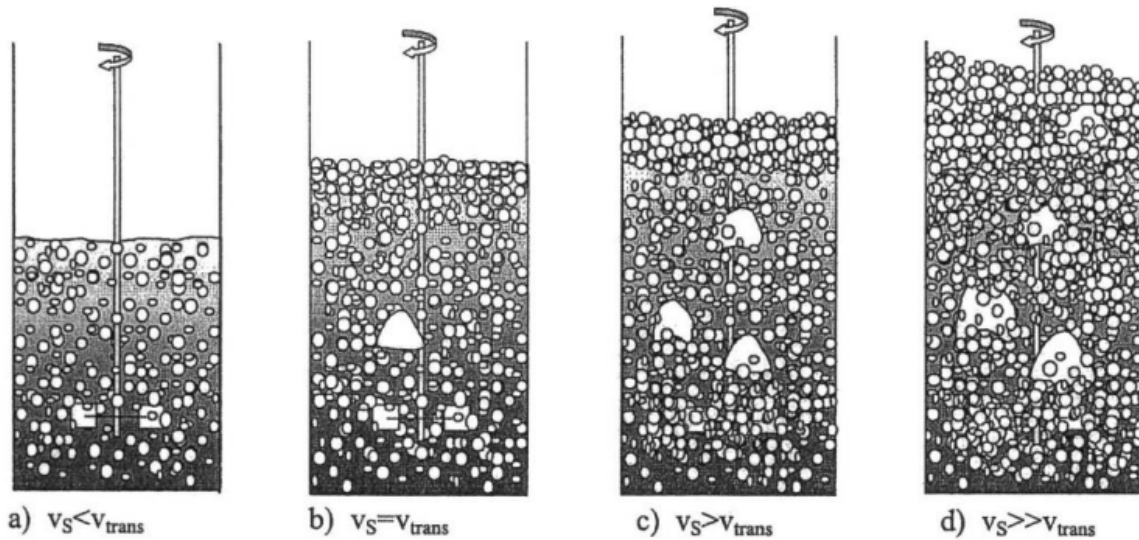


Figure 13: Illustration of homogeneous and heterogeneous distribution [17]

α - Global gas hold-up

The global gas hold-up describes the ratio between volume of the dispersed phase and the total volume. The total volume is the volume of the dispersed continuous phase.

$$\alpha = \frac{V_d}{V_d + V_c}$$

Equation 12: Gas hold-up

2.4.4 Dimensionless numbers in stirred reactors

The dimensionless numbers to describe the flow in stirred reactors are summarized in this section. The Reynolds number for a stirred reactor is calculated with Equation 13. For Reynolds numbers below 100 [16], the process is laminar and turbulent for greater than 10^4 [16]. The Froude number relates the inertial forces to gravity forces. The flow number is a dimensionless measure for the combination of gas flow rate and impeller speed.

$$Re_{SR} = \frac{\rho ND^2}{\mu}$$

Equation 13: Re – Reynolds number of an impeller

$$Fr = \frac{N^2 D}{g}$$

Equation 14: Fr - Froude number

$$Fl = \frac{\dot{G}}{ND^3}$$

Equation 15: Fl - Flow number

2.4.5 Flow pattern

In a multiphase stirred reactor, three main flow patterns can be distinguished depending on the gas flow rate and the impeller rotational speed. Figure 14 shows an illustration of a single impeller system at different operating conditions. The goal of the impeller is to disperse the bubbles within the reactor. The first flow pattern is called “*complete dispersion*” (1). In this regime the impeller disperses the bubble in the whole reactor. The second flow pattern is called “*loading*” (2). In this regime the impeller disperses the bubbles mainly above the disc level. The third flow pattern is called “*flooding*” (3&4) and is usually unwanted. It occurs when the gas flow rate is too high and the impeller cannot disperse the gas bubbles.

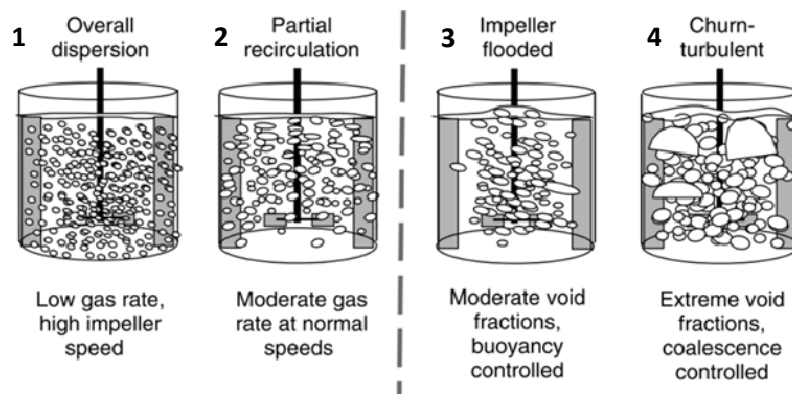


Figure 14: Flow patterns in a gas liquid stirred reactor [16]

For a system with a Rushton turbine, the flow pattern can be distinguished by observing the cavity structure behind the blades. Cavities are developed in low pressure regions in a reactor as they occur behind the rotating impeller blades. Bubbles accumulate and coalescence can occur behind the impeller. When gas continuously enters and exits a cavity, the cavity is said to be ventilated [19]. Four different cavity regimes are shown by Paglianti [20]. Figure 15 illustrates two dimensional views of a Rushton turbine from the top. The cavity regimes: vortex cavities, clinging cavities and 3-3 structure indicate an operation in a loading regime. A 3-3 structure is a regime with two different cavity forms on one impeller. There are small and big cavities, alternately around the impeller. Otherwise, ragged cavities indicate a flooded operation condition. Three dimensional illustrations of the cavities are shown in Figure 16. (a) shows a vortex cavity and (b) a large cavity.

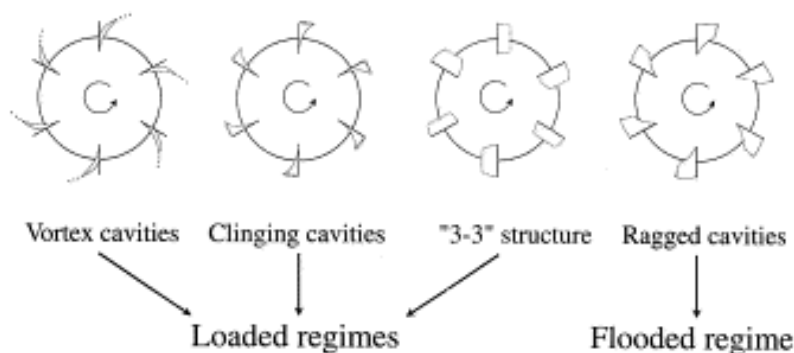


Figure 15: Cavity regimes in loading and flooding[20]

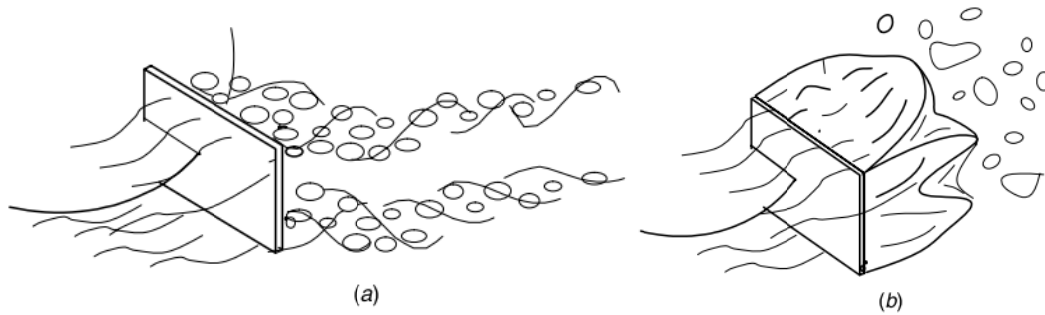


Figure 16: Cavity Structures behind a Rushton blade [16]

2.4.6 Flow regimes

Reactors can operate at various conditions. The gas flow rate and agitation speed can vary within a large range. Six different flow regimes can be identified for a system with Rushton impeller. Figure 17 shows the flow regimes in a so called flow map. The flow map is a logarithmic map dependent on the gas flow number and impeller Froude number. The flow map is based on empirical correlations found in the literature, which have been derived from experiments [16]. The first regime is “below minimum dispersion speed”. A stirred reactor with Fr Number < 0.04 behaves like a bubble column (below the - · - · in Figure 16) [16]. The impeller rotational speed is too low to disperse the gas phase. The second regime is called “vortex cavity, no recirculation”. Vortex cavities are shown in Figure 16 (a). Recirculation means that the bubbles follow the liquid flow so that they get in contact with the impeller several times. The third regime is called “vortex cavities with recirculation”. The cavity shape is also a vortex cavity but the bubbles recirculate within the impeller compartment. The fourth regime is called “flooding”. Here, the gas flow rate is too high and the impeller cannot disperse the gas phase. The cavity regime in this case is ragged cavities.

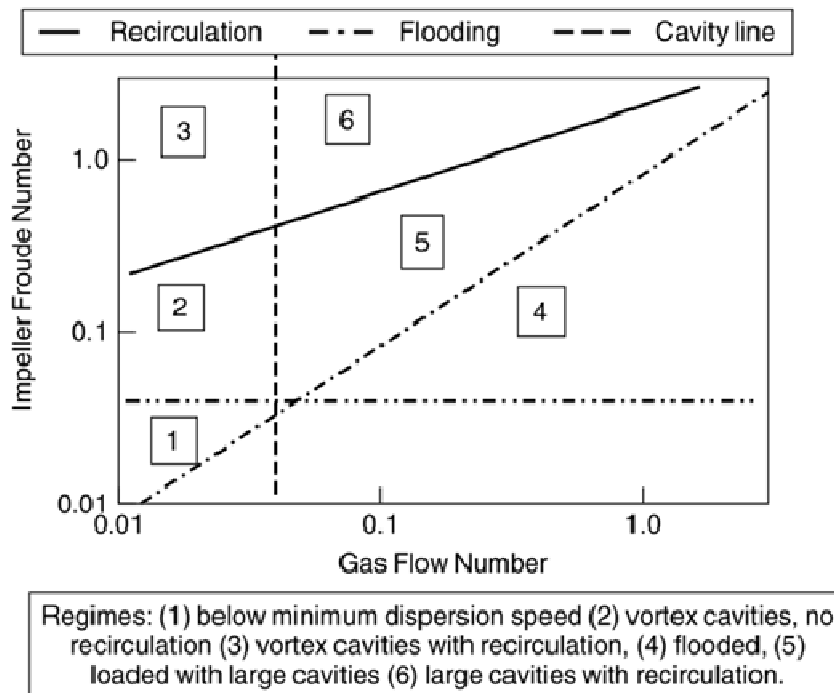


Figure 17: Flow map for single Rushton impeller [16]

The fifth regime is called “loaded with large cavities”. In this regime the bubbles are well dispersed. The cavity regime is large cavities, as illustrated in Figure 16 (b). The last and sixth regime is called “large cavities with recirculation”. This regime is similar to regime four, but with recirculation. The operation in the transition region should be avoided. The regime could flip unstably and cause serious mechanical and operational problems [16].

The flow map for a multiple impeller system is shown in Figure 18. The regimes 1 to 6 are in the regions as in the single impeller system (Figure 17). In multiple impeller systems the cavity regimes can be different on the impeller levels. Regime 5 is divided into two parts. In (A) large cavities appear at the lowest impeller and vortex cavities on the impellers above. In (B) large cavities occur on all impellers.

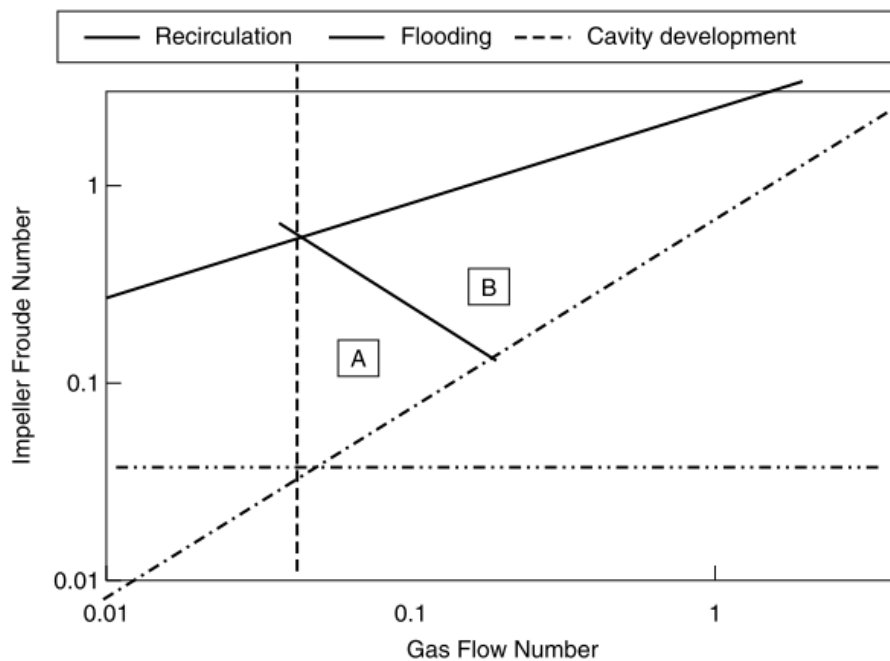


Figure 18: Flow map for a triple Rushton Impeller reactor [16]

2.4.7 Regime recognition

Industrial reactors are usually made of stainless steel. A visual observation of the flow pattern is possible through sight glasses only. The liquids are rarely transparent, most of the cases deal with non-transparent liquids. In these cases visual observation is limited to the vicinity at sight glass or at free surface. Even in transparent fluid a visual observation is affected through the gas bubbles. In case of high gas hold-up a detailed visual observation is impossible. Bombac et al. [1] introduced a methodology to identify the current cavity regime of impellers by analyzing the resistivity with a needle probe close to the impeller blades. Note that resistivity is the reciprocal value of the electrical conductivity. They recorded the resistivity for several impeller revolutions and applied a fast Fourier frequency analysis to the obtained conductivity curve (see Figure 19). The frequency spectrums show different shapes depending on the cavity regime. They were able to identify the following six different cavity regimes: Vortex cavities (VC), one large cavity (1L), two large cavities (2L), three small cavities (S33), three large cavities (L33) and ragged cavities (RC). The frequency spectrums show a significant peak at the blade frequency (f_b) in each case.

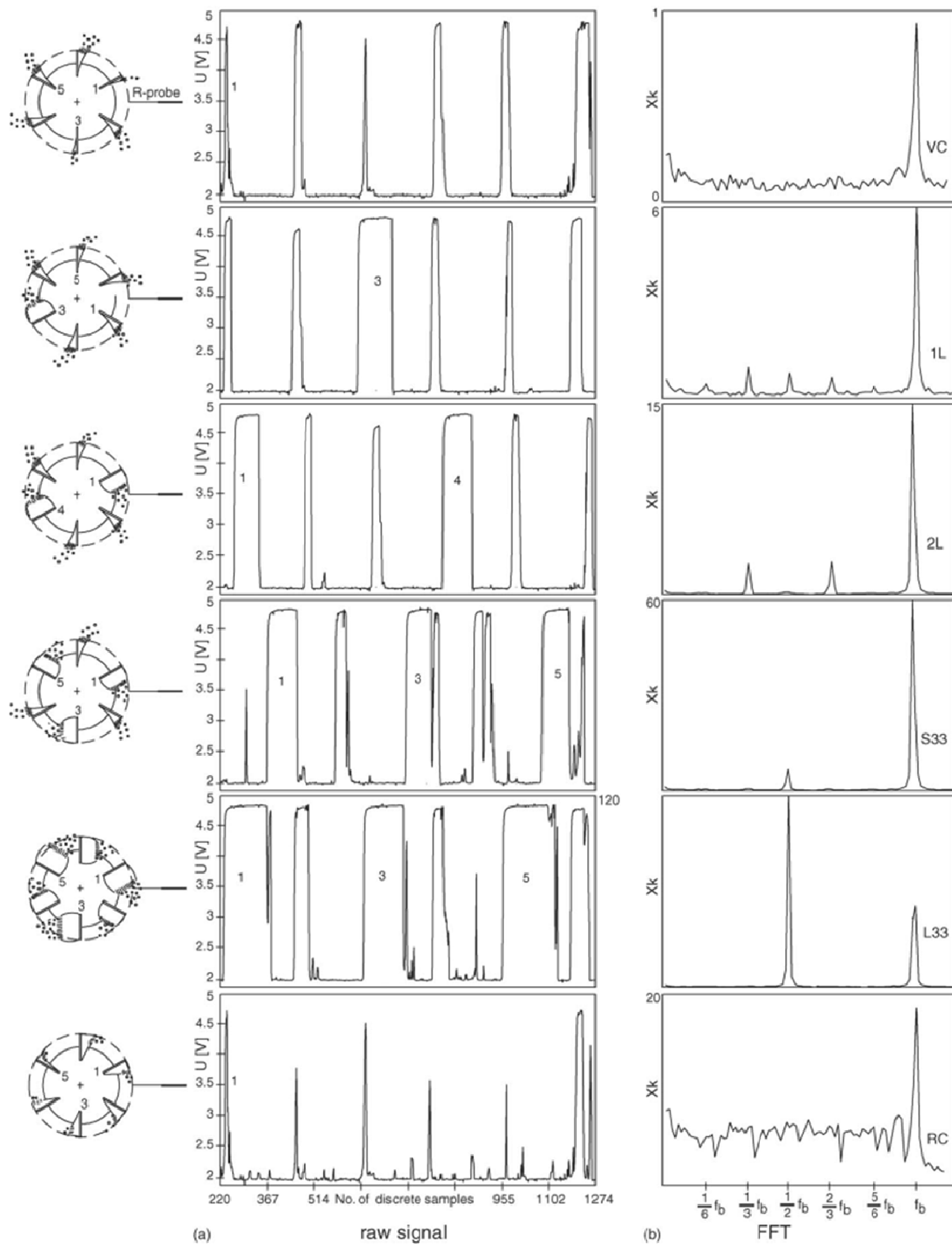


Figure 19: Flooding recognition with a resistivity probe: (a) raw signal; (b) frequency spectrum [2]

3 Measurement system

3.1 Principle

In this chapter, the principle of the conductivity measurement will be discussed. The measurement principle was developed during a previous conducted design study [21]. Figure 20 shows the block diagram and the ideal signal curves of this system. It consists of four main parts:

1. **Analog output:** Generates a continuous sine voltage signal
2. **Conductivity probe:** The resistance depends on the medium between two measurement points
3. **Analog input:** Measures the current over the conductivity probe
4. **Data processing:** Calculates the conductivity curve

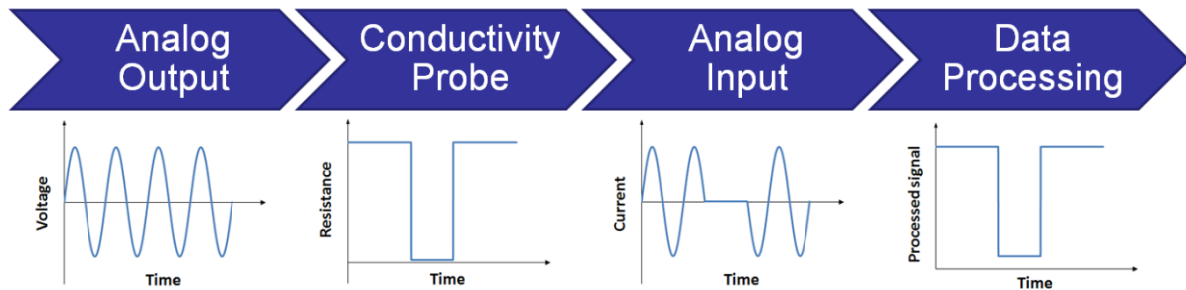


Figure 20: Illustration of the measurement principle [22]

3.2 Signal generation

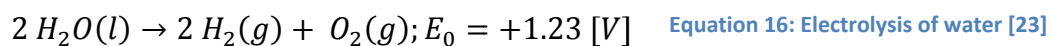
The choice of a proper signal, which will be applied to the conductivity probe, is an important factor. An improper signal can cause several unwanted effects, namely:

1. Parasitic capacities

In electrical circuits, parasitic capacitance is an unavoidable and usually unwanted capacitance. This effect exists between parts of an electronic component or circuit due to their proximity to each other. The main parasitic capacities in our case are caused by an electrical double layer at the electrode surface. In order to prevent parasitic capacities, it is necessary to use an alternating signal with high frequency. Therefore, a sine signal with a frequency of 1 [kHz] is applied to the conductivity probe.

2. Electrolysis

Electrolysis is a chemical reaction to split or separate chemical components with direct electrical current (DC). Therefore, it is necessary to know the electrolysis voltage of the used components. This will restrict the upper voltage limit of the measurement signal. The reaction in equation 16 suggests that the reaction takes place at the voltage of 1.23 [V]. Higher voltage will result in electrolysis and consequently measurement errors.



3. Changes of the electrodes surface

This change is caused by dissolving the electrodes by applying a voltage above their standard electrode potential or deposition of ion on the probe surface. Furthermore, according to the electrochemical standard potentials, the amplitude of the sine signal is limited by electrochemical effects in similar manner with the dissolution of the material. It is important that a low current density is generated at the electrode surface to avoid any physical changes at this surface.

The applied sine signal in this work has a frequency of 1 [kHz] and amplitude of 500 [mV].

3.3 Probe

A single tip probe design has been selected in the previous conducted design study [21], which is used in the work. The conductivity probe is shown in a three-dimensional view in Figure 21. The main component of the probe is the needle with the tip electrode, which is demonstrated in Figure 22. The drawings of the probe can be found in the appendix. The conductive surfaces are gilded in order to increase the chemical resistance according to the standard electrode potentials (see Table 1).

Table 1: Standard electrode potentials of copper and gold [15]

Standard electrode potentials	[V]
$\text{Cu}^{2+} + 2e^{-} \leftrightarrow \text{Cu}(s)$	+0.34
$\text{Au}^{3+} + 3e^{-} \leftrightarrow \text{Au}(s)$	+1.50

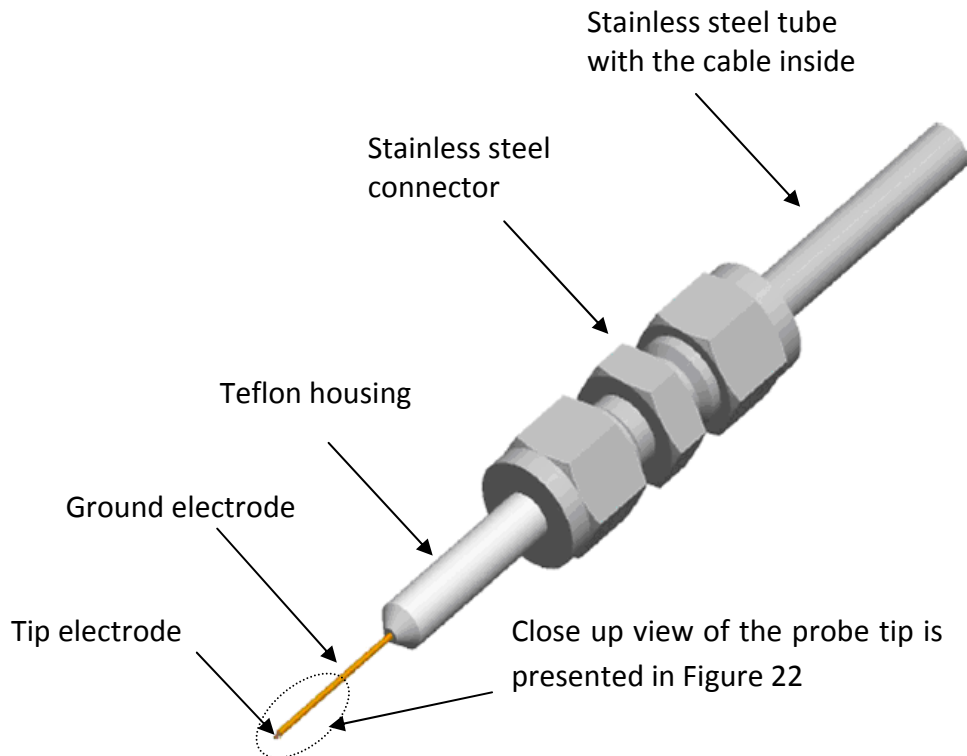


Figure 21: 3D View of the conductivity probe

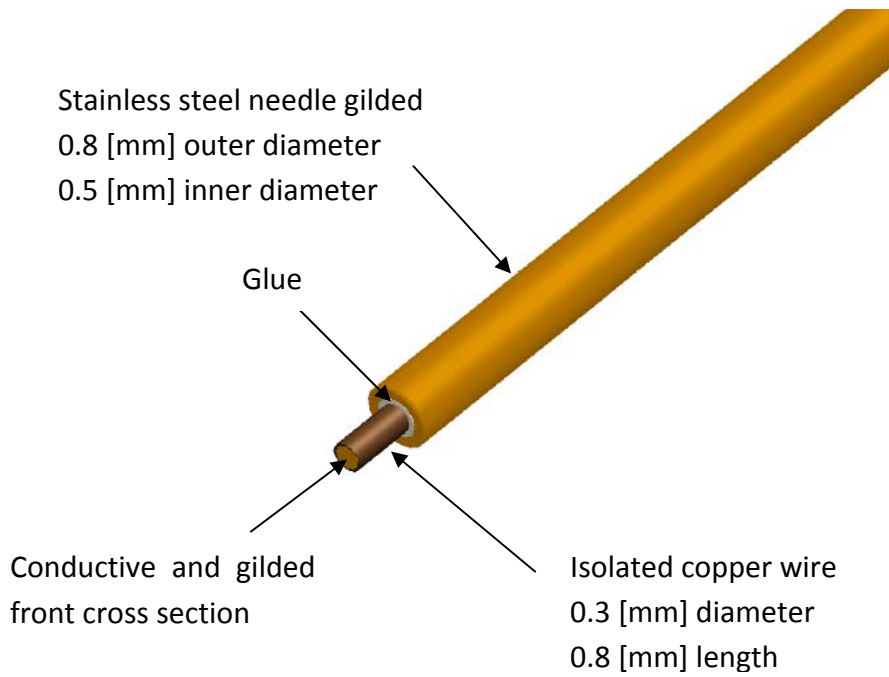


Figure 22: 3D view of the conductivity probe tip, highlighted in the ellipsoid in figure 21

Next, Figure 23 illustrates the change of the resistance on the conductivity probe. The conductive areas of the probe are highlighted in red. The left illustration shows the probe in contact with a gas bubble. The bubble covers the electrode tip. Consequently, the probe's resistance increases significantly, i.e., conductivity across the probe decreases. The right illustration shows the probe in contact only with the liquid phase which leads to a low resistance of the probe.

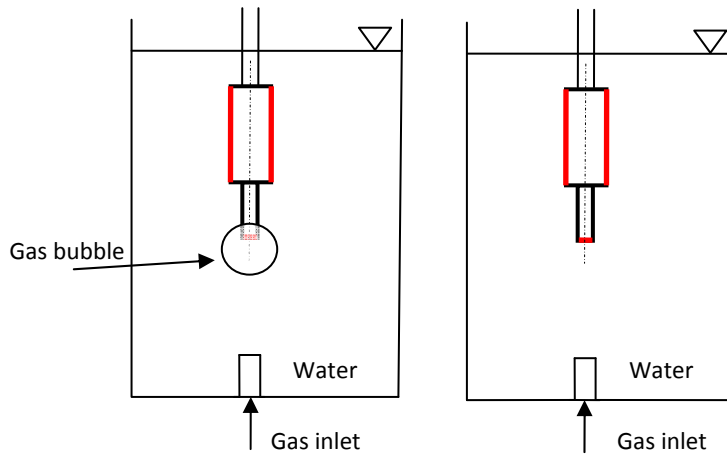


Figure 23: Illustration of the needle probe in a water-filled vessel

3.4 Signal acquisition and processing

The signal applied to the probe is an alternating sinus voltage with an amplitude of 500 [mV] and a frequency of 1 [kHz]. The current flow is acquired with a sampling rate of 50 [kHz] to determine the conductivity. The current flow depends on the specific conductivity and the probes cell constant. The combination of our experimental setup causes current flow between 0-30 [μ A] with tap water. The low current is susceptible to electromagnetic interference (EMI). Figure 24 shows two periods of the acquired raw signal in blue. The EMI causes unwanted deviations from the real curve. The signal is filtered with a band pass filter, to smooth out this noise. The filter signal is shown as the green curve.

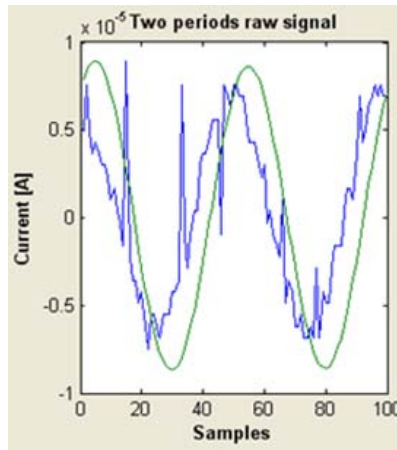


Figure 24: Raw signal and filtered signal

As an alternating current is used, the signal must be treated before we obtain the conductivity curve. The root-mean-square (RMS) value of the sine curve is calculated. The RMS value from a set of data points is calculated by Equation 17. The obtained RMS signal has a time resolution of 1 [kHz].

$$x_{RMS} = \sqrt{\frac{x_1^2 + x_2^2 + \dots + x_n^2}{n}}$$

Equation 17: RMS of a set of data points

3.5 Circuit of the measurement system

Figure 25 shows the electrical circuit of this system. It shows how the needle probe is connected to the DAQ hardware. An analog output module is used to generate the sine signal voltage with constant amplitude. The generated signal is applied to the probe. The current flow in the system is measured with an analog input module.

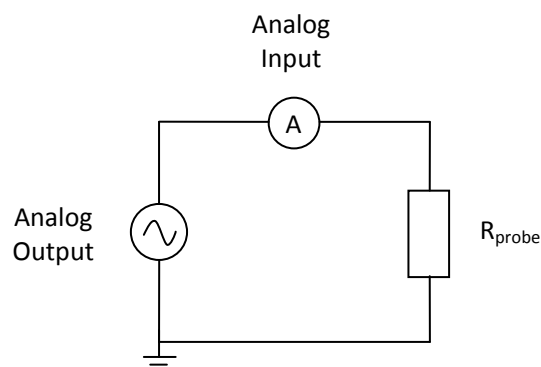


Figure 25: Electrical circuit of the measurement system

3.6 Data acquisition

The measurement software is programmed with commercial software called Matlab® including the data acquisition toolbox. The software is designed such that important measurement parameters are generated, monitored and measured within a single program. The task of the software comprises of:

- Signal generation
- Data acquisition
- Signal handling (normalize, band pass filter)
- Reconstruct the conductivity curve
- Online gas hold-up calculation
- Data logging

Figure 26 shows the developed graphical user interface GUI. It has three parameter input fields, six graphs, two indicators and a run button.

The input sections are located in the middle of the GUI. They are clustered in three panels.

- **Signal parameters panel:** the voltage and frequency can be set in this panel
- **Gas hold-up parameter panel:** the threshold and averaging time can be set in this panel
- **Save data panel:** this panel contains the parameters for the saving function of the program, measurement sets and data source can be defined
- **Run button:** starts the measurement

The indicators are placed on the top and the bottom of the GUI. The diagram “two periods raw signal” shows the measured raw signal (blue) and the same section of the signal after the filter procedure (green). A shift of the phase between the raw signal and the filtered signal is due to the filter algorithm. The diagram “RMS Signal” shows the obtained RMS curve of the last measured second in a normalized form. The threshold is also shown as a red curve in this diagram. The diagram “gas hold up” shows the gas hold-up curve obtained for the defined average time. The diagram “Min (blue) and max (red) Values of the RMS” show curves of the minimum and maximum measured conductivity. The blue curve represents the measured conductivity of the dispersed phase and the red curve of the continuous phase. A change of the specific conductivity or temperature change can be seen in these diagrams. The diagram “Averaged Gas Hold-Up” shows a curve of the averaged gas hold-up over the measurement period. This indicator can be used to define a statistically necessary measurement time. The indicator panel “Analysis of the Indicated Data” shows the gas hold-up values for RMS data displayed in the diagram “RMS Signal”. The indicator “Gas hold up overall” shows the numeric value for the gas hold-up of the acquired RMS curve throughout the beginning. The averaged values can be reset with the button “Reset displays”.

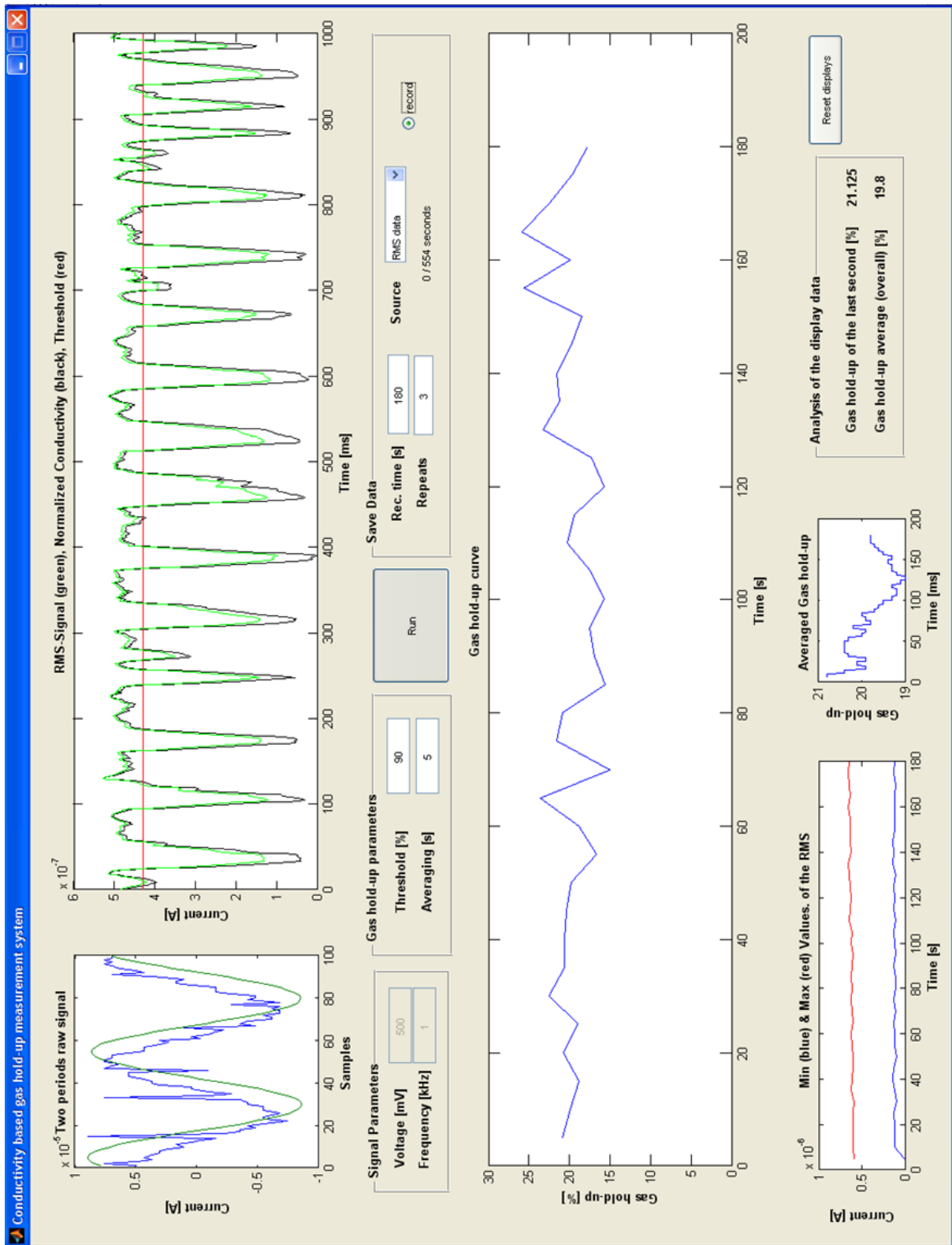


Figure 26: Graphical user interface (GUI) of the measurement software in Matlab®

3.7 Verification with an image analysis technique

3.7.1 Verification setup

A cubic Plexiglas® box is used to run the verification with single air bubble in water. The box has a dimension of $L=280$ [mm], $W_{PB}=280$ [mm] and $H=280$ [mm] (see figure 27). The box is made of transparent Plexiglas® which allows visual investigations.

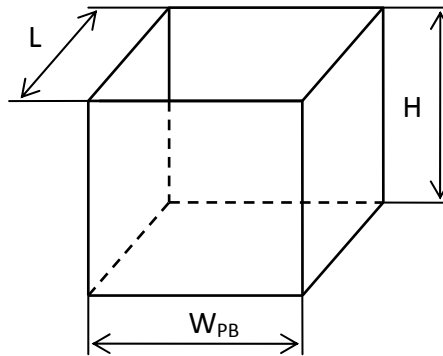


Figure 27: Illustration of the box for single bubble experiments

3.7.2 Verification

The verification of the developed conductivity-based measurement system was carried out by a comparison with images obtained from a high speed camera. Figure 28 shows an illustration of the experimental setup. The Plexiglas box was filled with tap water. The probe was located in the middle of the box and bubbles were consequently injected below the probe with a syringe. The objective of the validation is to evaluate the consistency between both methods.

Bubble generator

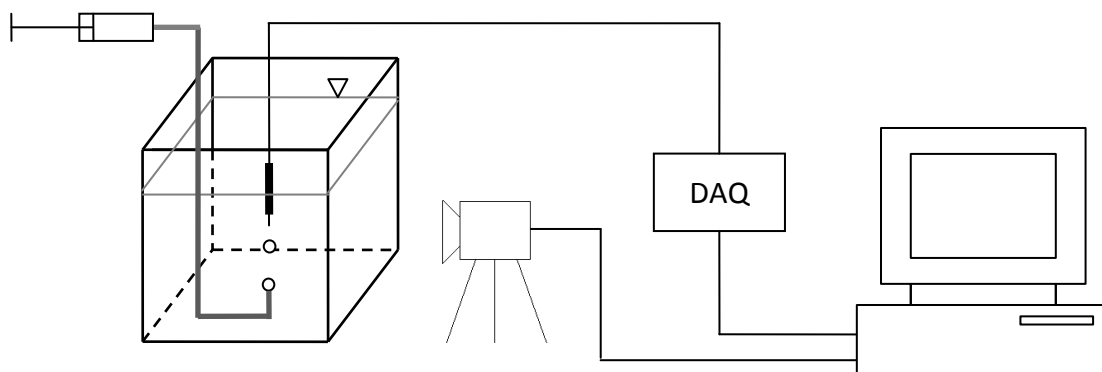


Figure 28: Illustration of the verification setup

Figure 29 shows snapshots obtained with the high speed camera. The images show a close up view of our measurement probe tip and a rising bubble. The images were taken with a frequency of 1000 [Hz], that means 1 snapshot was taken at every millisecond. The images show that the rising bubble is in contact with the conductive probe tip from the second to the second last depicted images. It correlates a contact time of 7 [ms].

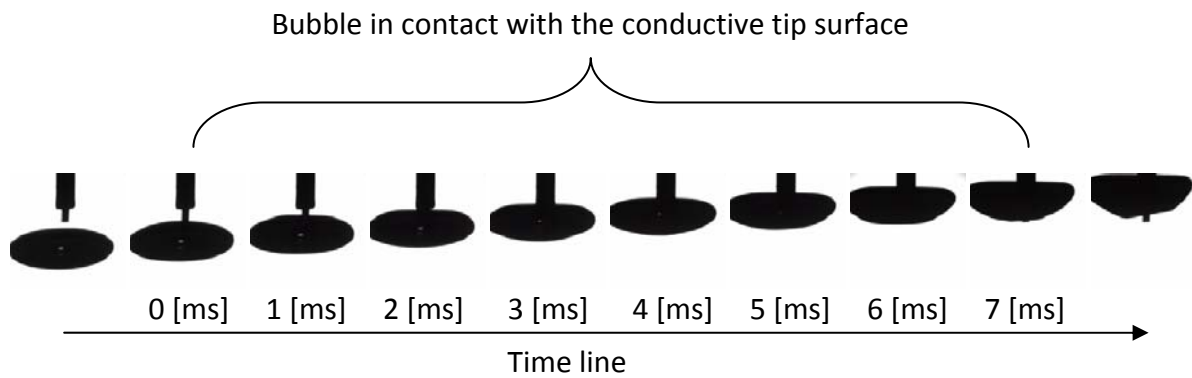


Figure 29: Snapshots of a rising bubble with the M3 high-speed camera at 1000 [Hz]

3.7.3 Matlab® post processing

A Matlab® script was programmed to investigate and compare the data from both methods. The flow diagram of the program is illustrated in Figure 30. The first step is to load the measurement file. Next, the loaded conductivity curve is normalized to the liquid conductivity and the minimum value of the conductivity curve. The next step reconstructs the conductivity curve with threshold level of 90 percent. Subsequently, the bubbles and their contact times are determined. The last post processing step is to visualize the obtained data. The Matlab® code is attached in the appendix and on the volume.

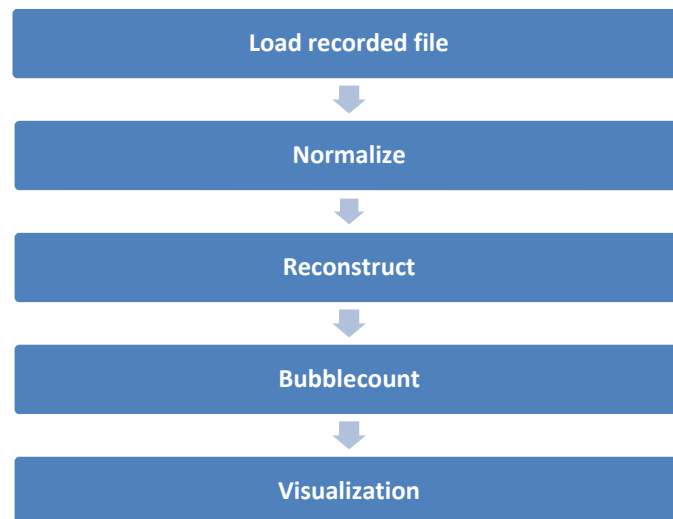


Figure 30: Illustration of the Matlab® post processing for the image analysis

3.7.4 Calculation of the theoretical contact time

The bubble size was altered within the experiments. Figure 31 shows characteristic snapshots of the three generated bubble dimensions. In Figure 31 (c), since the bubble size is greater than the range of the high speed camera, the missing parts of the bubble were estimated with an ellipse. The estimated ellipse is illustrated as a dotted line in the figure. The generated bubbles are all in the elliptic regime. The dimension in h , which is important for the measurement, does not change significant with the applied bubble size. It varies from 1.4 [mm] to 1.7 [mm]. This dimension in combination with the terminal velocity is used to determine the theoretical contact time with the probe tip.

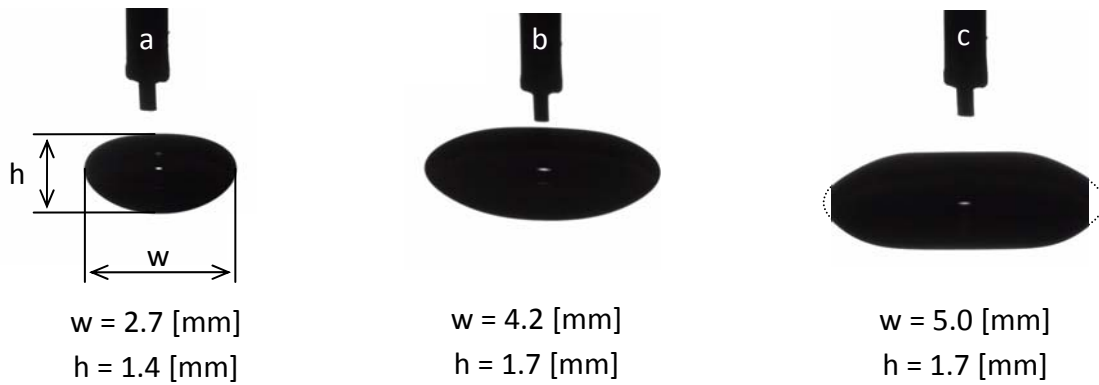


Figure 31: Snapshots of characteristic bubbles of the verification procedure

Table 2 shows the calculation of the theoretical contact time. The first step was to estimate the bubble volume with the volume of an ellipsoid. The equivalent bubble diameter was calculated from this volume. The terminal velocity was obtained with a correlation (Equation 18) for the ellipsoidal part of the terminal velocity diagram (Figure 5). The Re Number and Eö Number were calculated and compared with the bubble shape diagram (Figure 6). The bubbles are in the ellipsoidal regime. The assumptions for the theoretical contact time are:

- The bubble does not feel any resistance of the probe
- The bubble hits the probe in the middle

Therefore, the theoretical contact time is calculated with the bubble diameter and the terminal velocity. The table shows that the theoretical contact time lies in the range between 4 and 6 [ms].

$$u_t = \sqrt{\frac{2.14\sigma}{\rho d_e} + 0.505gd_e}$$

Equation 18: Correlation for the terminal velocity in pure water and $d_e > 1.3$ [mm] [14]

Table 2: Calculation of the theoretical contact time

Bubble size	w	h	V_{eps}	d_e	u_T	Re	Eö	theoretical contact time
	[mm]	[mm]	[mm ³]	[mm]	[m/s]	[-]	[-]	[ms]
a	2.7	1.4	1.70	1.48	0.34	496	0.30	4.2
b	4.2	1.7	5.00	2.12	0.29	613	0.61	5.9
c	5	1.7	7.08	2.38	0.28	661	0.76	6.1

3.7.5 Results of the verification

Several experiments to verify the measurement system were performed. Figure 32, Figure 34 and Figure 36 show the conductivity curves and the reconstructed signals obtained by a verification experiment with bubble sizes as shown in Figure 31. The signal curves have been reconstructed with a threshold of 90%. The approach to verify the measurement system was to compare the contact time and the interval between two bubbles of both methods. The contact time is the duration when the bubble is in contact with the conductive area of the probe tip. The interval between two bubbles is calculated from one falling edge to the next falling edge of the reconstructed conductivity curve. The interval comparison for the conducted verification experiments is summarized in Table 3 and shows a perfect match.

Figure 33, Figure 35, and Figure 37 show a close up view of the bubble interaction sections Figure 32, Figure 34, and Figure 36, respectively. The diagrams show the conductivity curve, the threshold and the reconstructed signal. In the close-up for bubble 1 in Figure 34, the contact time is depicted. It can be seen that the bubble interaction causes similar signal drops by comparing the shape of the drops. The results of the image and conductivity curve analysis are shown in Table 4. The comparison of the contact times shows a deviation of approximately 140% from the image analysis contact time. One assumes that the deviation is caused by influencing the electric field at the probe vicinity. Two approaches to compensate the deviation were taken into consideration. The first approach uses the threshold. It sets the threshold to a level that the contact times match with the results from the high speed camera. The second approach uses a compensation factor to obtain agreement between the contact times. The compensation has the advantage that the measurement system can capture a half signal drop due to the bubble contact, e.g. Figure 33 bubble 3. The deviation is compensated by dividing the contact time gained by the conductivity measurement with a compensation factor of 2.4 and a perfect match was obtained.

Table 3: Comparison of the obtained intervals between image analysis and conductivity measurement (IA .. image analysis; CM .. conductivity measurement; Dev .. deviation)

Interval				Bubble size a			Bubble size b			Bubble size c		
Bubbles				IA	CM	Dev	IA	CM	Dev	IA	CM	Dev
				[ms]	[ms]	[%]	[ms]	[ms]	[%]	[ms]	[ms]	[%]
1	&	2	t_{12}	29	29	0%	399	399	0%	43	42	2%
2	&	3	t_{23}	30	30	0%	45	46	-2%	46	46	0%
3	&	4	t_{34}	34	34	0%	50	50	0%	50	50	0%
4	&	5	t_{45}	37	37	0%	55	54	2%	54	53	2%
5	&	6	t_{56}	35	35	0%	64	64	0%	65	66	-2%
6	&	7	t_{67}	39	39	0%	70	70	0%	72	72	0%
7	&	8	t_{78}	41	41	0%	86	86	0%	93	93	0%
8	&	9	t_{89}	43	44	-2%	113	113	0%	131	131	0%
9	&	10	t_{910}	53	51	4%	179	179	0%	315	315	0%
10	&	11	t_{1011}	61	62	-2%	544	544	0%	-	-	-
11	&	12	t_{1112}	69	70	-1%	-	-	-	-	-	-

Table 4: Comparison of the contact times (IA .. image analysis; CM .. conductivity measurement; Dev .. deviation)

Contact time		Bubble size a			Bubble size b			Bubble size c		
Bubble		IA	CM	Dev	IA	CM	Dev	IA	CM	Dev
		[ms]	[ms]	[%]	[ms]	[ms]	[%]	[ms]	[ms]	[%]
1	t_{c1}	6	14	133%	7	16	129%	7	15	114%
2	t_{c2}	7	17	143%	6	15	150%	6	15	150%
3	t_{c3}	5	13	160%	6	15	150%	6	15	150%
4	t_{c4}	5	15	200%	6	15	150%	6	15	150%
5	t_{c5}	5	13	160%	7	16	129%	7	16	129%
6	t_{c6}	7	16	129%	7	16	129%	6	15	150%
7	t_{c7}	5	13	160%	8	17	113%	8	17	113%
8	t_{c8}	5	14	180%	7	16	129%	7	17	143%
9	t_{c9}	5	13	160%	7	16	129%	7	16	129%
10	t_{c10}	6	16	167%	7	16	129%	6	16	167%
11	t_{c11}	6	15	150%	6	16	167%	-	-	-
12	t_{c12}	5	14	180%	-	-	-	-	-	-
		5.6	14.4	158%	6.7	15.8	135%	6.6	15.7	138%

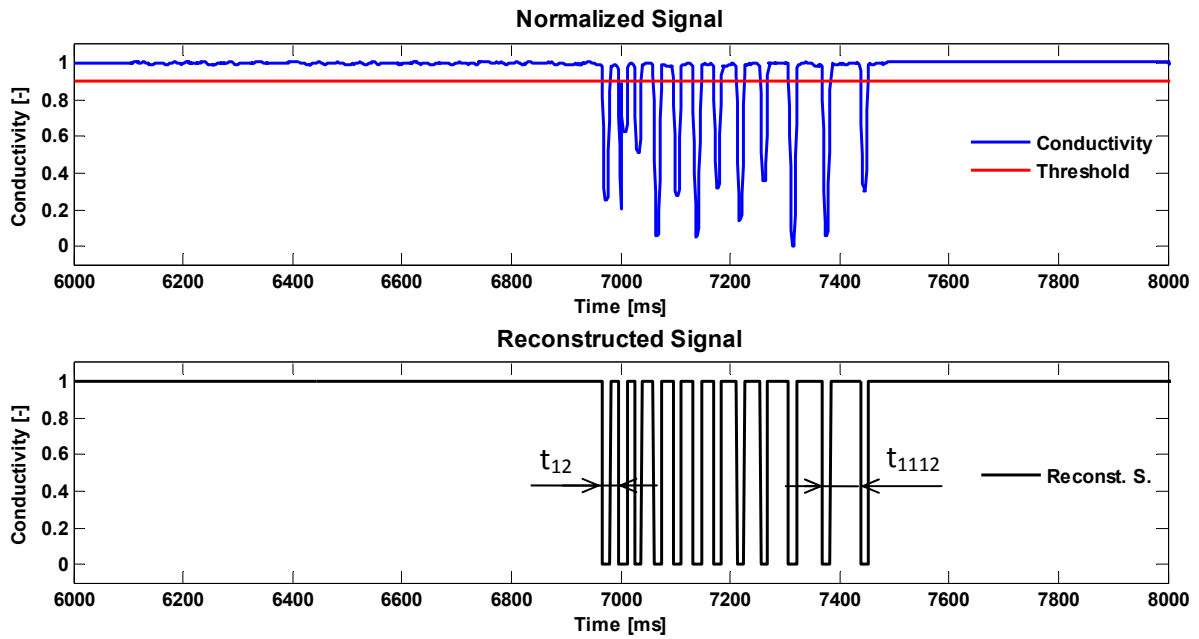


Figure 32: Conductivity curve obtained from the verification experiment with bubble size (a)

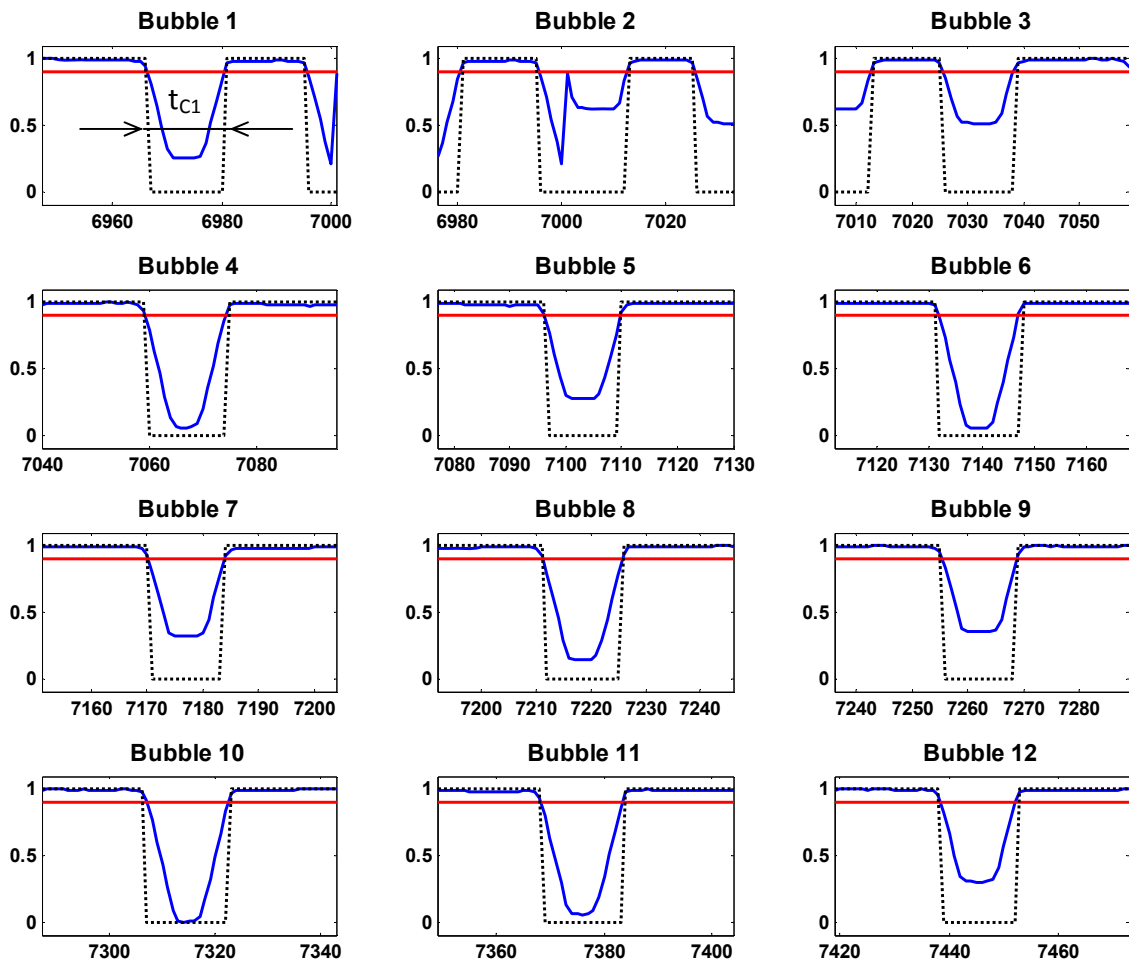


Figure 33: Zoom of the bubble interactions in Figure 32 (- threshold, -conductivity, -- reconstructed signal)

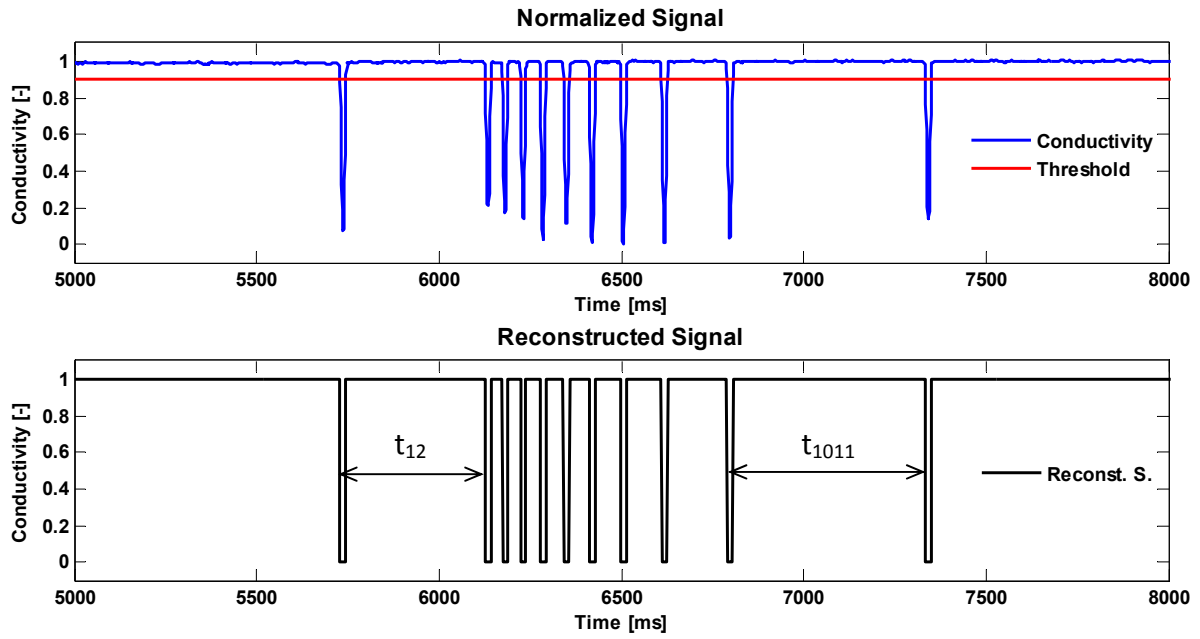


Figure 34: Conductivity curve obtained from the verification experiment with bubble size (b)

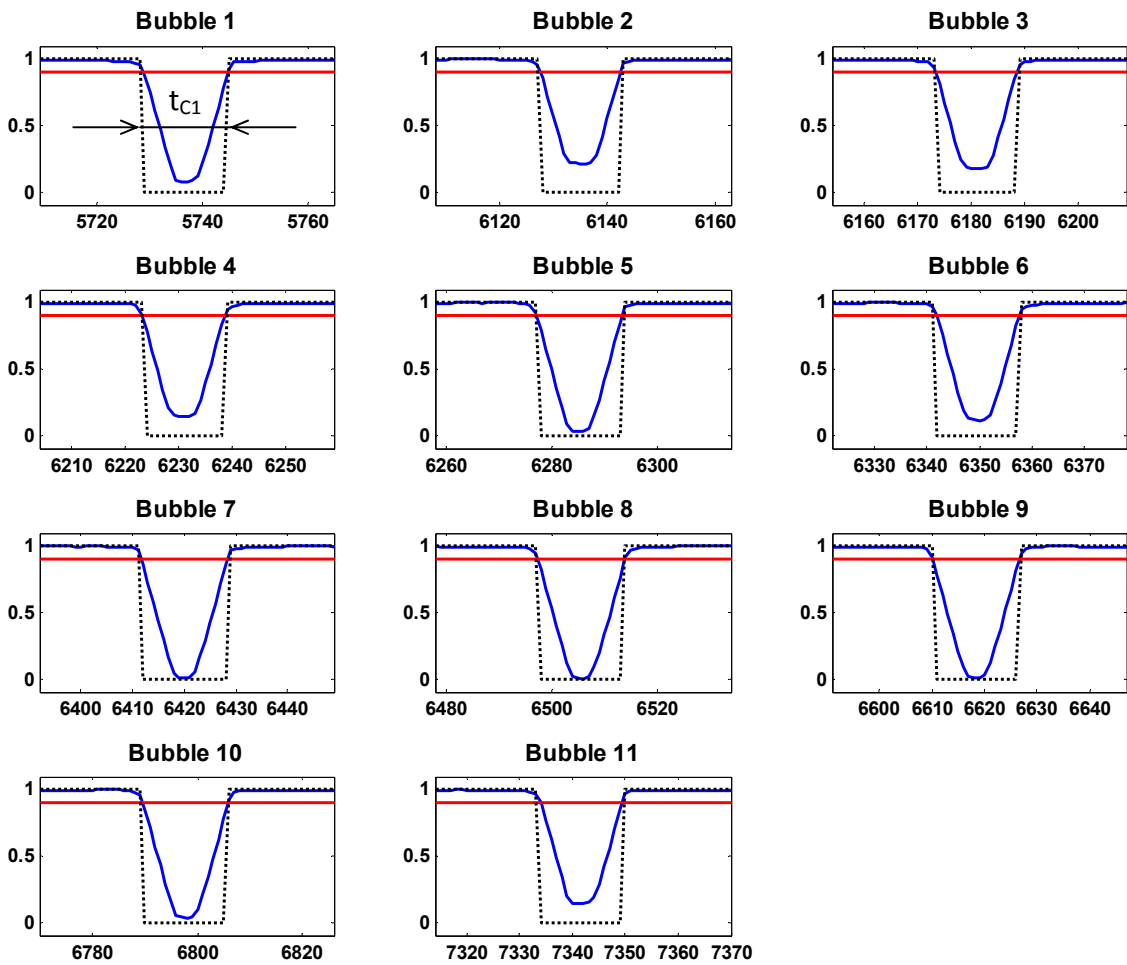


Figure 35: Zoom of the bubble interactions in Figure 34 (- threshold, - conductivity, -- reconstructed signal)

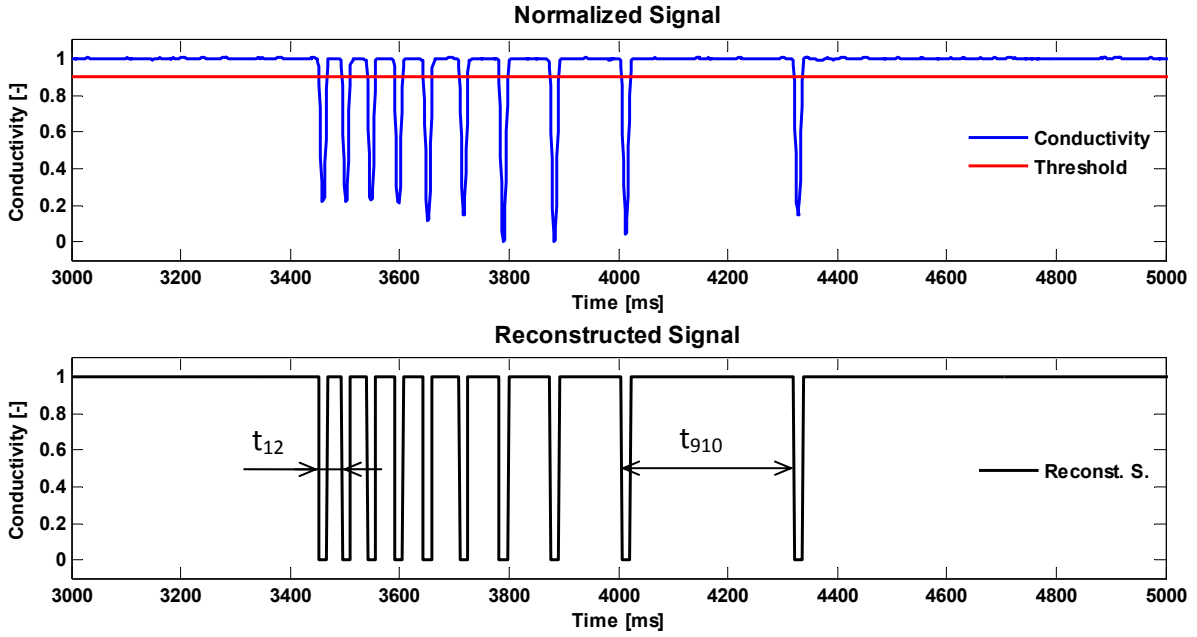


Figure 36: Conductivity curve obtained from the verification experiment with bubble size (c)

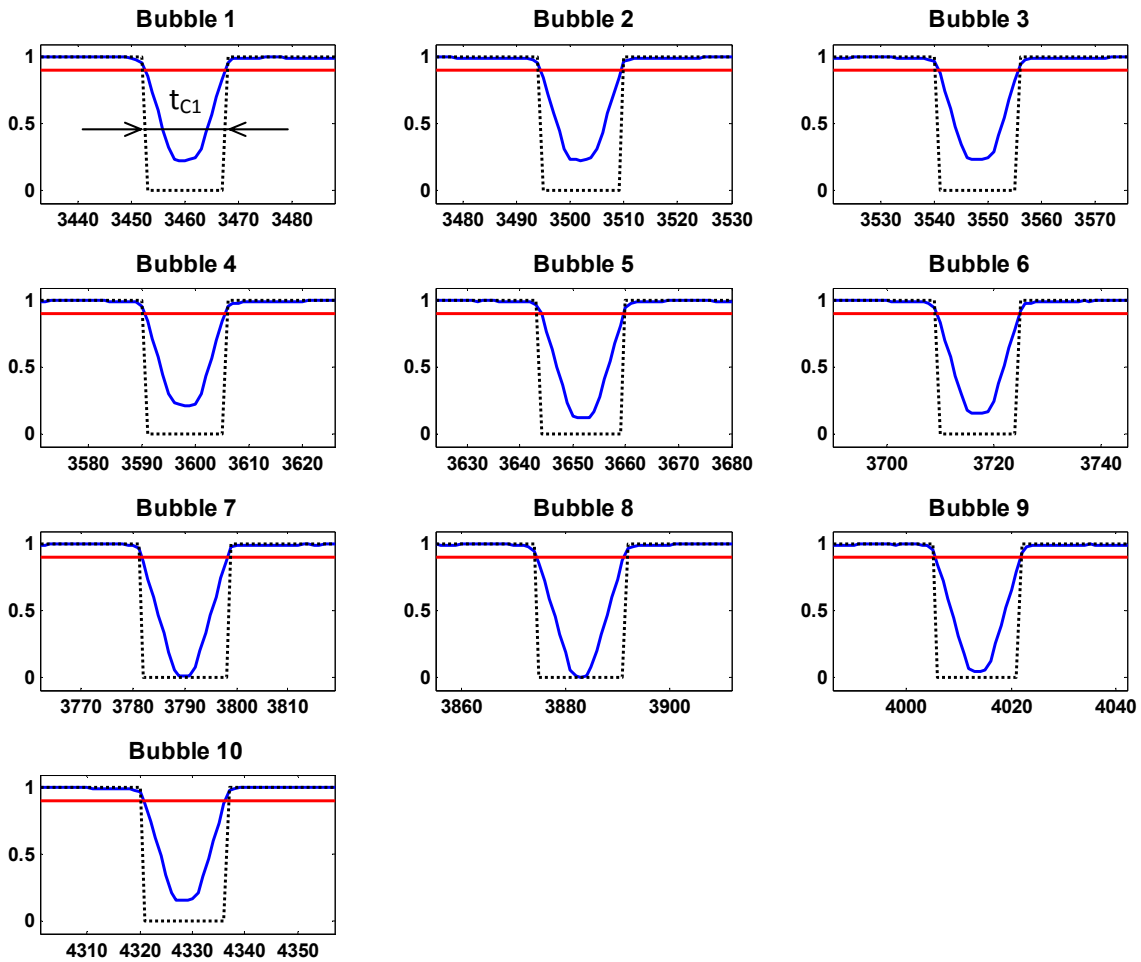


Figure 37: Zoom of the bubble interactions in Figure 36 (- threshold, -conductivity, -- reconstructed signal)

4 Test facilities

4.1 Laboratory reactor

One part of this work was to design and construct a multiple-impeller laboratory-scale reactor. The reactor and its dimensions are illustrated in Figure 38. It is a cylindrical tank reactor with flat bottom. Four baffles are located perpendicular inside the tank. The impellers are mounted on a shaft from the top. A ring air sparger is placed below the lowermost impeller. A cylindrical tank causes optical distortion in case of different mediums on the wall. The industrial handbook of mixing [16] suggests two solutions to allow undisturbed visual observations. In the first solution, the cylindrical reactor is placed inside a rectangular box as shown in Figure 39 (a). The reactor and the box are filled with the same liquid. The second solution is to apply a small box with a plane surface on the cylindrical reactor as shown in (b). The box is filled with the same liquid. Solution (a) was chosen, which allows us to investigate the flow from every direction.

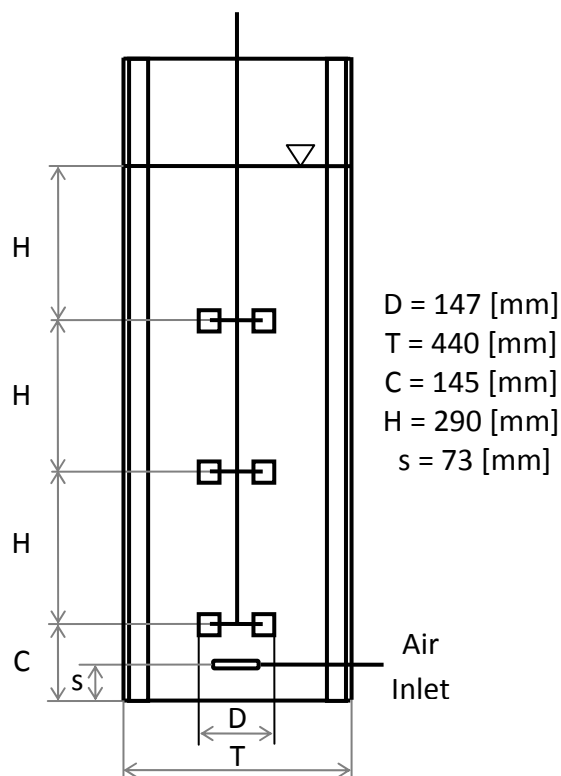


Figure 38: Illustration of the laboratory stirred reactor

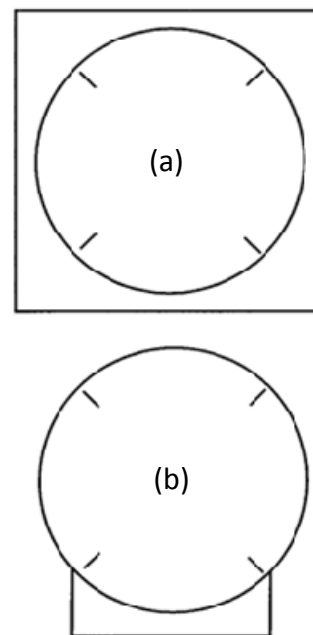


Figure 39: Visual observation in transparent vessels [16]

The design of the reactor has been performed with the commercial design tool ProEngineer Wildfire 5.0. Figure 40 show a photograph (left) and a three dimensional view (right) of the laboratory reactor with all main components. The Plexiglas reactor is placed on a pedestal to allow visual observations from the bottom. A mirror is located below the reactor, which enables us to investigate the reactor from the bottom. This makes it possible to see the cavities on the lower most impeller. The motor and shaft are mounted on the wall cage.

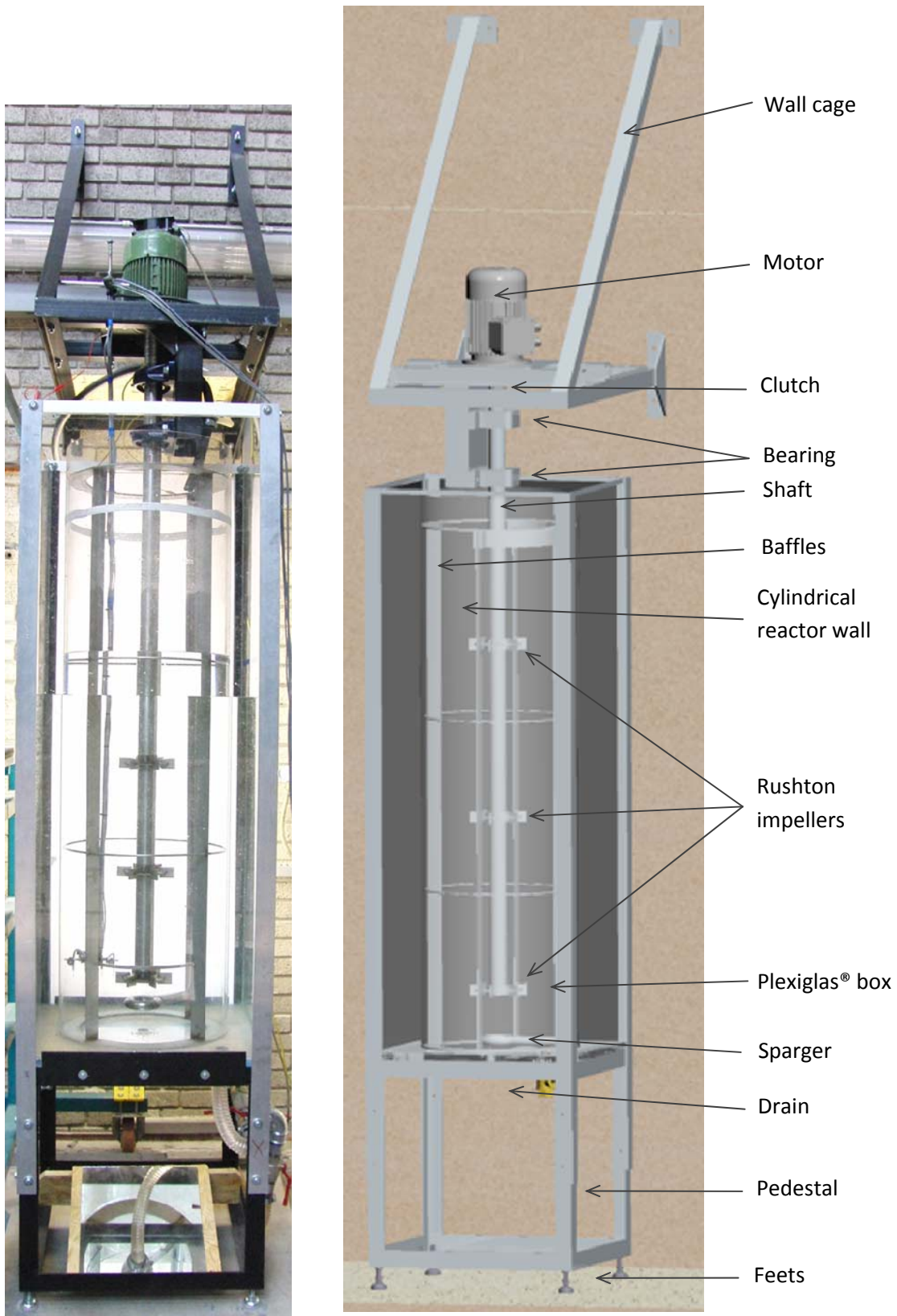


Figure 40: Photo and three dimensional view of the reactor in ProEngineer

A Rushton turbine has been chosen for the laboratory reactor. Figure 41 shows a photograph and a three dimensional illustration of the impeller. It is a disc turbine with 6 blades. The drawing of the Rushton impeller is in the appendix. Its main dimensions are summarized in Table 5.

Table 5: Impeller dimensions

Dimension	[mm]
Disc diameter	110
Blade height	30
Blade width	37
Outer blade diameter	147
Blade & disc thickness	5
Shaft diameter	50

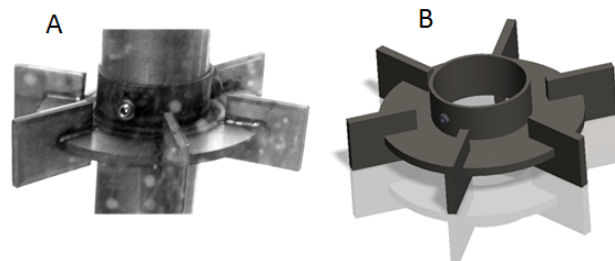


Figure 41: Photograph (A) and three dimensional ProEngineer illustration (B) of the Rushton turbine

A ring sparger was chosen for this work. A three dimensional view is shown in Figure 42. It has 36 holes with 2 [mm] diameter. The drawing of the sparger can be found in the appendix.

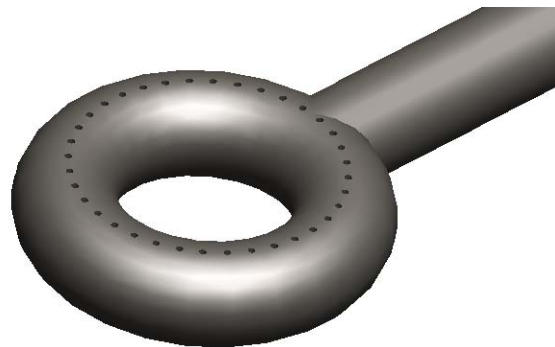


Figure 42: Three dimensional ProEngineer illustration of the ring sparger

A special probe holder for the developed conductivity needle probe has been designed. Figure 43 shows a photograph of the probe holder with four probes. The probes are tightened on a horizontal rail, which anon is tightened to a retainer. The retainer is guided on the baffles. The level of the horizontal rail and therewith the probe position can be adjusted from the top. Figure 44 shows the positions as it is used in the experiments. The measurement points are located on a line in the xy plane collateral to the x-axis in the middle of the reactor.

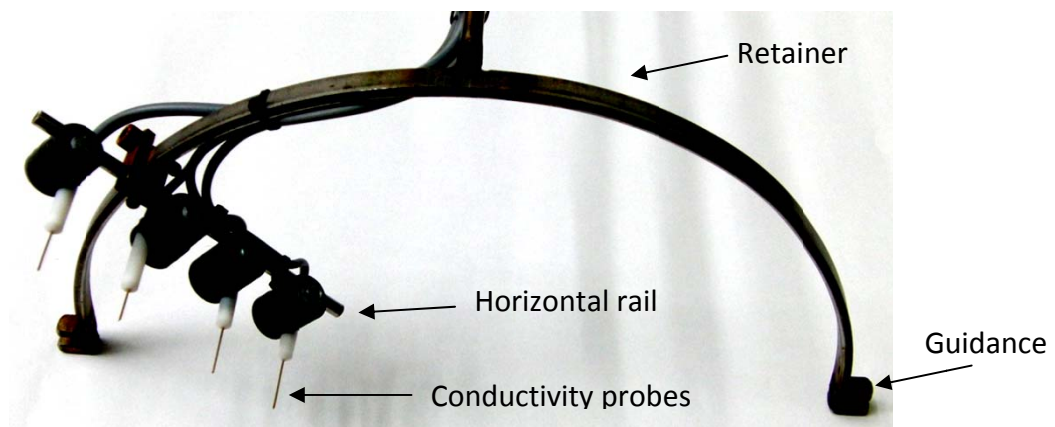


Figure 43: Photograph of the probe holder

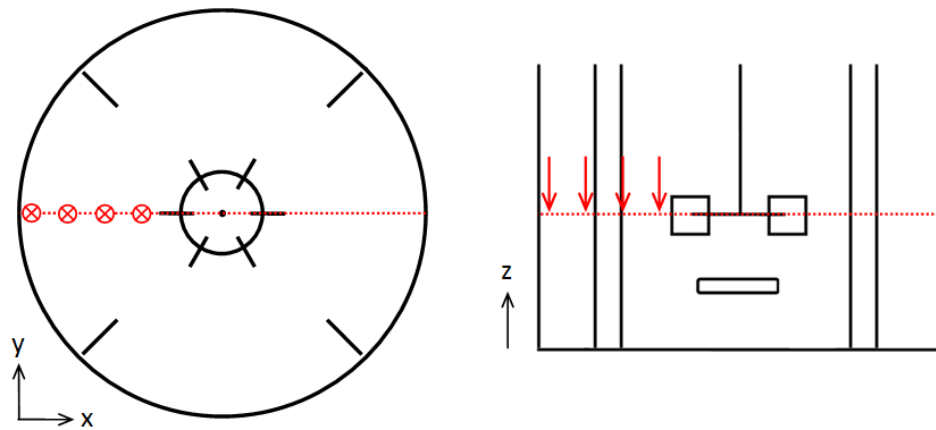


Figure 44: Illustration of the probe positions

The laboratory-scale reactor can be equipped with other impeller, sparger and baffles. Furthermore, the mediums can be varied within the chemical resistance range of Plexiglas®. This makes the reactor as multifunctional test equipment for gas liquid stirred reactors.

4.2 Bubble column – Becker case

The laboratory bubble column following the work of Becker et al. [24] was designed and assembled at the institute by Pucher [25]. The dimension of the bubble column is 1:2 scaled to the original Becker bubble column [24]. The bubble column is illustrated in figure 45. The bubble column has the dimensions of $D=81$ [mm], $W=250$ [mm] and $H=870$ [mm]. The air inlet is located eccentrically at the bottom. It was designed to produce bubble swarm with transient behavior, i.e. meandering from one side to another.

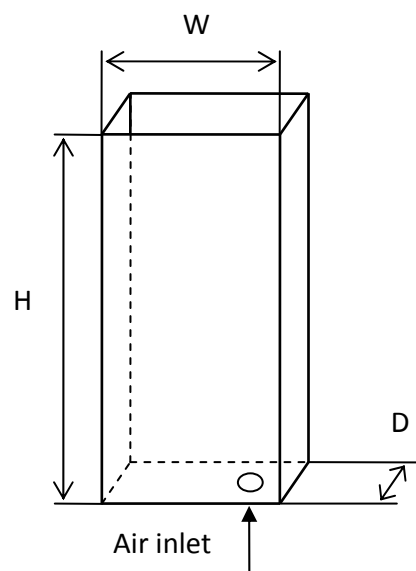


Figure 45: Illustration of the bubble column

5 Experimental work

Several gas hold-up experiments have been conducted. Gas hold-up profiles were measured in a bubble column and continuous stirred tank reactor. The results of the measurements are shown in the following to subchapters.

5.1 Bubble column experiments

The presented gas hold-up results of a Becker bubble column with an air water system are parts of previous work [21] [22]. The experiments were made to show the capability of the measurement system. The gas hold-up has been measured in three compartments of the bubble column along the grey dotted lines, as shown in Figure 46. The Data acquisition (DAQ) was performed with commercial available software called Labview®. The post processing algorithm was done with Microsoft Excel 2007. The algorithm did not normalize the conductivity curve or apply the correction factor, which lead to an uncertainty of the gas hold-up magnitude. However, the trends of the gas hold-up profiles show a good agreement with visual observation.

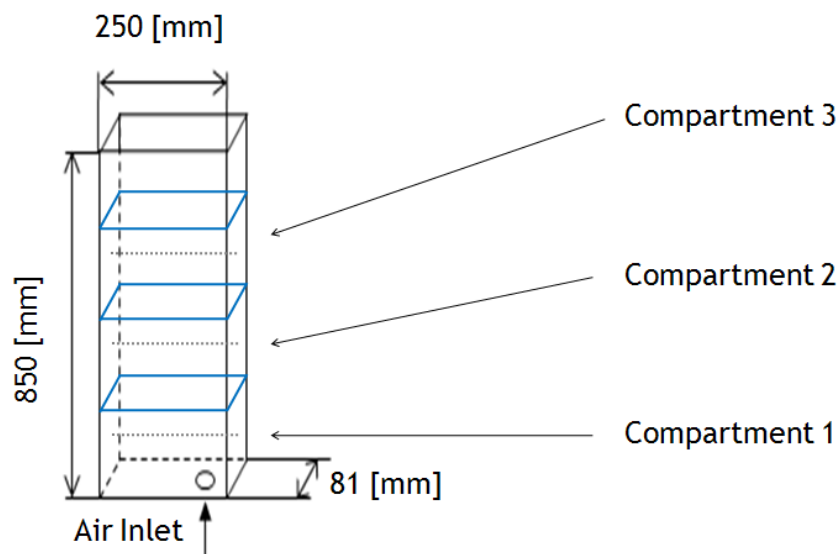


Figure 46: Compartment of the bubble column

Figure 47 shows snapshots of the bubble column and the measured gas hold-up profiles at three different gas flow rates. In (A) the gas flow rate of 1 [l/min] was applied. The bubbles are mainly located in the right side of the compartments. It can be observed that the bubble flow has inherent transient behavior as they are not moving upwards in a straight line, but meandering left and right within a small range. Similar behavior was observed in the work of Becker et al. [26]. In (B) a gas flow rate of 5 [l/min] is applied. The bubbles are mainly located in the right side of the column, but a liquid vortex induced by the bubble rise, carries some bubbles into the left side. This can also be seen in the measured gas hold-up profile. The result of the third experiment with 10 [l/min] is depicted in (C). The induced liquid vortex at this air flow rate is stronger and carries more bubbles to left side of the compartments. This can also be identified in the presented gas hold-up profile.

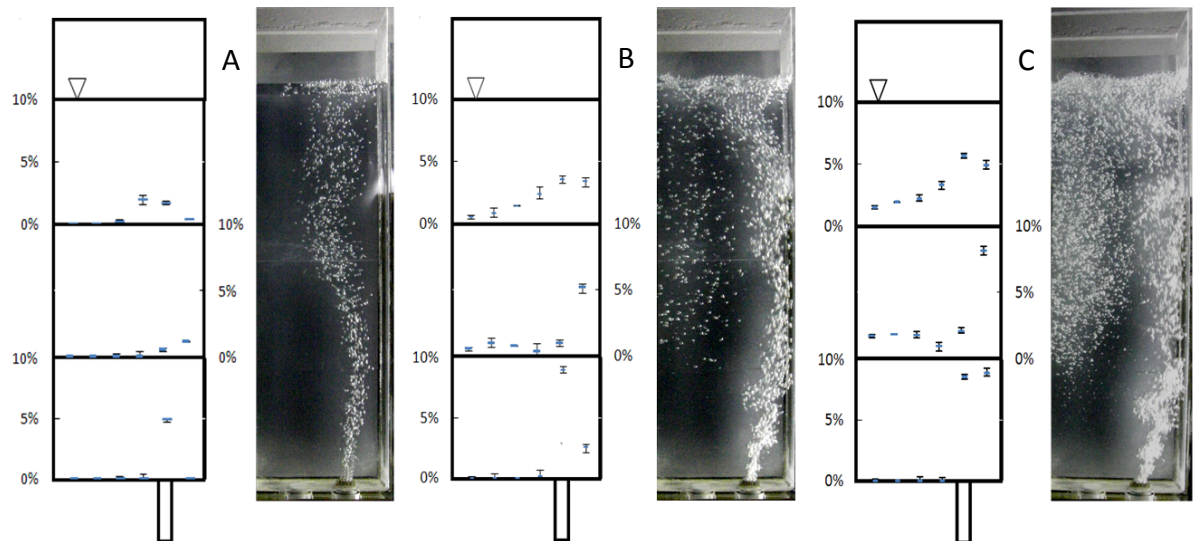


Figure 47: Summary of the snapshots and gas hold-up profiles obtained of the bubble column experiments at different air flow rates (A: 1 [l/min], B: 5 [l/min], C: 10 [l/min]) [22]

5.2 Laboratory stirred reactor experiments

The experiments were conducted with tap water and compressed air. The DAQ and analysis were performed with the developed Matlab® algorithm. The developed measurement system measures the conductivity locally. Thus, representative points within the reactor had to be chosen. A two dimensional plane between the baffles as illustrated in Figure 48 has been defined. This plane is divided into seven measurement levels, each containing 4 points. In total, the local gas hold-up is measured on 28 points within the reactor. The mixing time experiments were conducted at one point, namely at the closest probe in the jet of the lowermost impeller (L1.4). Furthermore, snapshots from the front of the reactor were taken at each experiment.

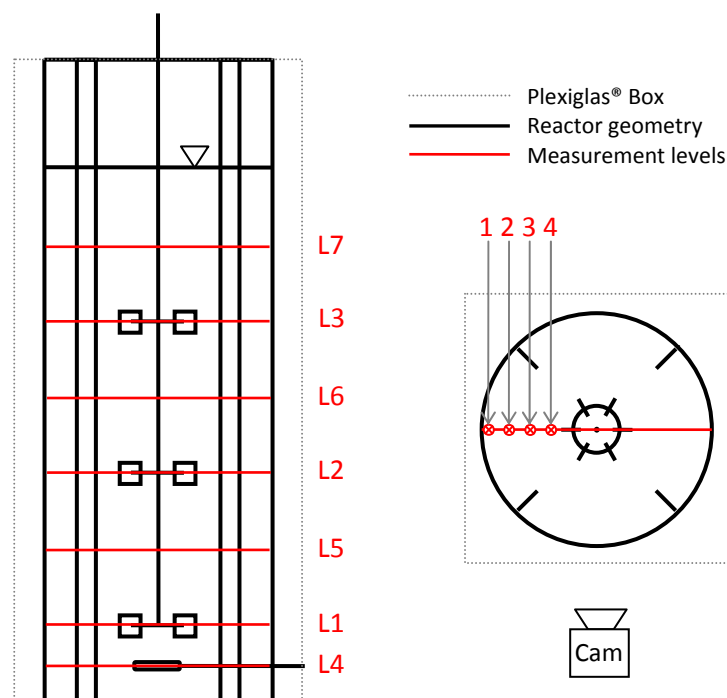


Figure 48: Illustration of the measurement levels

In addition, the volume increase caused by the dispersed phase has been recorded to gain values for the global gas hold-up. This method is only a rough approximation since it relies on visual observation of the liquid height of a fluctuating free surface. Another important parameter is the power consumption of a liquid stirred reactor. Thus, the current consumption of the electric motor has been recorded and hence the power consumption is calculated. It is compared between an aerated and un-aerated operating condition.

The experiments were performed for various conditions. The parameters were chosen based on the flow map in Figure 49. The flow map distinguishes between six flow regimes in aerated liquid stirred reactor (F1-F6). The flow regimes are explained in chapter 2.4 and the applied experimental parameters are shown in Table 6.

Table 6: Operating conditions of the experiments

Flow regime	Fr	Fl	N	N	f _B	\dot{G}	\dot{G}	U _s	vvm
	-	-	[min ⁻¹]	[rps]	[Hz]	[l/min]	[m ³ /h]	[cm/s]	[min ⁻¹]
F1	0.15	0.02	190	3.2	19	11.9	0.71	0.13	0.08
F2	0.8	0.02	440	7.3	44	27.4	1.64	0.30	0.18
F3	1.1	0.05	516	8.6	52	80.3	4.82	0.88	0.54
F4	0.15	0.05	190	3.2	19	29.6	1.78	0.32	0.20
F5	0.5	0.12	348	5.8	35	129.9	7.79	1.42	0.87
F6	0.15	0.5	190	3.2	19	296.4	17.78	3.25	1.98

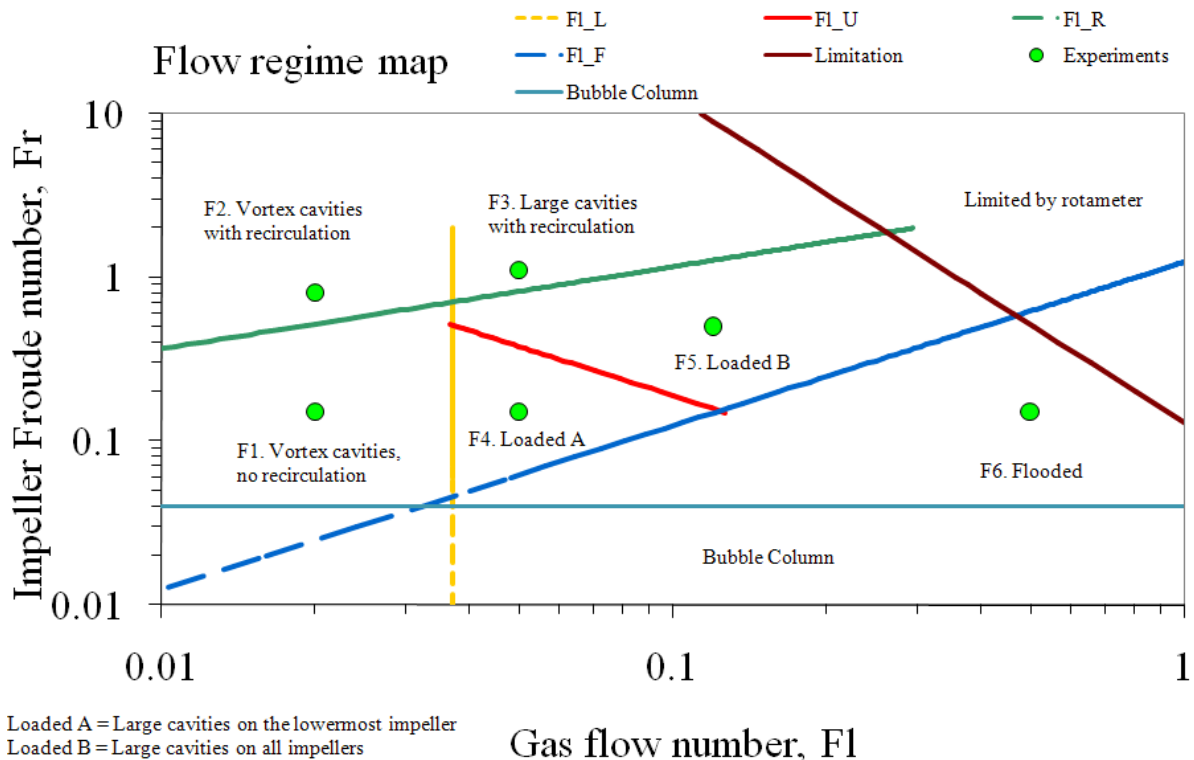


Figure 49: Flow map of the laboratory reactor [Internal report, R. Sungkorn]

5.2.1 Gas hold-up experiments

5.2.1.1 Post processing of the measured data

The measured conductivity has been recorded for 180 seconds for three times on every point. The measurement time was chosen to get a statistically representative result. The sampling rate of the conductivity curve was 1 [kHz]. One measurement file contains therewith 180,000 points. The gas hold-up is calculated with a post process algorithm in Matlab®. The work flow of the algorithm is illustrated in Figure 50. The first step is to load the recorded measurement file. The second step, removes a drift caused by possible temperature change during the experiment. Next, the script normalizes the conductivity curve to the average conductivity of the liquid phase and minimum measured conductivity, which represents a full contact with the dispersed phase. The local gas hold-up is calculated as a ratio between the cumulative time where the probe is contact with the dispersed phase and the measurement time. The threshold of 90% and a compensation factor of 2.4 are results from conducted verification (see chapter 3.7.). The last step is the visualization of the gas hold-up profiles. The developed Matlab® codes are in the appendix and on the appended volume.

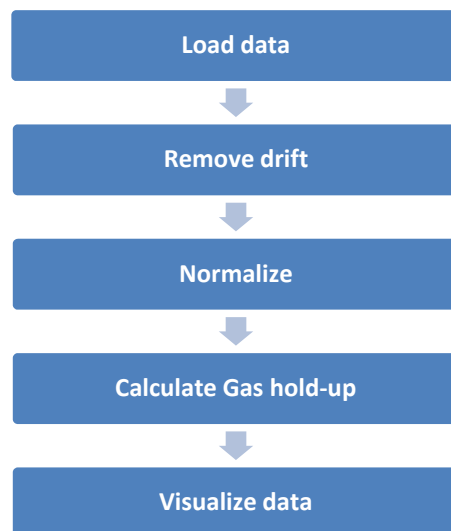


Figure 50: Work flow of the gas hold-up measurement post processing

5.2.1.2 Results

The measured gas hold-up profiles and images for every point in the flow map, as well as analysis of the measured conductivity signal are shown in Figure 51 - Figure 66. The basic meaning of the figures is explained in this paragraph. Detailed explanations of the results for each flow regime are in the next paragraphs. The Image (a) shows a snapshot of the unstirred reactor with the gas flow rate according to the flow map. Images (b) & (c) are snapshots of the stirred reactor at the operating condition according to the flow map. A comparison between a,b&c shows effect of the rotating impeller to the dispersed phase. Each impeller creates its own flow compartment. The white dotted lines show their borders. The white arrows illustrate the bubble flow path within the reactor. Illustration (d) shows a simplified sketch of the reactor geometry and the measured gas hold-up profiles (blue line). The measurement levels are illustrated as grey dotted lines and are coincidentally the zero axes for the profiles on each level. The scaling of the profiles is different from flow regime to flow regime in order to see the trend of the curve clearly. It is shown with a vector in the

right side of the illustration. Its length correspond with the space between the measurements levels L1-L5. Diagram 1 shows the measured conductivity curve (blue curve) and threshold level (red line) on radial closest position to the impeller over the measurement time. Diagram 2 shows the first five seconds and diagram 3 shows only the first second of the conductivity curve. Diagram 4 shows the reconstructed signal of diagram 3. Diagram 5 shows a histogram of the measured conductivity curve and diagram 6 the frequency spectrum obtained with the fast Fourier transform (fft) algorithm included in Matlab®. Furthermore, Table 7 shows a summary of the obtained results, e.g. gas hold-ups, power inputs, temperature and specific conductivity, which were recorded during the experiments.

Flow regime 1 (Figure 51) is called *vortex cavities and no recirculation*. This regime has a low gas flow number (0.02) and low Froude number (0.15). The snapshots show that the impeller is able to disperse the gas phase above the first impeller effectively. The dispersed phase follows mainly the lower loop of the Rushton impeller and the distinct compartments are homogeneously distributed. In addition, no recirculation of the dispersed phase has been recognized. The measured gas hold-up profile has the highest value with 6.7% at the closest probe on the first impeller level L1. The gas hold-up decreases with the distance from the impeller. The level below has just one point with contact with the dispersed phase. This is due to the influence of the sparger. The outermost measurement points gets in contact with some bubbles. The impeller develops a vortex in the bottom loop, which flow in a toroidal shape around the reactor. The profile at the second impeller level L2 has a similar shape and the highest value is close to the impeller. The profile on the third impeller level L3 shows a different trend. The closest point has the highest value but the second closest point has the lowest value this time. The profiles between the impellers show a similar trend with higher gas hold-up to the middle of the reactor. Whereas, the top level shows an opposite trend with the highest gas hold-up at wall of the reactor. The conductivity curve analysis of L1.4 shows that most of the cavity interactions cause just a partial signal drop, due to a small cavity size. The histogram shows a mono-modal shape. The frequency spectrum has a peak close at the blade frequency f_b , which corresponds with the results shown from Bombac [2] (see chapter 2.2). The conductivity curves of L2.4 and L3.4 show a similar trend but with less bubble interactions and therewith lower gas hold-ups. The averaged value of the gas hold-up profile (0.98%) has been compared to the global gas hold-up determined by visual observation and volume increase. The deviation between both methods was 3.7%. The power demand between the aerated and un-aerated operations shows no measurable reduction.

Flow regime 2 (Figure 54) is named *vortex cavities with recirculation*. This regime has the same gas flow number (0.02) as the previous regime, but a higher Froude number (0.8). The snapshots show that the impellers are able to disperse the gas flow effectively. The bubble follow now both loops of the Rushton turbines and it comes to recirculation of the dispersed on the loops above the first impeller level. The flow disturbance of the sparger impedes the recirculation in the bottom loop of the first impeller. The borders of the observed compartment are lower than in the previous regime (see white dotted line). The profiles are

scaled to 10 % and the measured profiles on the impeller levels are similar to the previous, except for higher magnitude. The highest value is at L1.4 with 8.9 %. The profile on L4 has higher magnitude compared to the previous one. The vortex in the bottom half is stronger due to the higher Froude number. It carries more bubbles in the bottom half. The profiles between the impeller have a different trend. The highest gas hold-up is now close to the reactor wall. This can be explained by the earlier mentioned compartment shift, which causes the probe to be inside the bottom loop. The top level shows also a trend with higher gas hold-ups in the wall regions. The conductivity analysis shows that most of the cavities cause just a partial signal drops, this is due to cavity size and impeller velocity. The histogram shows a mono-modal distribution. The frequency spectrum shows a significant peak at 35 [Hz]. The conductivity analyses of L2.4 and L3.4 show similar results. The blade frequency is 44 [Hz]. This result is not a match with data from Bombac et al., we assume that our probe was not close enough to obtain the correct frequency. The comparison of the global gas hold-up shows again good agreement (4.4% deviation). A reduction in power demand caused by the dispersed phase was measured with 17%.

Flow regime 3 (Figure 57) is termed as *large cavities with recirculation*. In this regime the reactor operates at high Froude number (1.1) and moderate gas flow number (0.05). The snapshots show that the impeller is able to disperse the gas phase within the reactor above the first impeller level. Recirculation takes place on the second and third impeller and also on the upper half of the first impeller. It can be seen that a detailed visual observation is limited to systems with low gas hold-up. The distinct compartments are shifted again (see white dotted line). The gas hold-up profiles are now scaled to 30%. The highest gas hold-up is again at L1.4 with 26%. The profile L4 shows the highest gas hold-up values within the conducted experiments. L4.1 has 2.8% and L4.2 has 0.6% gas hold-up the other point on this level are zero. The levels L5, L6, L7 show a homogeneous gas hold-up distribution. The conductivity curve analysis of L1.4 shows that almost every cavity results in a full signal drop. The histogram of the curve shows a bimodal distribution. The small peak on the left hand side represents the dispersed phase and the tall peak at the right hand side the continuous phase. The analyses of the conductivity curves L2.4 and L3.4 show a different cavity interaction with the probe. The curves show mainly partial signal drops, this can be due to smaller cavities. The reconstructed signal shows a similar recurring pattern for every impeller. This pattern can be identified with the frequency transformation. The spectrum shows peaks at multiples of 20 [Hz]. The curve resembles to the frequency spectrum Bombac et al. found for large cavities on every blade [2]. The blade frequency $f_B=52$ [Hz] does not match with the frequency spectrum in this case. The comparison of the global gas hold-up shows a deviation of approximately 25%. The power demand of the aerated reactor in this flow regime was reduced by almost 30%.

Flow Regime 4 (Figure 60) is called *loaded with large cavities on the lower most impeller*. This regime operates at low Froude number (0.15) and moderate flow number (0.05). The snapshots show that the impellers are able to disperse the gas phase above the first impeller within the reactor. The distinct compartments are distributed homogeneous in between the impellers. The highest local gas hold-up with 12.4% is at L1.4 again. The profile on L4 is

almost zero. A few bubbles are carried with a toroidal shaped vortex around the reactor. Thus, the dispersion of the first impeller is not effective in the bottom loop. The measurement levels between the impellers (L5 and L6) show a trend to higher gas hold-ups in the middle of the profile. Whereas, the profile on L7 shows a trend to higher gas hold-up at the reactor wall. The conductivity curve analysis of L1.4 shows that the cavities cause partially full signal drops and partial signal drops. The frequency spectrum shows peaks at 19 and 30 [Hz]. The analyses of the L2.4 and L3.4 show a different trend. Just a small amount of the bubble interactions, compared to L1.4, were recorded. The frequency spectrum shows peaks at 19 and 40 [Hz]. The peaks at 19 [Hz] in this case match with the blade frequency f_b . The different shape of the frequency spectrum indicates a different cavity regime on the first impeller compared to the second and third impeller. The comparison of the global gas hold-up shows a good agreement with a deviation of 4.23%. The power demand showed no measurable reduction.

Flow regime 5 (Figure 63) is termed *loaded with large cavities on all impellers*. The reactor operates at moderate Froude number (0.5) and higher flow number (0.12). The snapshots show that the impellers can disperse the gas phase above the first impeller effectively. Recirculation occurs on every impeller, with the exception of the lower half of the first impeller. The gas hold-up profiles are scaled to 30 [%]. The highest gas hold-up with 21.8% is again at L1.4. The profile shows a turning point on L1.2 and a trend to higher gas hold-up at L1.1. The shape of the L2 is similar, but with different magnitudes. L4 shows good agreement with the visual observations, that just a few bubbles are located in the bottom loop of the first impeller. They are mainly located close to the reactor wall. The profiles between the impellers show a trend to higher gas hold-up to the center of the reactor. On L7 the same trend has been observed. The conductivity analysis of L1.4 shows that almost every cavity causes a full signal drop. The conductivity curves on L2.4 and L3.4 show that the cavities cause mainly partial signal drops. The comparison of the reconstructed curves of L1 to L3 shows a similar recurring pattern. The frequency spectrums show peaks at multiplies of 17.5 [Hz] in each case. This indicates that the impellers operate in same cavity regime. The comparison of the global gas hold-up shows a deviation of 30.03%. This is due to the fact that the visual observation of a fluctuating surface is just a rough approximation. The aerated power demand of the operation condition was reduced by 23%.

Flow regime 6 (Figure 66) is called *flooding*. The reactor operates at high flow number (0.5) and low Froude number (0.15). The snapshots show that the impellers have almost no influence on the dispersed phase. The impellers are flooded and the reactor behaves like a bubble column. The liquid flow field develops one big loop in the reactor. This phenomenon has also been reported in literature by Shewale [6]. The superficial velocity $v_G=3.25$ [cm/s] is now in the heterogeneous regime and the bubble size shows a heterogeneous distribution as reported from Gezork [17]. The highest gas hold-up was at L3.1 with 9.3%. No bubbles are located below the first impeller. The points 1-3 have gas hold-up values of zero on the first impeller level, which indicates, that the first impeller is not able to disperse any bubbles. The bubbles are dispersed from its fluctuation due to shape instability, lift force, collision between each other and liquid flow with the height. This effect can be seen clearly in the gas

hold-up profiles. In the upper part of the reactor many bubbles are carried with the liquid vortex. The conductivity analysis shows a minuscule peak at 19 [Hz] on every impeller, which complies with the blade frequency f_B . The global gas hold-up has been compared and shows a large deviation 86% between both methods. The high gas flow and the flow pattern of the bubble column lead to a strong fluctuating free surface. Thus, the result of the visual observed gas hold-up cannot be taken as a representative value for the global gas hold-up.

Flow regime 1: Vortex cavities no recirculation

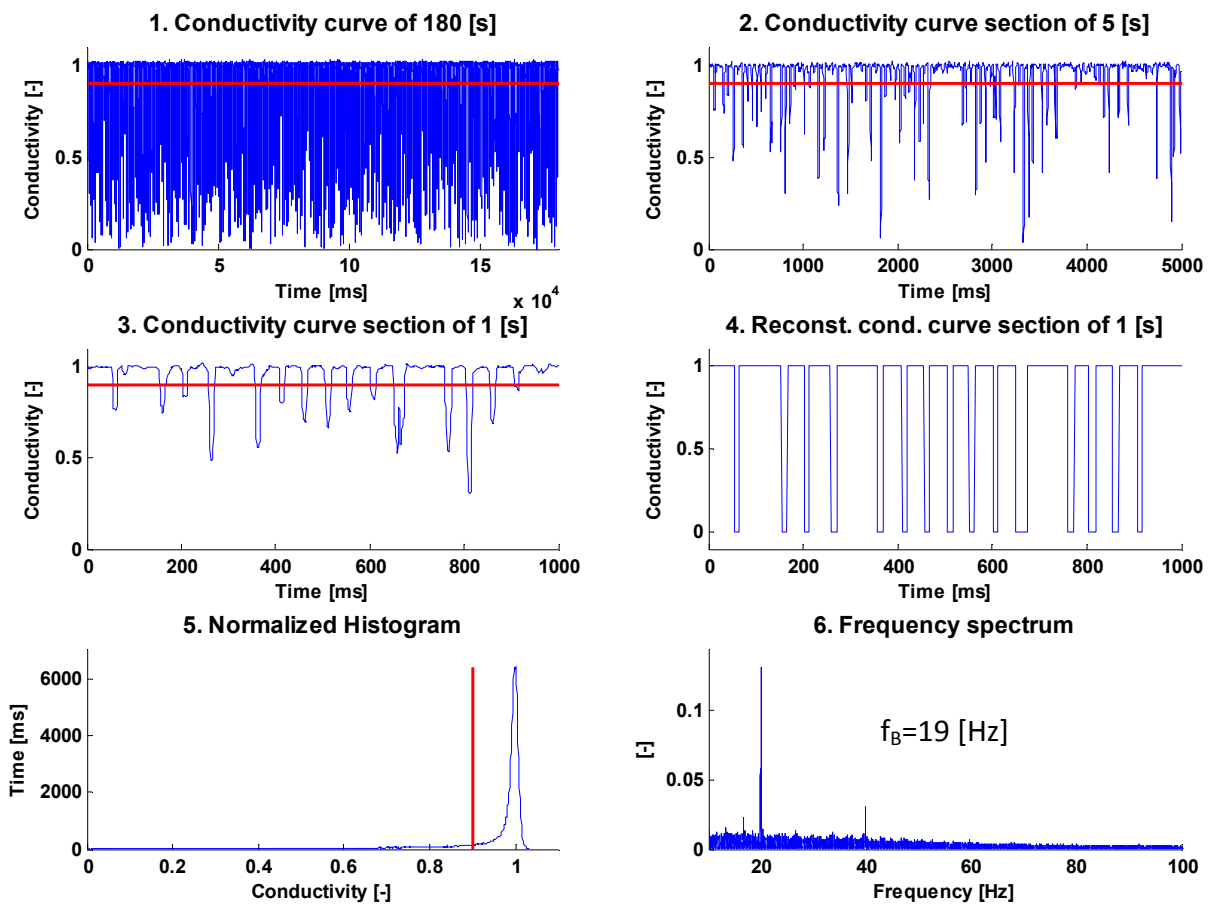
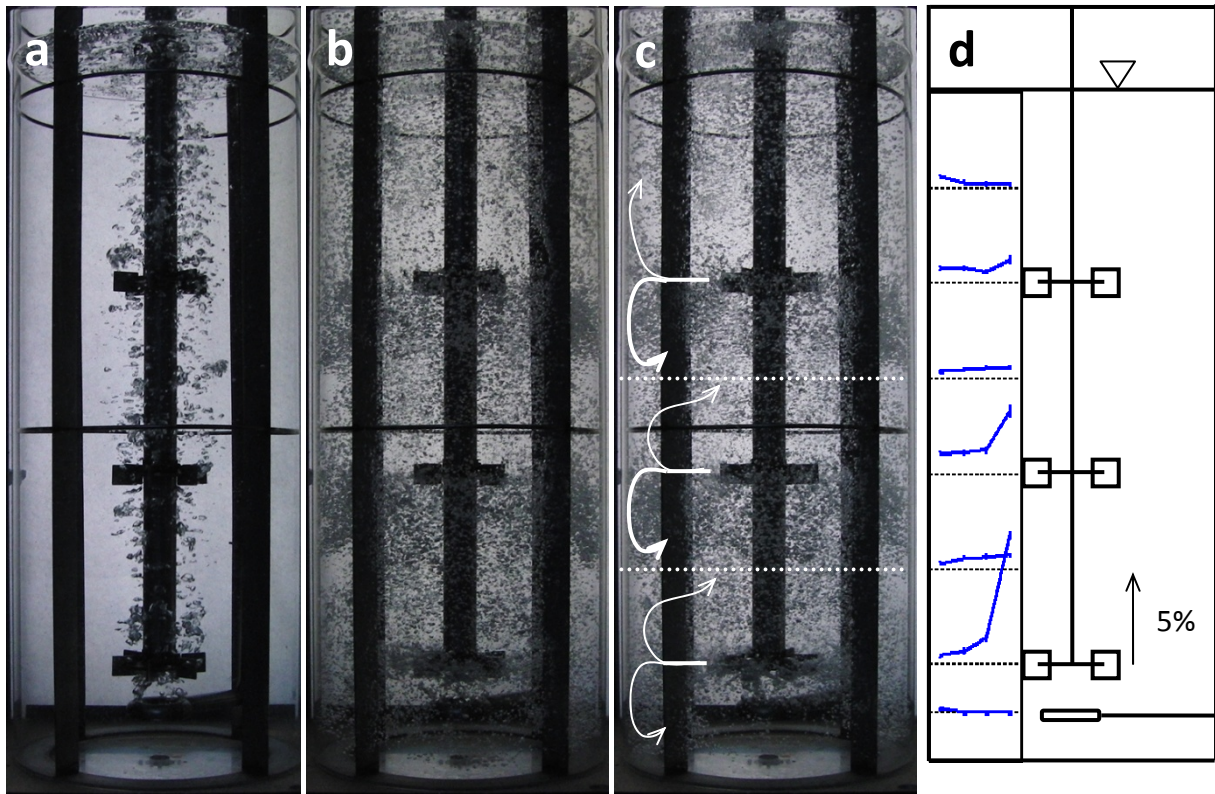


Figure 51: (F1) Snapshots and gas hold-up profile of the reactor & conductivity curve analysis at L1.4

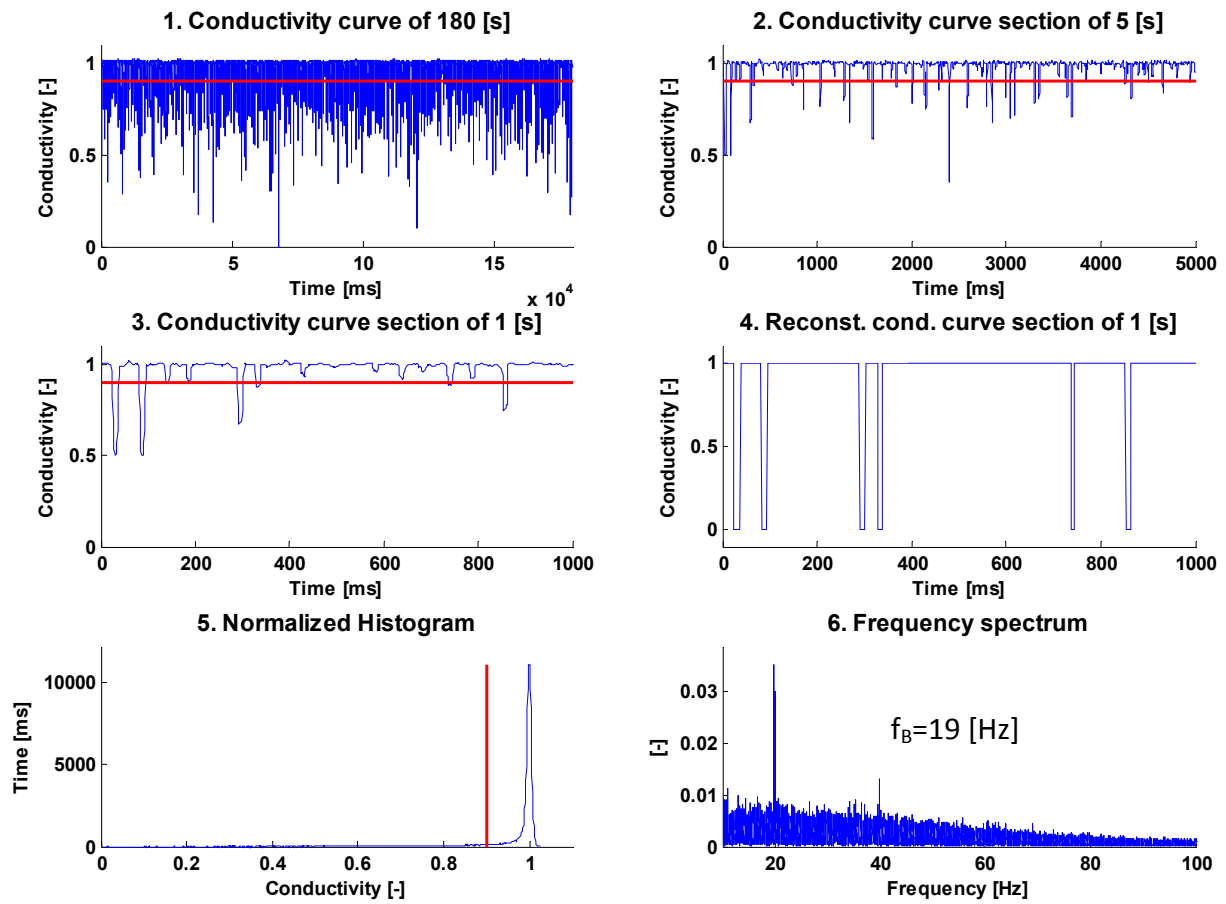


Figure 52: (F1) Conductivity curve analysis at L2.4

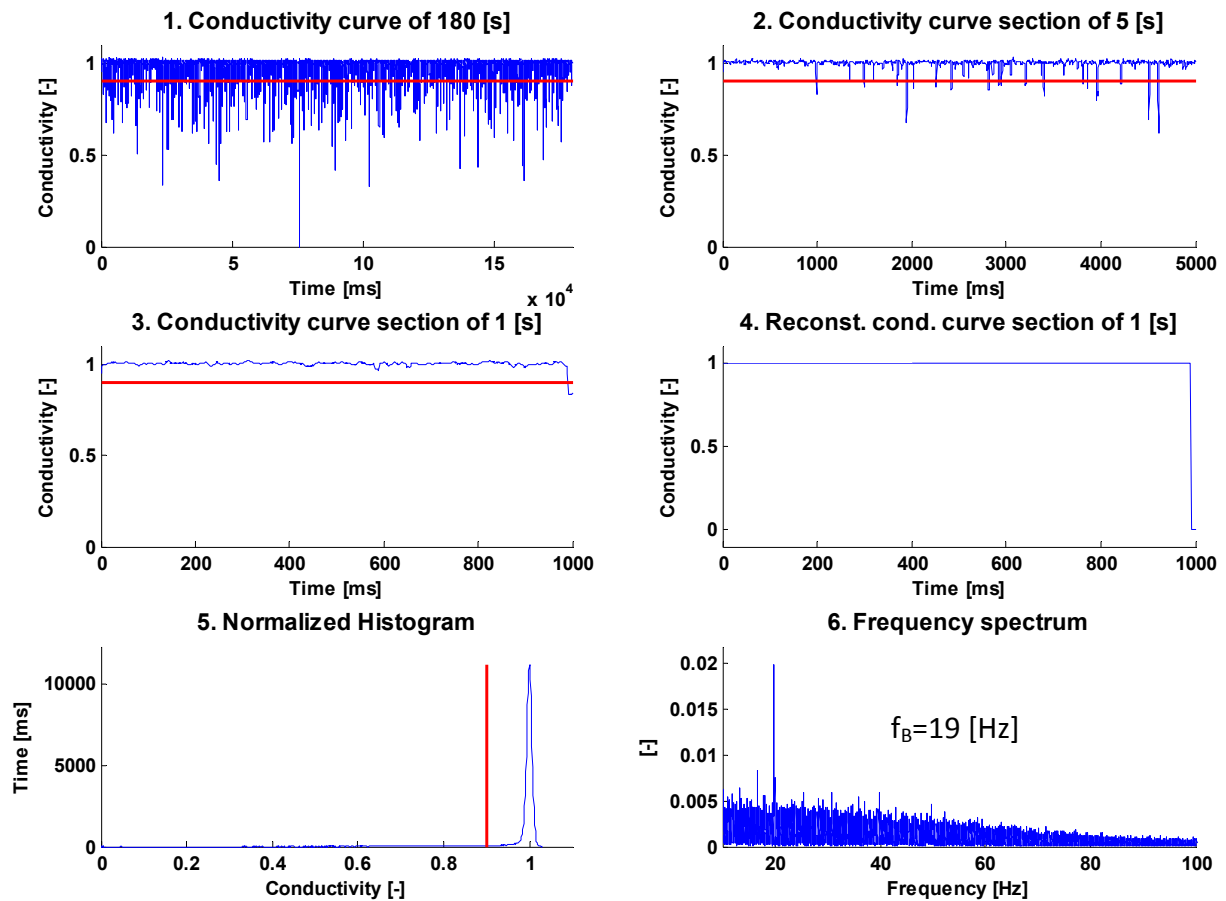


Figure 53: (F1) Conductivity curve analysis at L3.4

Flow regime 2: Vortex cavities with recirculation

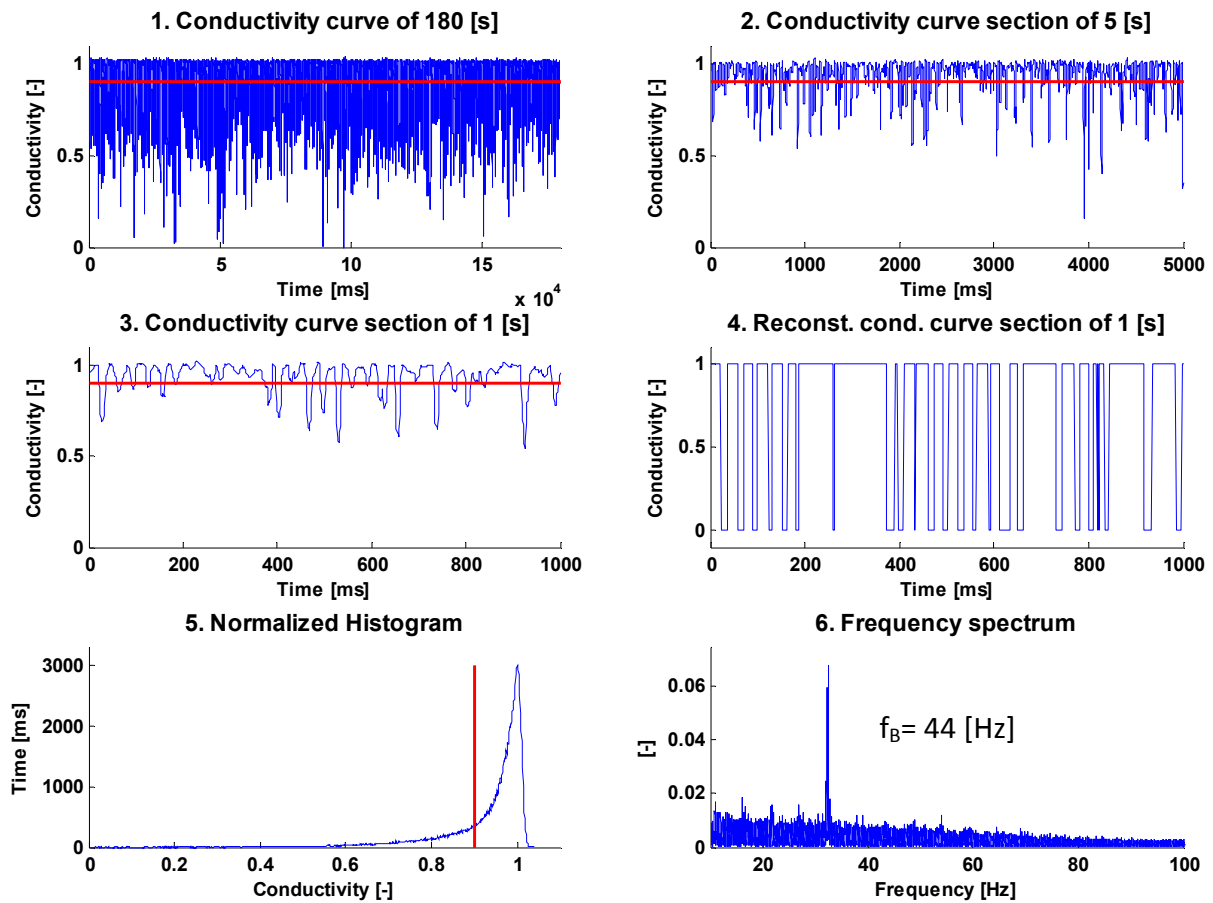
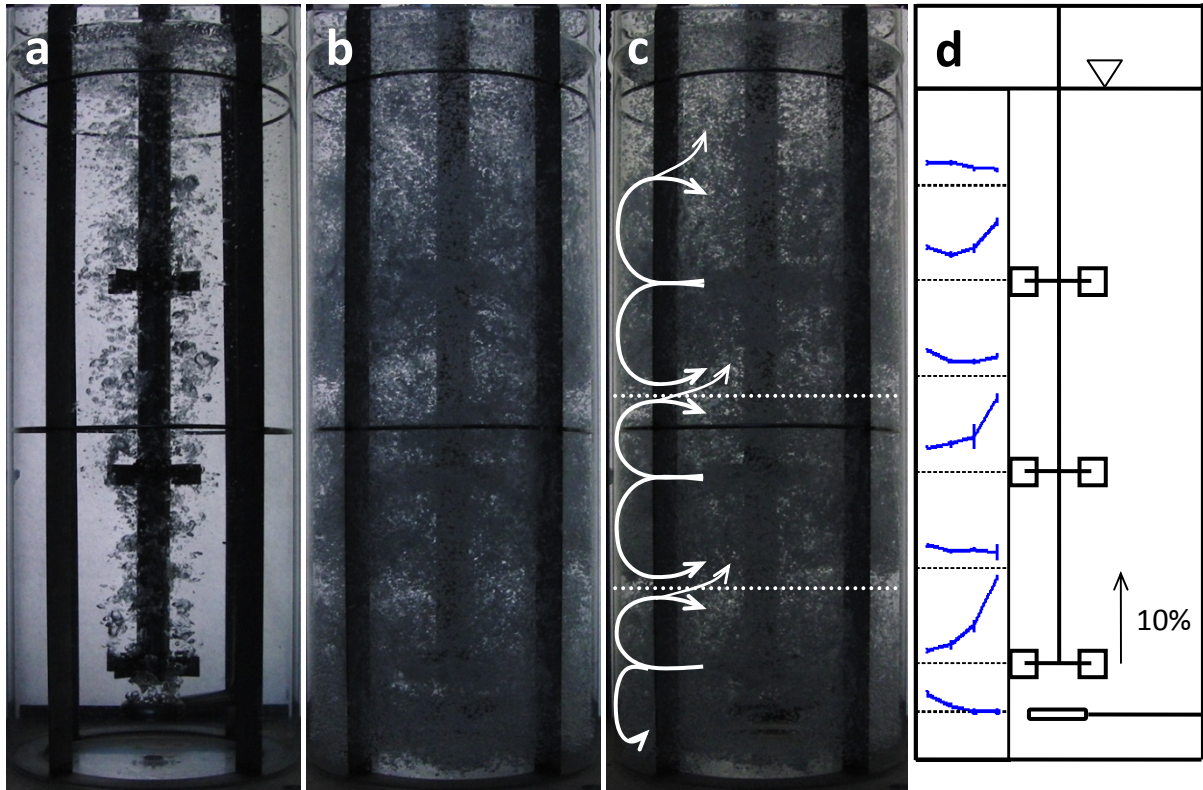


Figure 54: (F2) Snapshots and gas hold-up profile of the reactor & conductivity curve analysis at L1.4

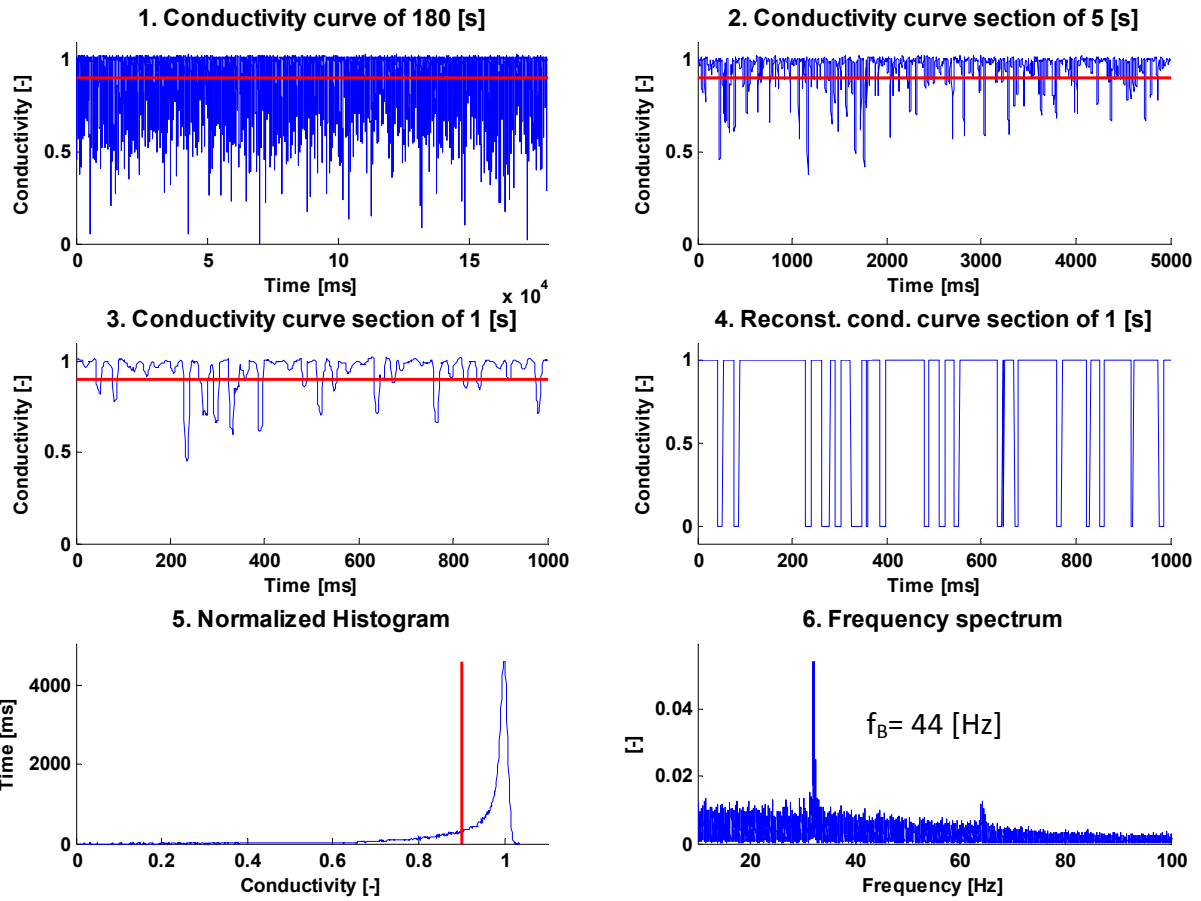


Figure 55: (F2) Conductivity curve analysis at L3.4

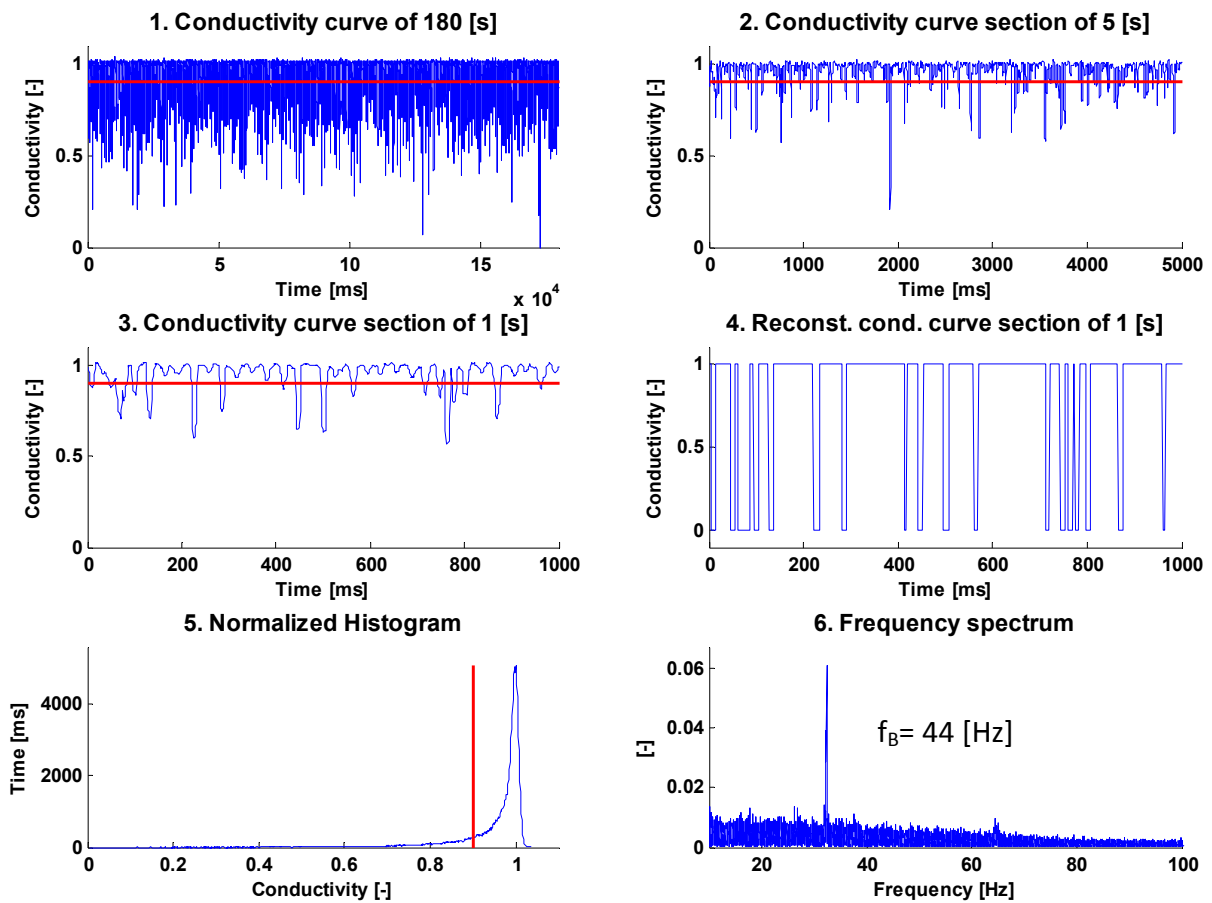


Figure 56: (F2) Conductivity curve analysis at L3.4

Flow regime 3: Large cavities with recirculation

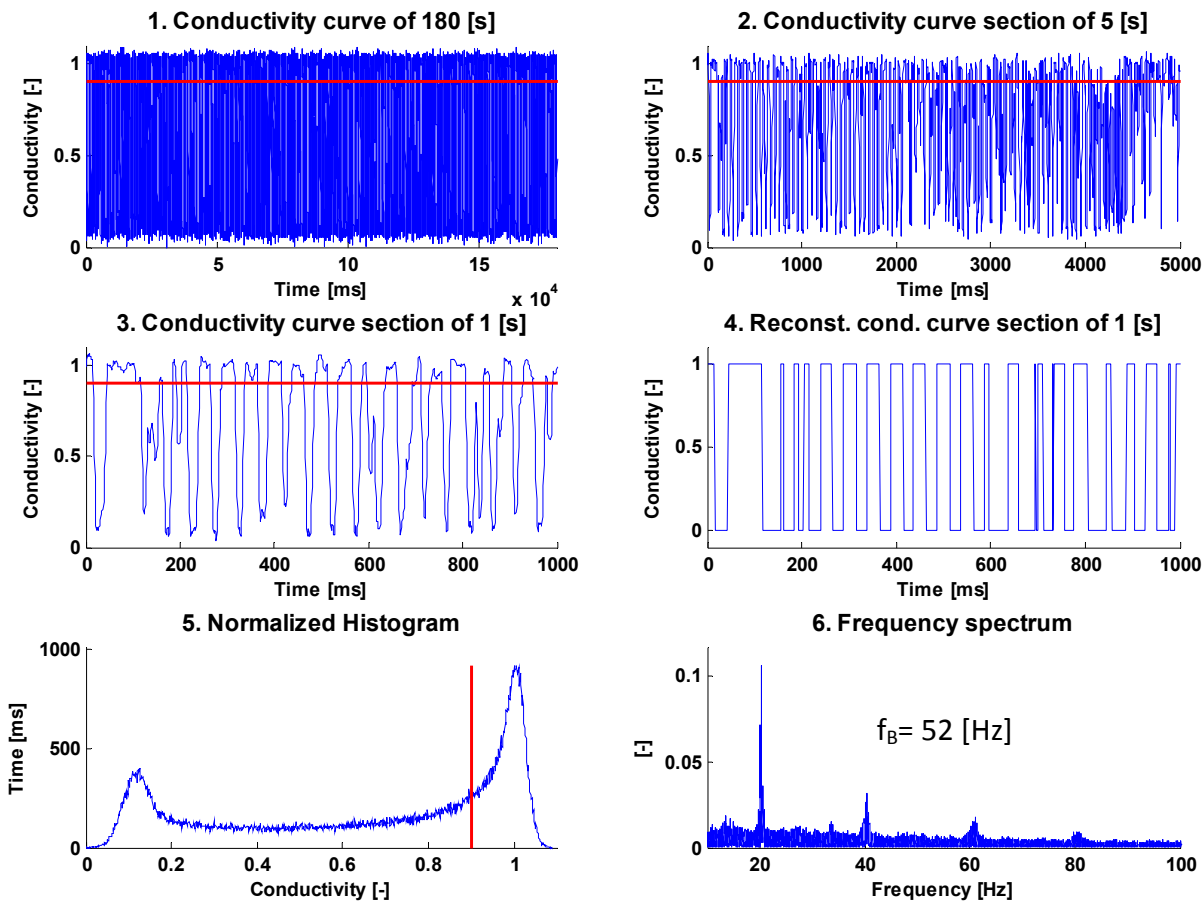
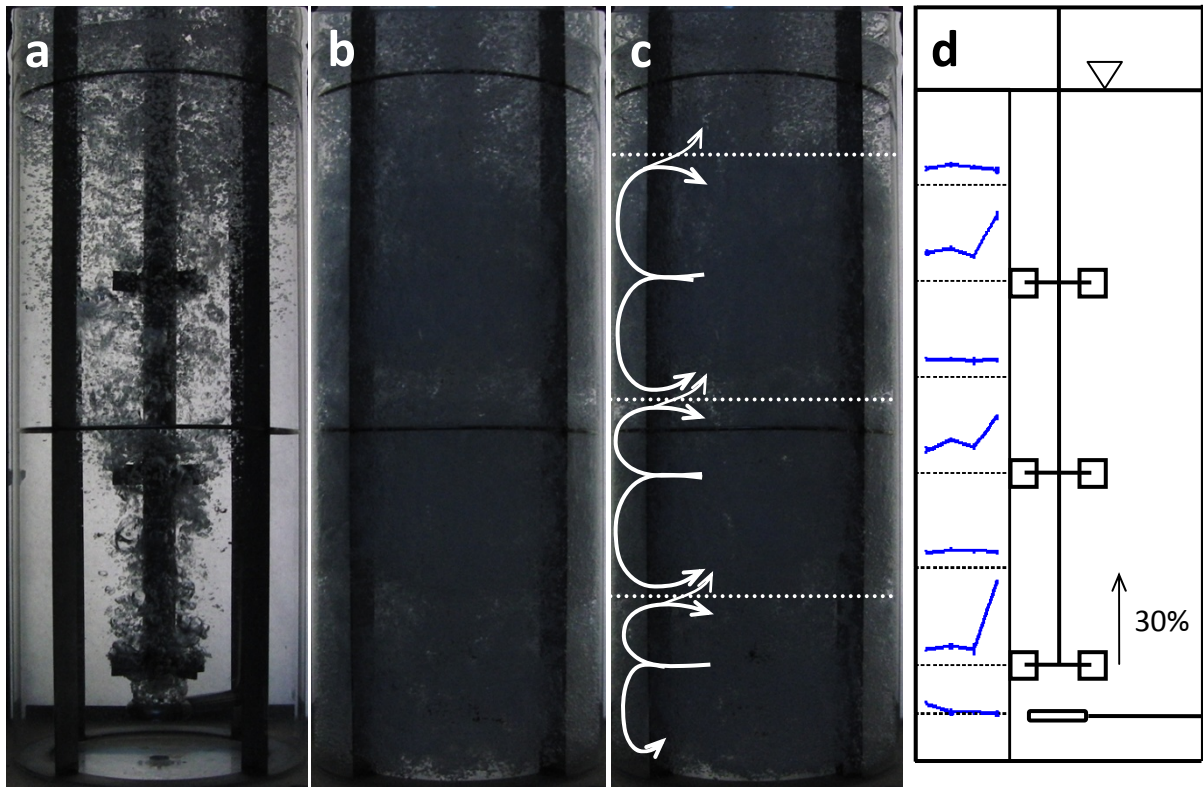


Figure 57: (F3) Snapshots and gas hold-up profile of the reactor & conductivity curve analysis at L1.4

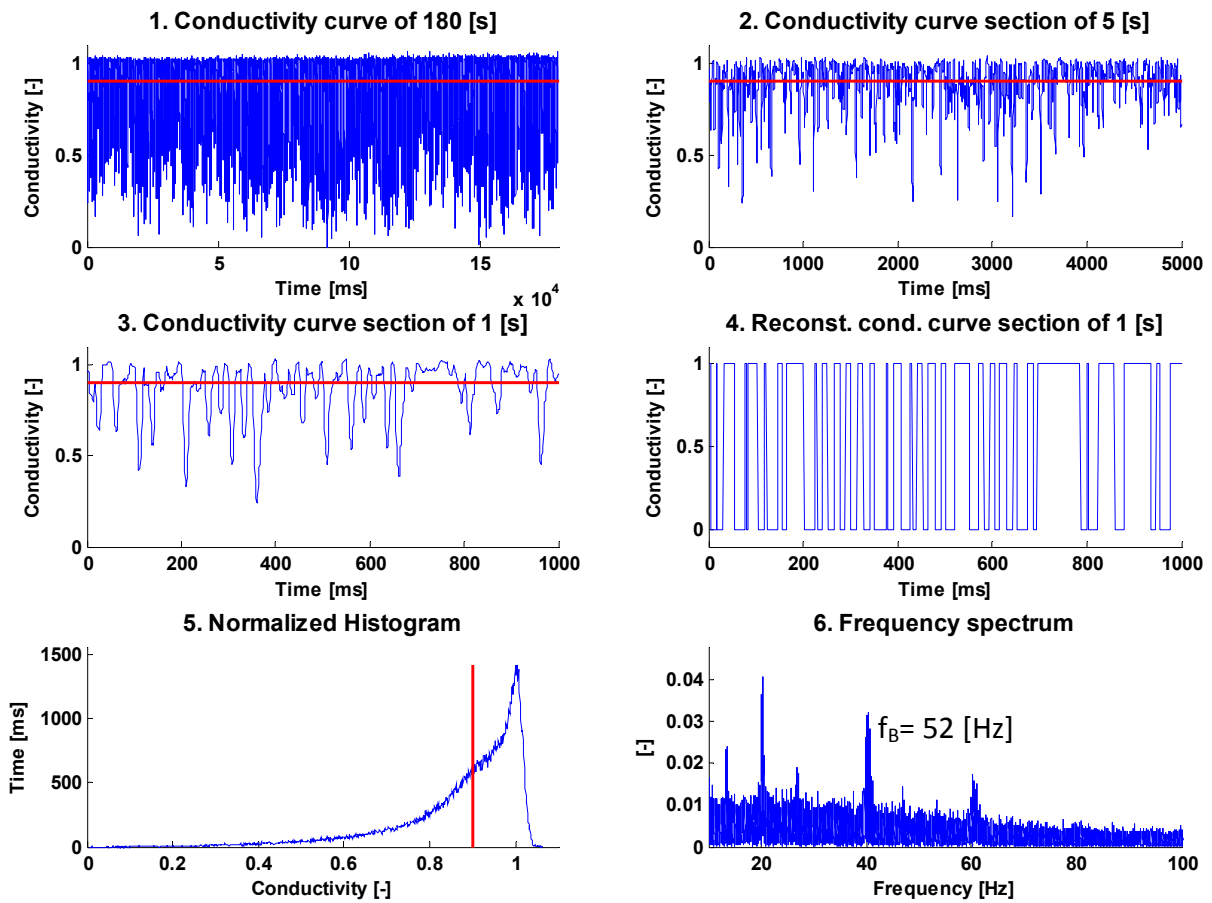


Figure 58: (F3) Conductivity curve analysis at L2.4

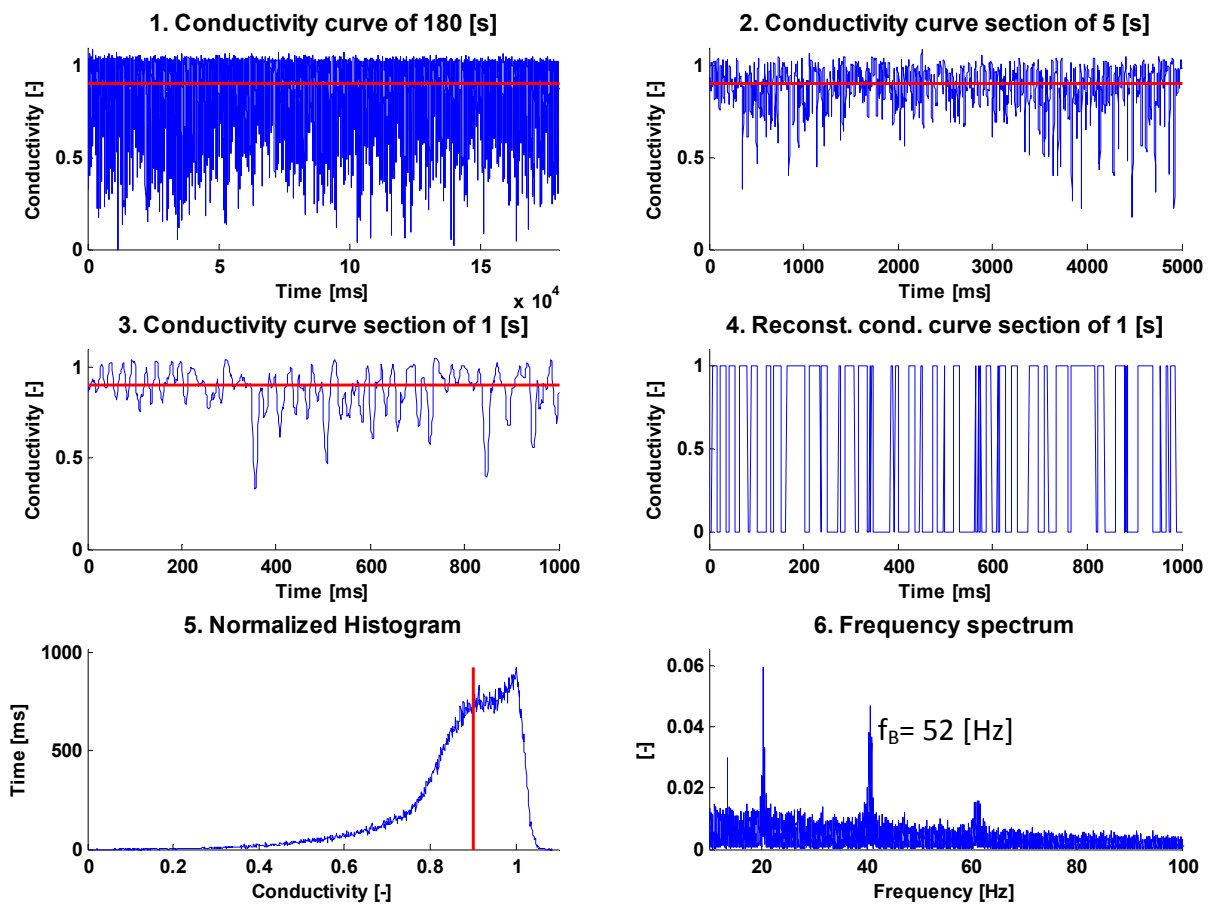


Figure 59: (F3) Conductivity curve analysis at L3.4

Flow regime 4: Loaded with large cavities on the lowermost impeller

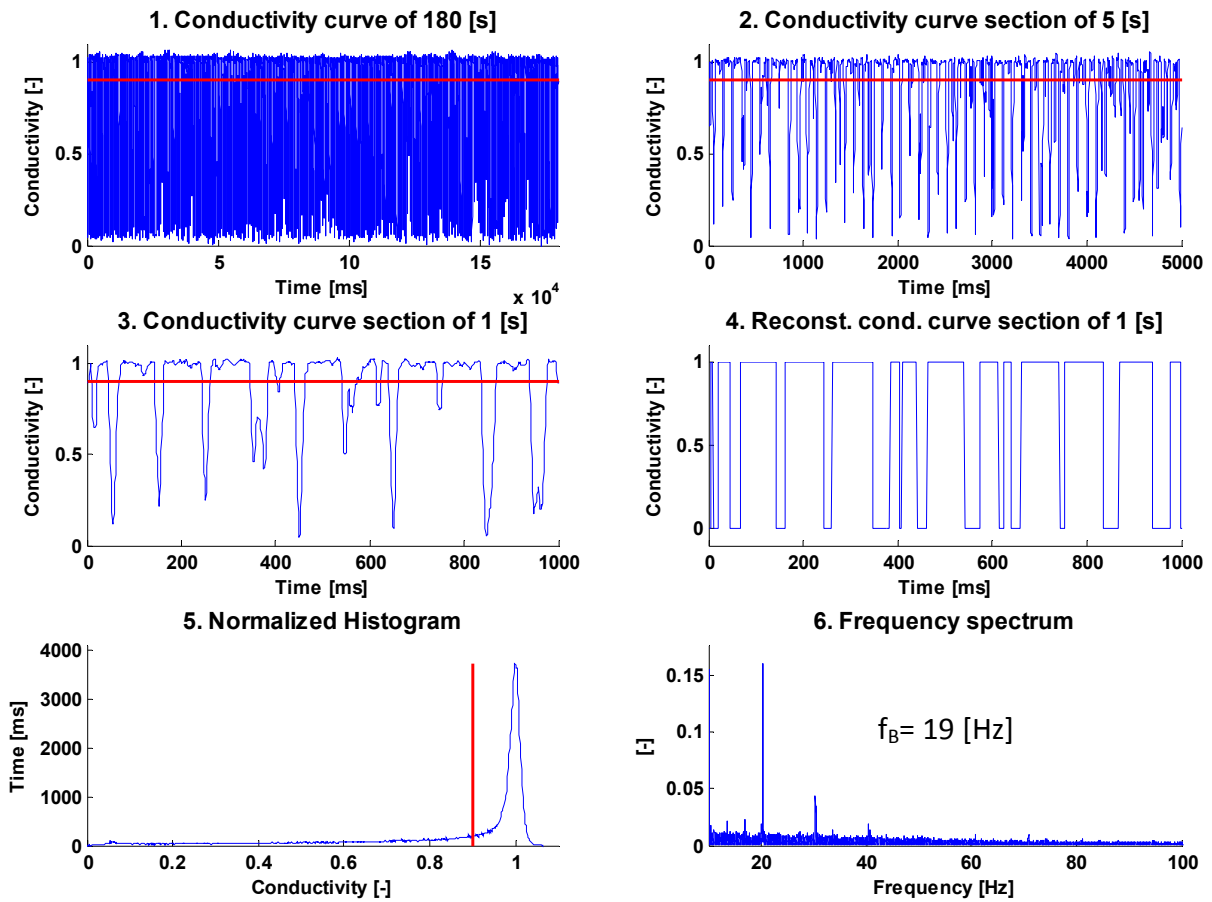
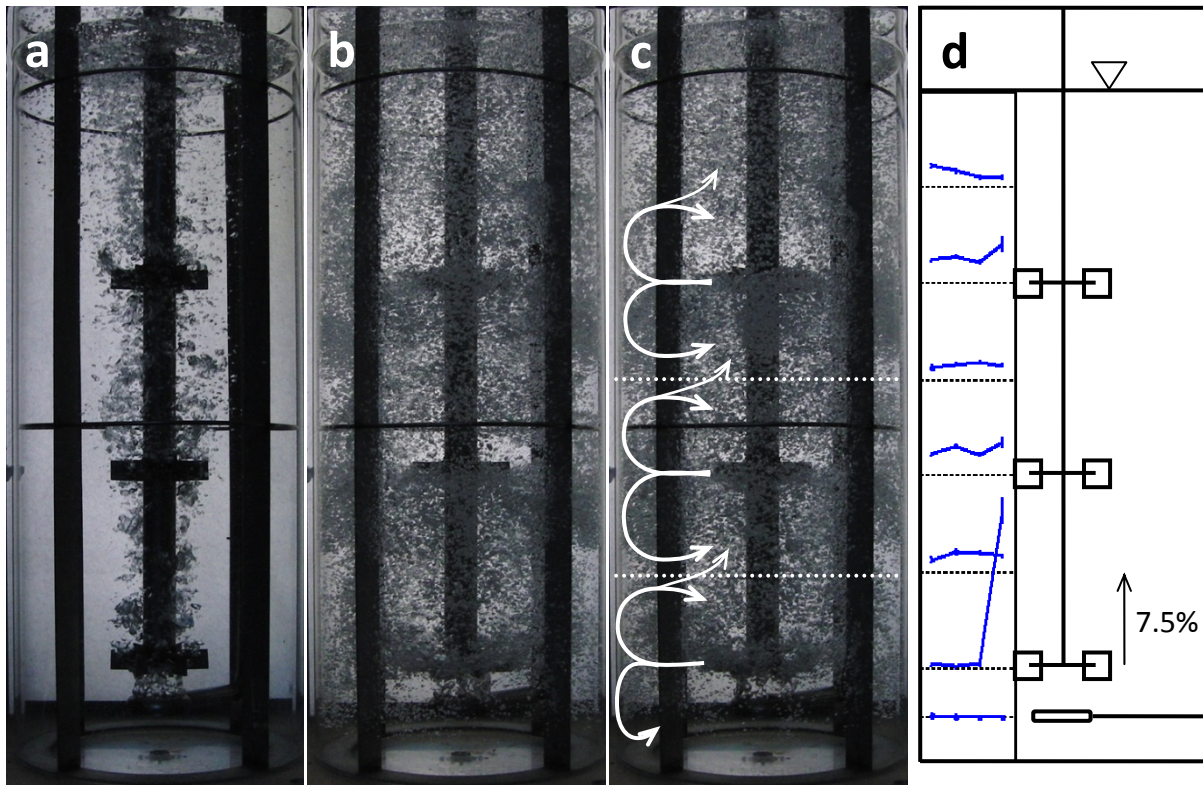


Figure 60: (F4) Snapshots and gas hold-up profile of the reactor & conductivity curve analysis at L1.4

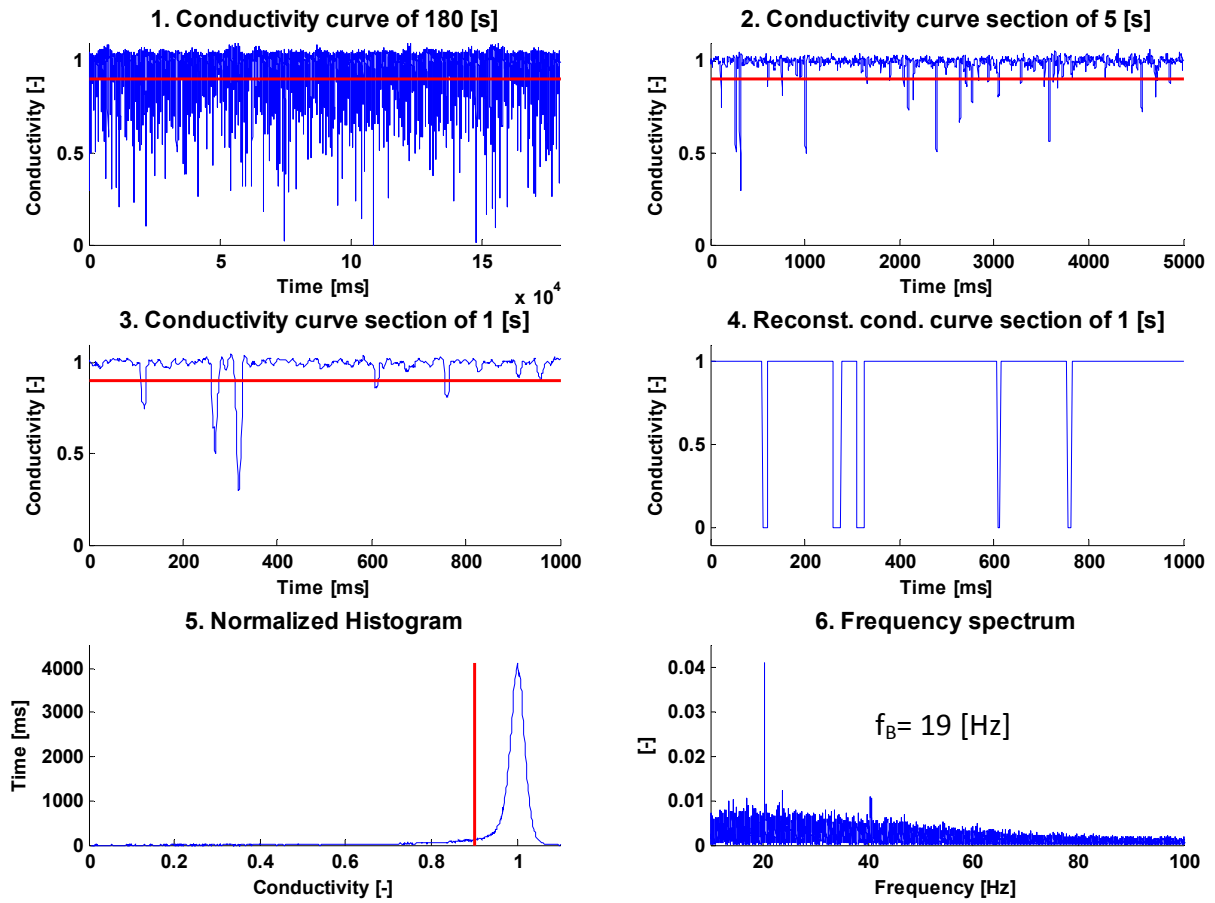


Figure 61: (F4) Conductivity curve analysis at L2.4

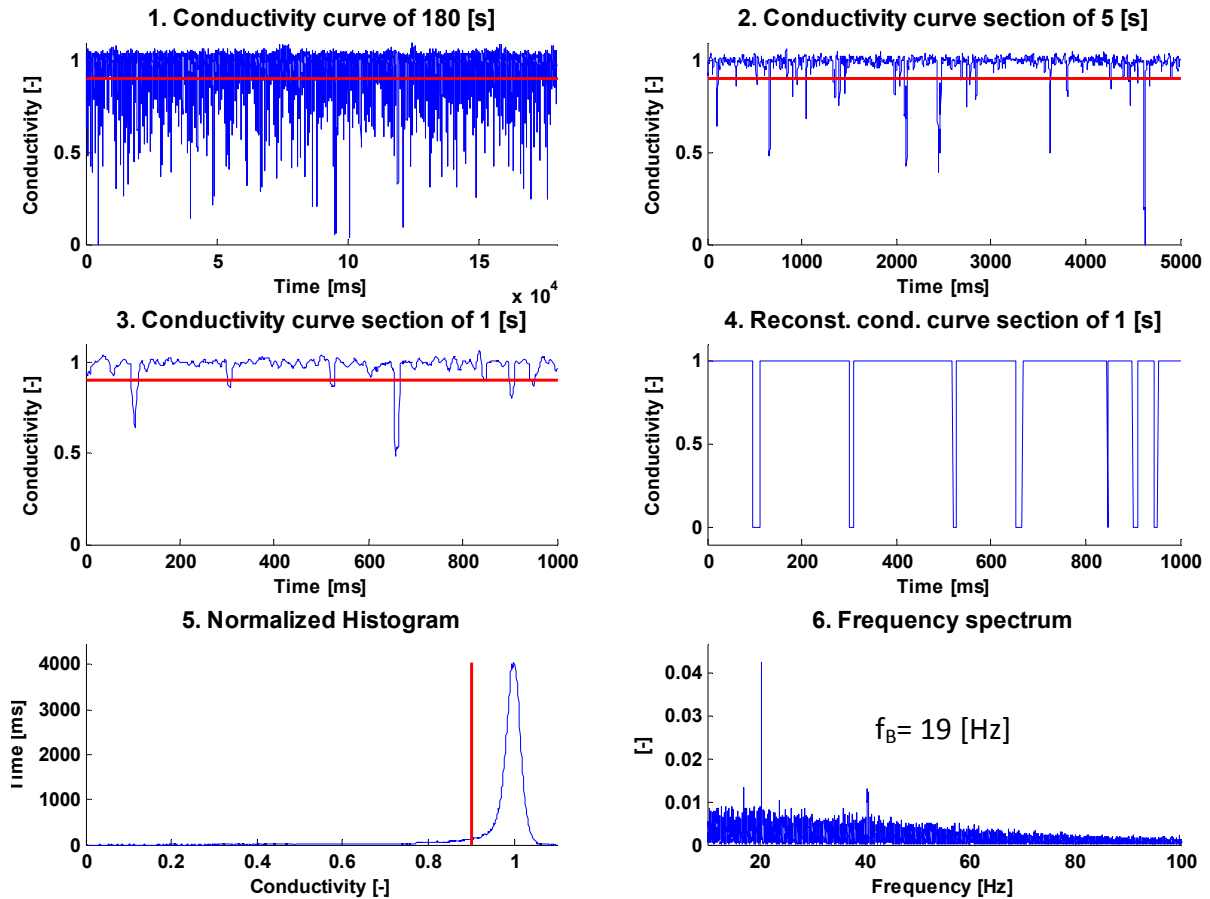


Figure 62: (F4) Conductivity curve analysis at L3.4

Flow regime 5: Loaded with large cavities on all impellers

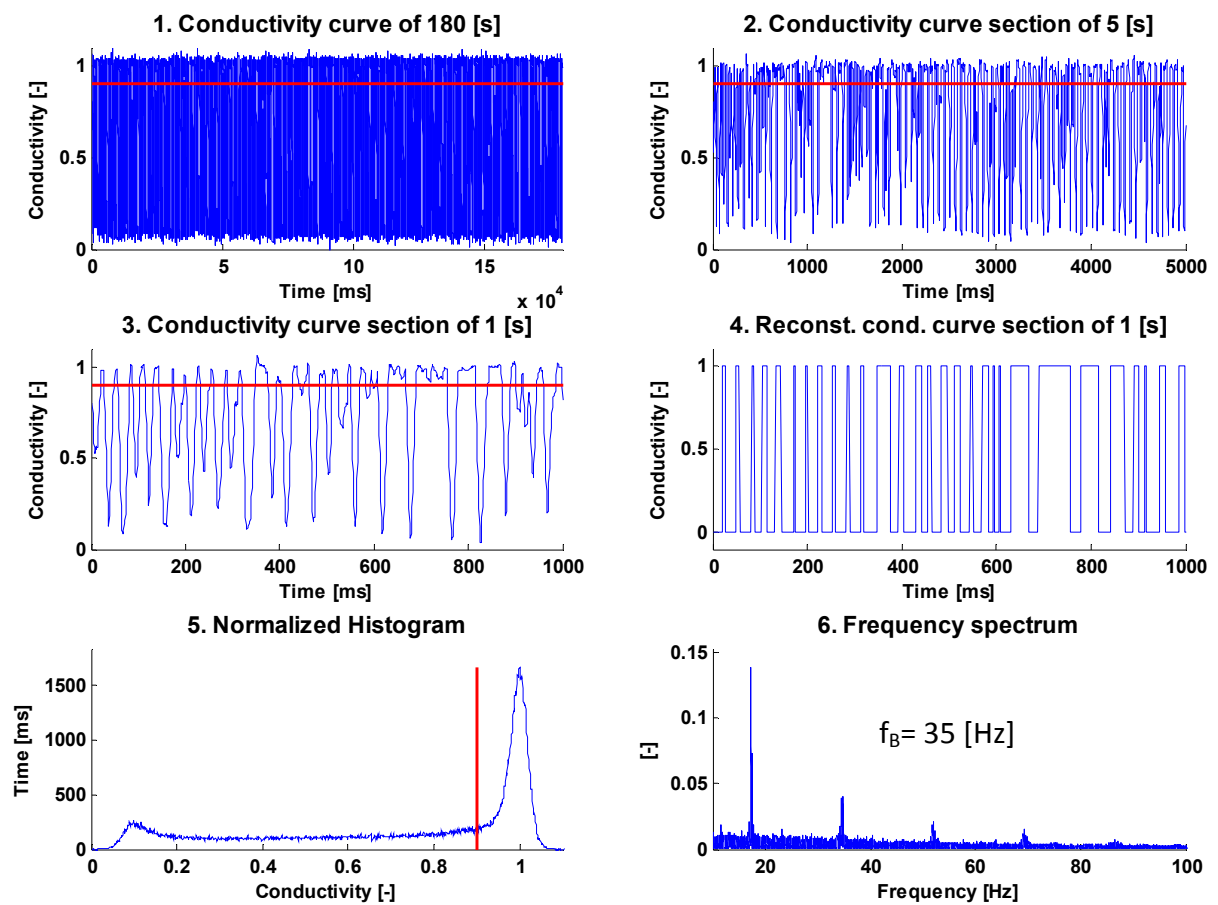
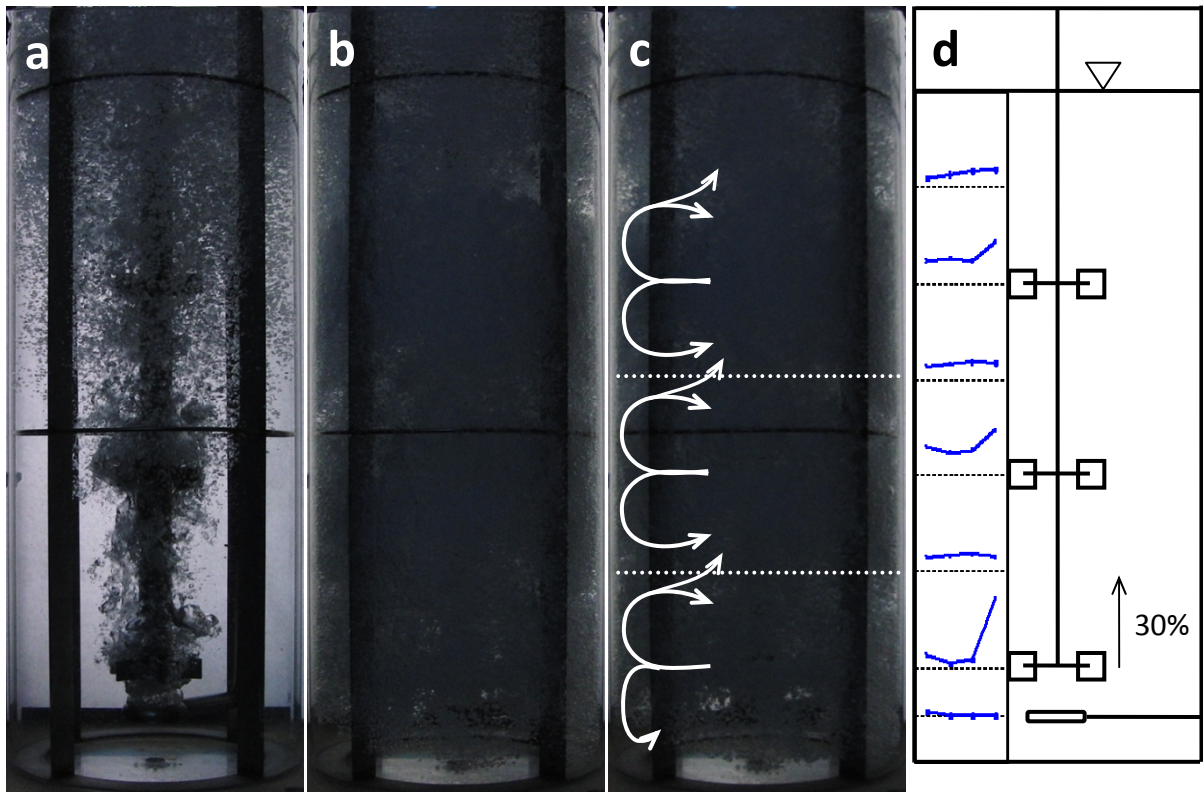


Figure 63: (F5) Snapshots and gas hold-up profile of the reactor & conductivity curve analysis at L1.4

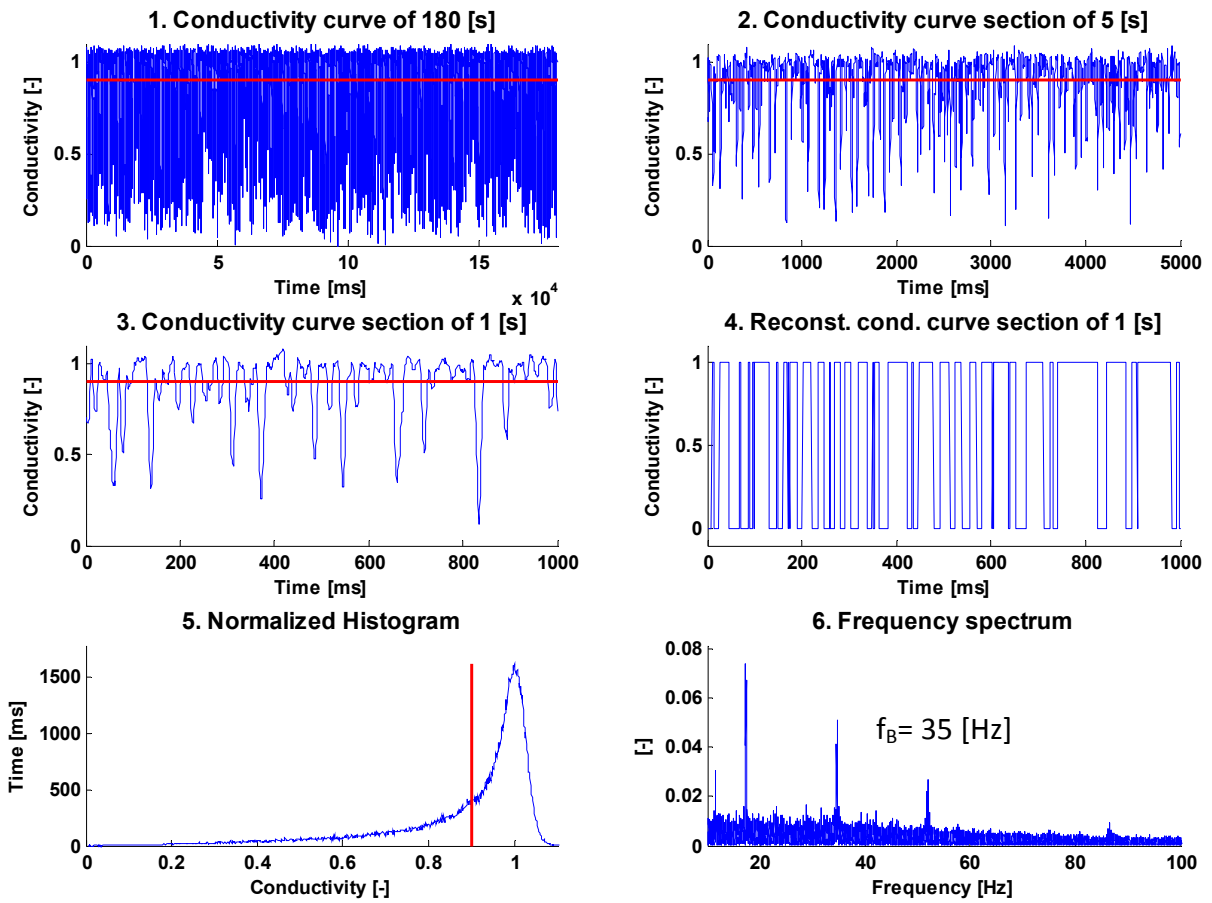


Figure 64: (F5) Conductivity curve analysis at L2.4

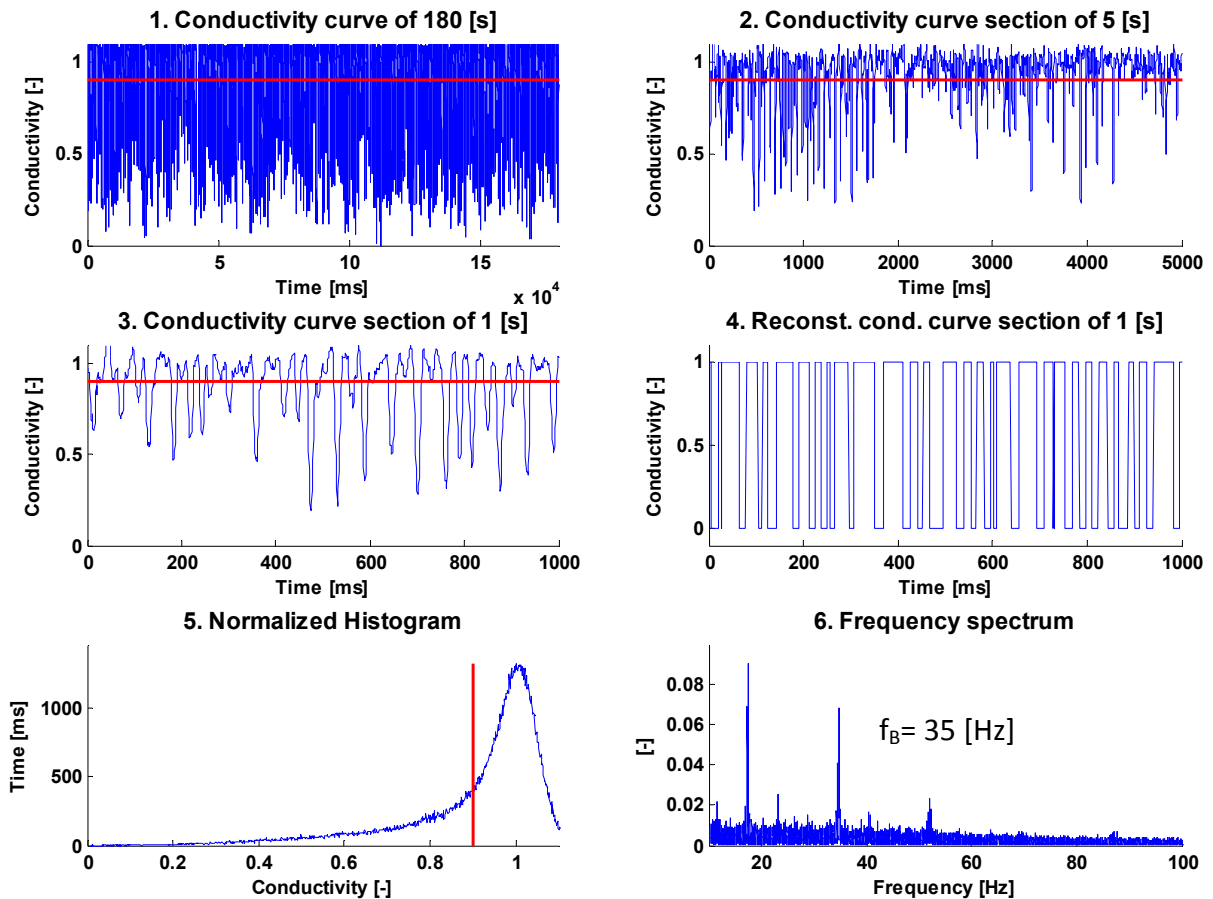


Figure 65: (F5) Conductivity curve analysis at L3.4

Flow regime 6: Flooding

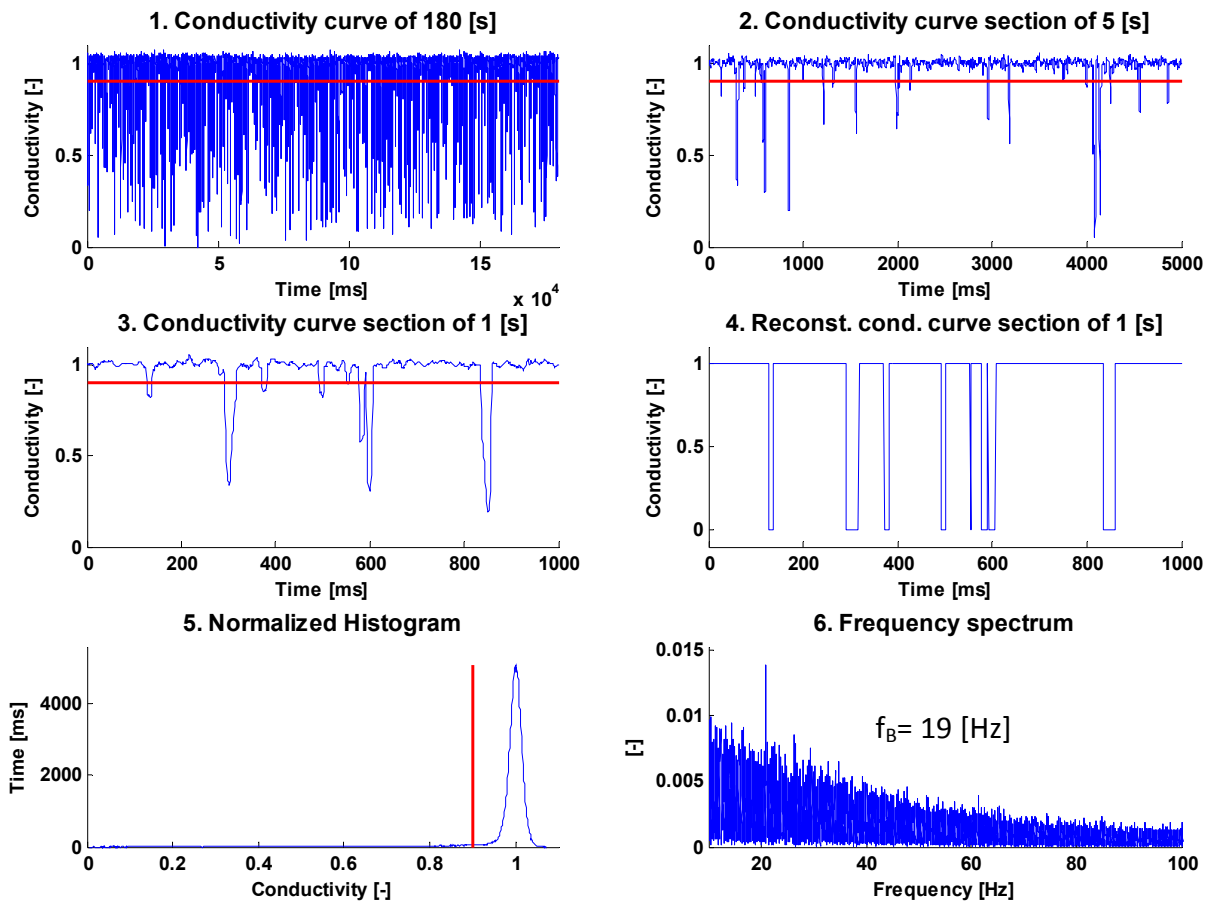
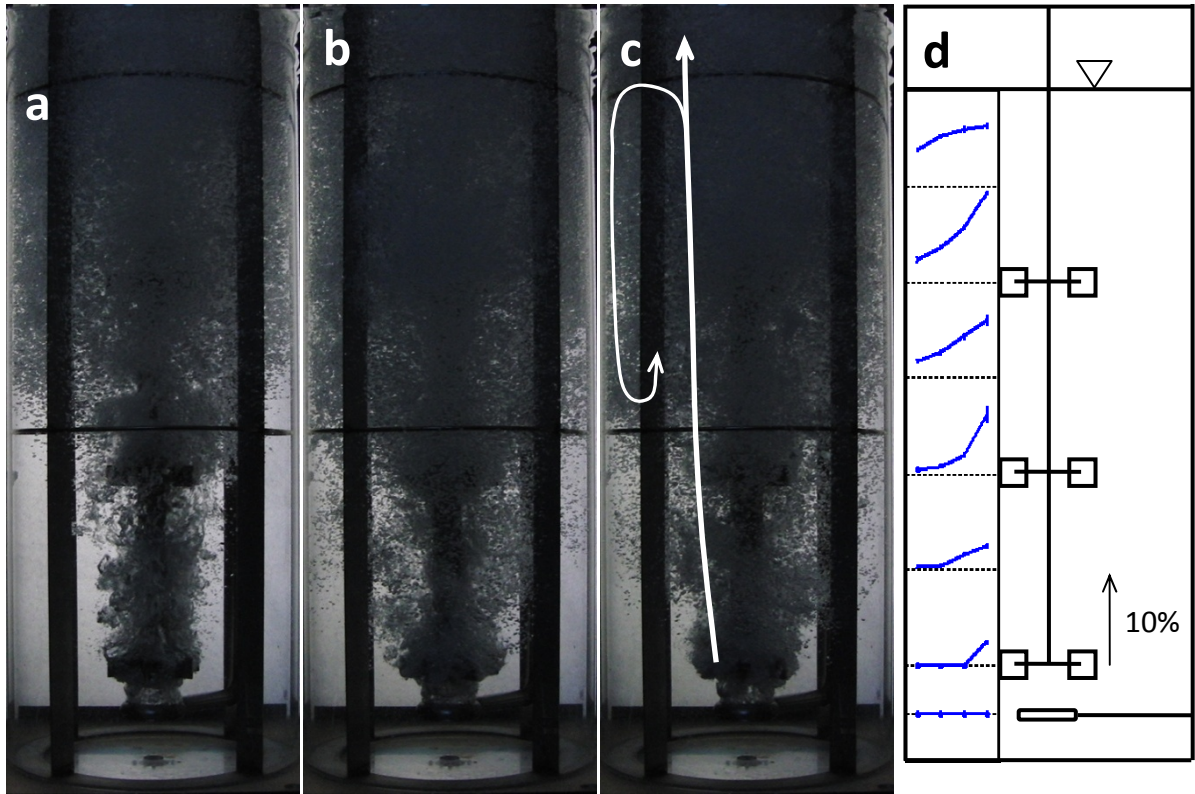


Figure 66: (F6) Snapshots and gas hold-up profile of the reactor & conductivity curve analysis at L1.4

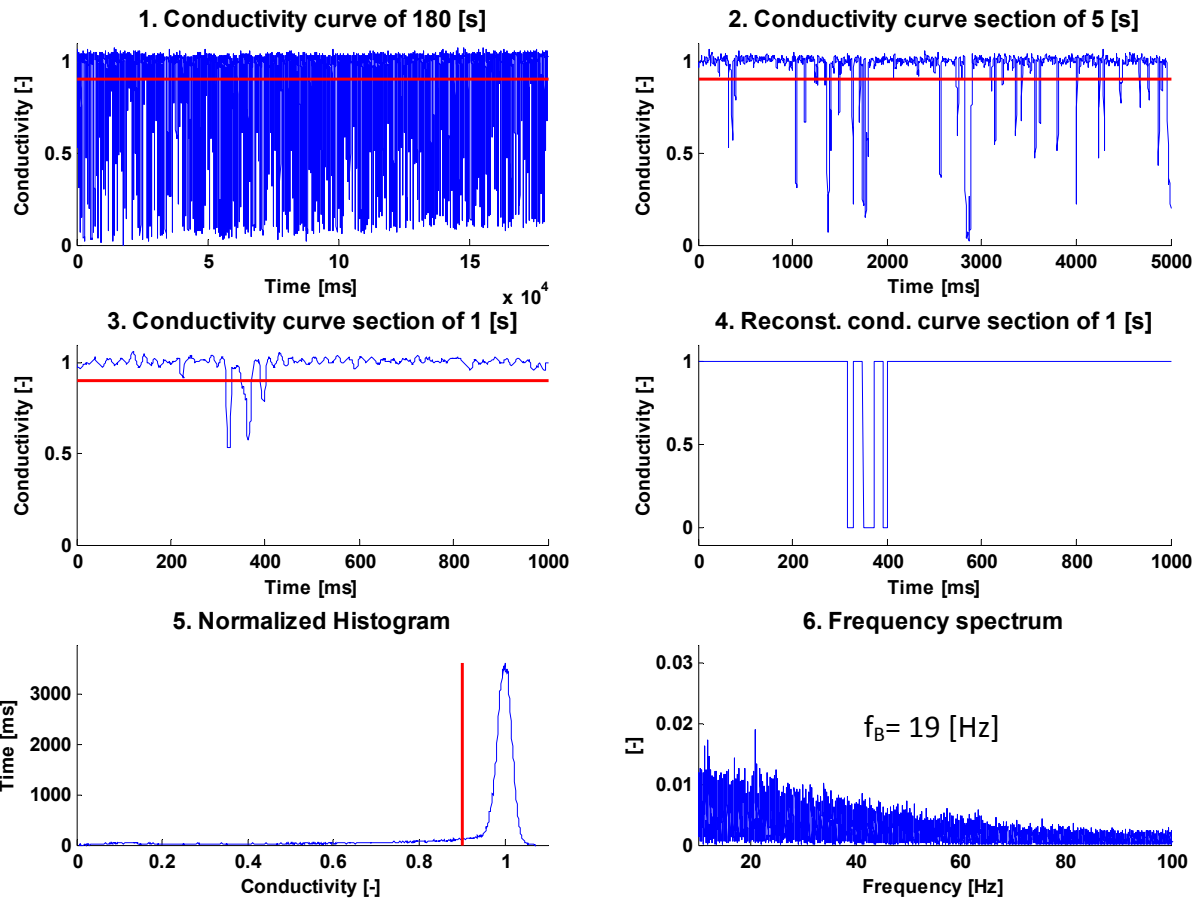


Figure 67: (F6) Conductivity curve analysis at L2.4

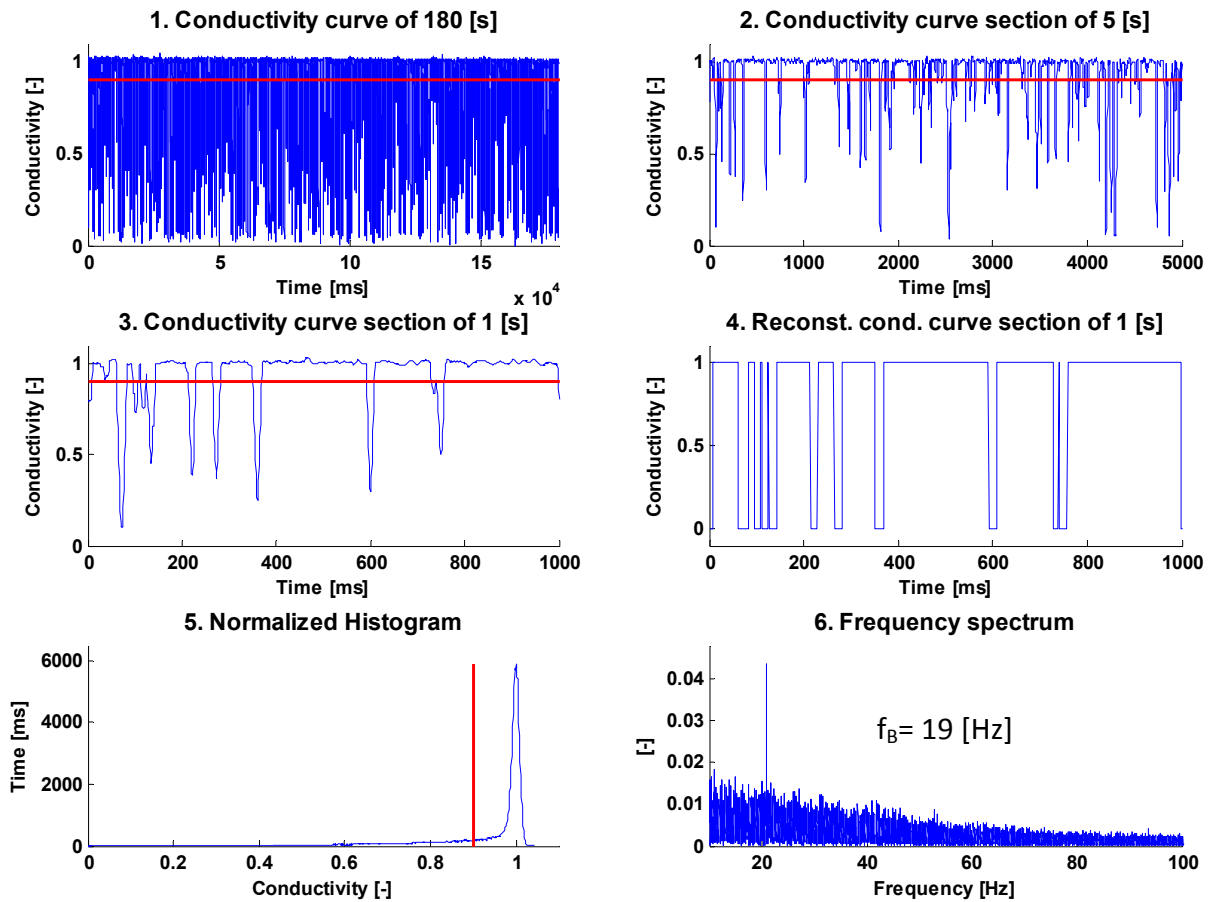


Figure 68: (F6) Conductivity curve analysis at L3.4

Comparison of the results for the different flow regimes

Table 7 shows a summary of the recorded experimental parameter and results from the comparison of the averaged local and global gas hold-ups. The power reduction cannot capture small changes in power demand since the electrical current reading accuracy is limited with one digit.

Table 7: Results of the flow regime experiments

FR	T [°C]	σ_{spec} [mS]	Power input [W]	Power liquid only [W]	Power reduction [%]	Gas hold-up visual obser. [%]	Gas hold-up Cond.Meas. [%]	Deviation [%]
F1	15.3	0.46	712	712	0%	0.98%	1.01%	-3.74%
F2	15.1	0.46	1246	1495	17%	2.93%	2.80%	4.38%
F3	15.9	0.45	1246	1744	29%	8.78%	7.05%	24.56%
F4	16.2	0.4	712	712	0%	1.95%	2.04%	-4.23%
F5	17.1	0.46	819	1068	23%	8.29%	6.38%	30.03%
F6	15.5	0.47	748	748	0%	6.34%	3.41%	85.86%

Figure 69 shows a comparison of the measured gas hold-up profiles. The scaling is illustrated as a vector in the right side of the illustration. In case F2-F3 and F5 recirculation takes place. Signification points to identify recirculation are the points on level 4. If the measured points are lower than one percent no recirculation occurs. In case of gas hold-ups higher than one percent recirculation is identified. Flooding can be identified by measuring the gas hold-up at the first impeller level. In a flooded operating condition the points L1.1-L1.3 are zero.

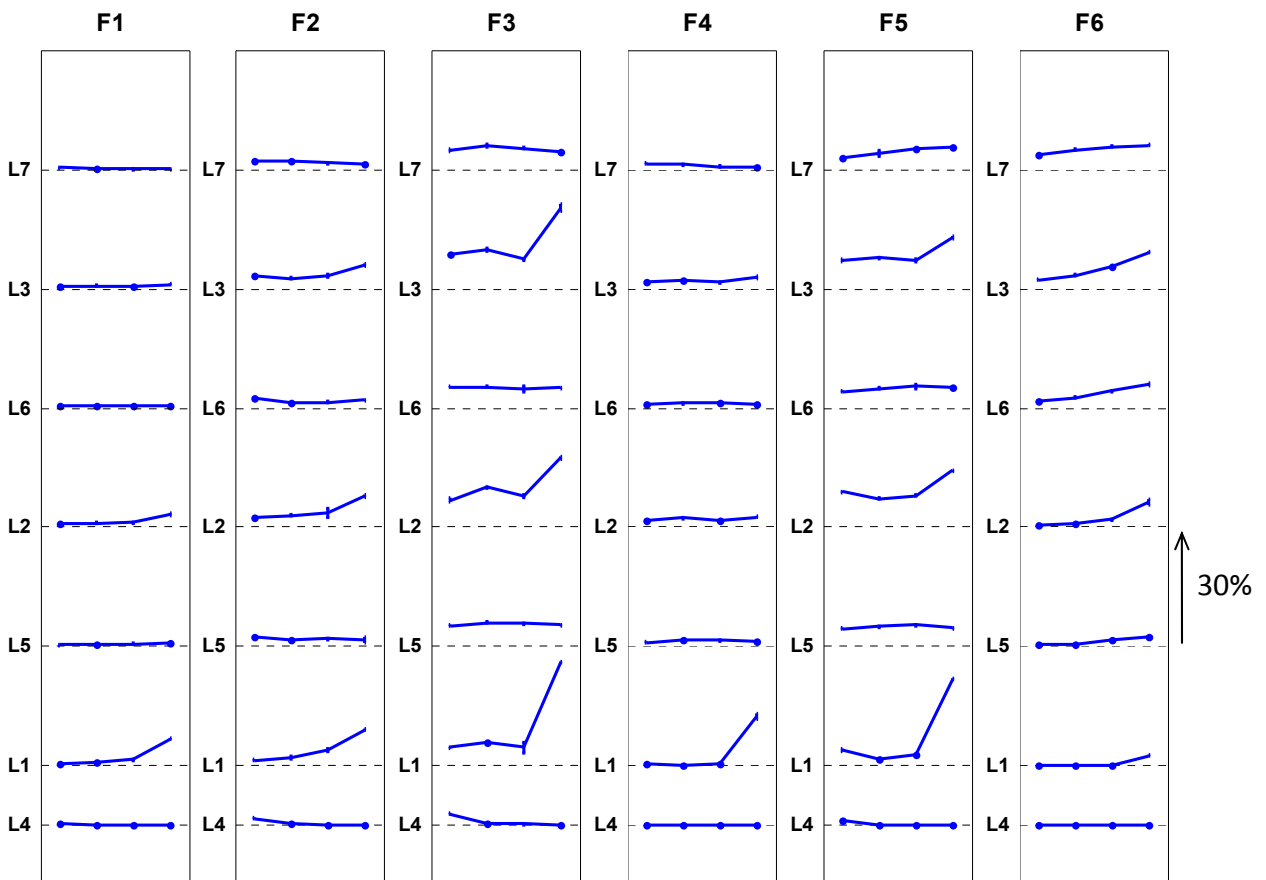


Figure 69: Comparison of the gas hold-up profiles

Figure 70 shows a comparison of the laboratory-scale reactor snapshots. It can be seen that the impeller is able to disperse the gas phase in every regime, except in F6. In F6 the reactor is flooded. Furthermore, it can be seen that a detailed visual observation of the impeller is not possible at higher gas hold-ups as in cases F3 and F5.

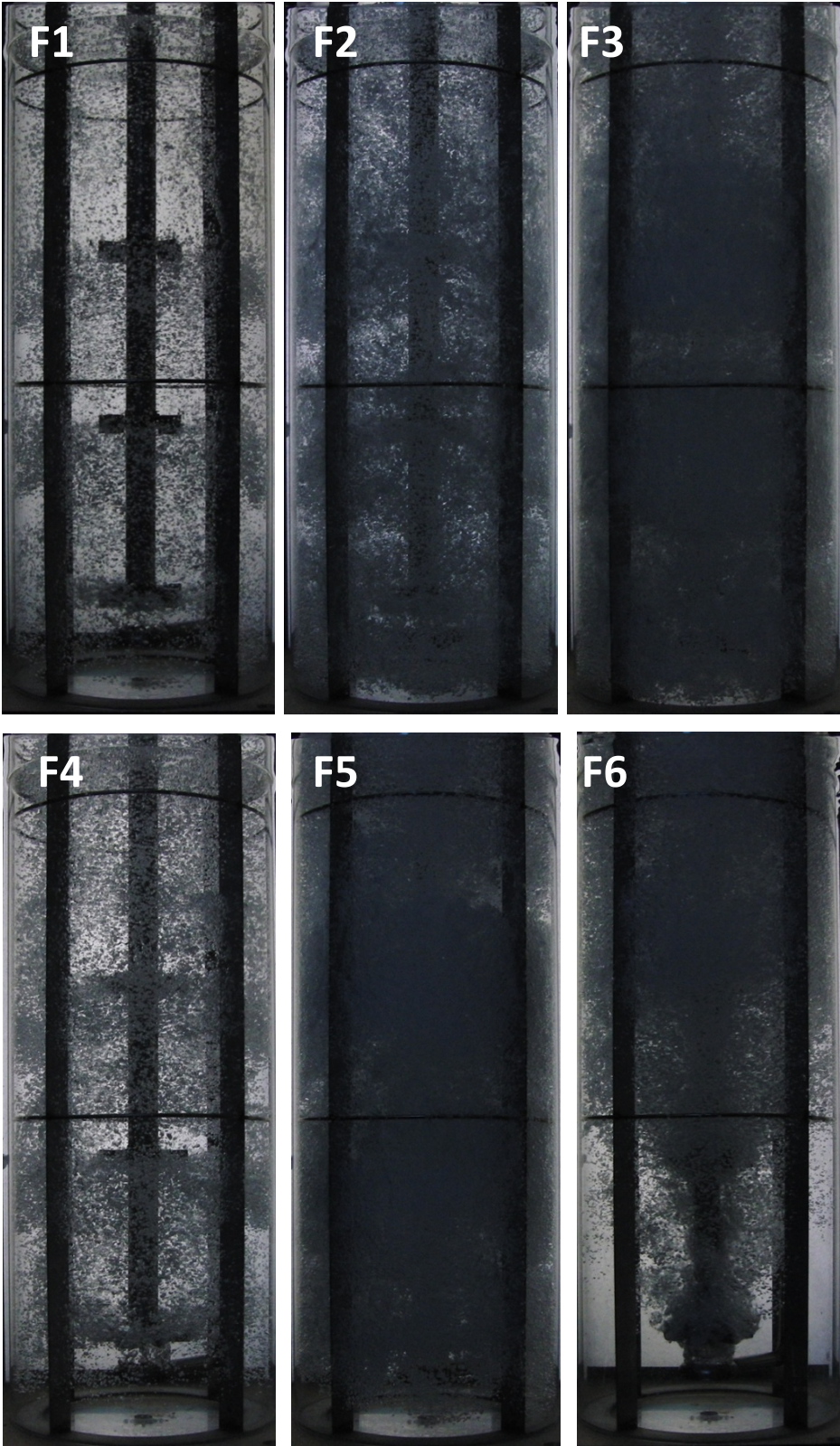


Figure 70: Comparison of the flow regime snapshots

5.2.1.3 Discussion

The measured local gas hold-up results show a good reproducibility with small deviation between experimental trials. The profiles show a good agreement with the visual observation in regions with low gas hold-up where visual observation is possible. The comparisons between the averaged local gas hold-ups and the global gas hold-ups showed good agreement in the points F1, F2 and F3. These flow regimes have a global gas hold-up lower than 3%. In the flow regimes F3 and F5 the comparison showed a deviation of approximately 30%, we assume that this deviation is caused by measurement uncertainty in the visual observation. This could also explain the large deviation of 80% in the flooding regime. The frequency pattern showed similar peaks at the blade frequency as reported in literature [1][2][20] in flow regimes 1,4,5,6. The mismatch of the flow regimes 2 and 3 cannot be explained so far, one assumption is that the distance between conductivity probe and impeller blade was too far. Thus, this mismatch should be investigated in future work.

5.2.2 Mixing experiments

The mixing experiments were conducted three times for every point in the flow map. The conductivity was recorded at the location L1.4 in the outflow jet of the lowermost impeller. A tracer was added from the top surface of the reactor. The conductivity change was recorded and analyzed. Zahradnik et al. [27] investigated the effect of electrolytes on bubble coalescence. They have found that electrolytes almost prevent bubble coalescence when it exceeds a certain concentration. Figure 71 shows coalescence percentage Ψ as function of the electrolytes concentration. We decided to use NaCl as a tracer for our mixing experiments. It can be seen that the tracer concentration should not exceed 0.1 [mol/L]. Table 8 shows the basic calculations for the tracer experiments. A tracer of 10 [g] per experiment has been chosen. The calculation shows that the applied tracer does not change the coalescence behavior of the system.

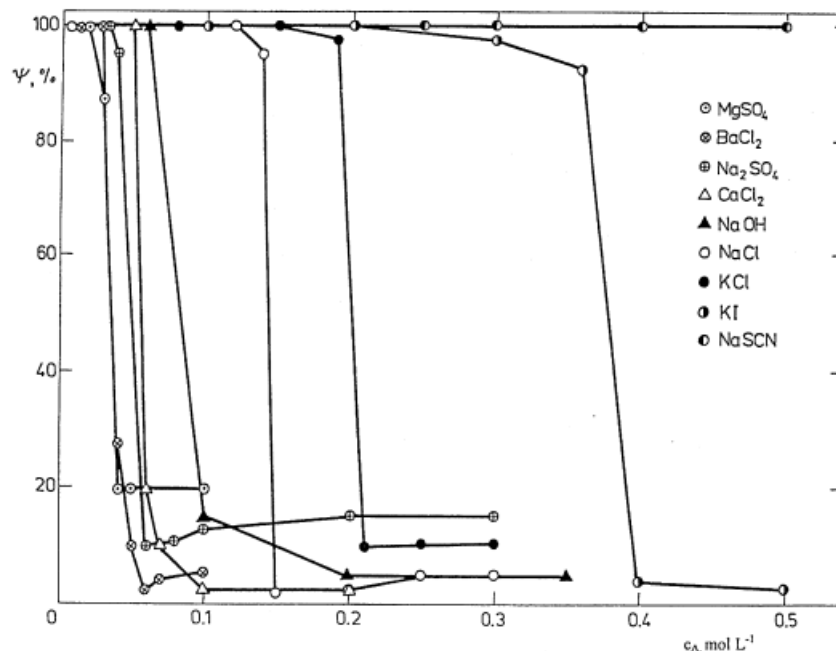


Figure 71: Coalescence percentage in aqueous solutions of electrolytes[27]

Table 8: Basic tracer calculations

Molar mass NaCl	58.44	[g/mol]
Liquid volume	150	[l]
max. Concentration	0.1	[mol/l]
max. Tracer	876.6	[g]
Tracer	10	[g]
Tracer	0.17	[mol]
Concentration	0.0011	[mol/l]

5.2.2.1 Post processing of the measured data

Figure 72 shows the work flow of the post processing algorithm. The first step is to load the recorded data. The recorded data for one experiment of F1 is shown in Figure 73 (1). The next step removes the bubble interactions of the conductivity curve. Therefore, the conductivity curve is divided in sections of 100 [ms]. The conductivity curve is reconstructed by taking the maximum value of every section. The reconstructed curve is shown in Figure 73 (2). Next, a conductivity change caused by a temperature drift is removed from the liquid conductivity curve. In addition, the curve is smoothed with a moving average filter. After that, the curve is normalized to the constant conductivity levels before and after the tracer addition. Figure 73 (3) show the result of the last four steps. The mixing time t_{90} is calculated from moment of the tracer addition to the moment when the conductivity remains stable above the 90 % of the normalized conductivity change. The post processing ceases with the visualization of the results.

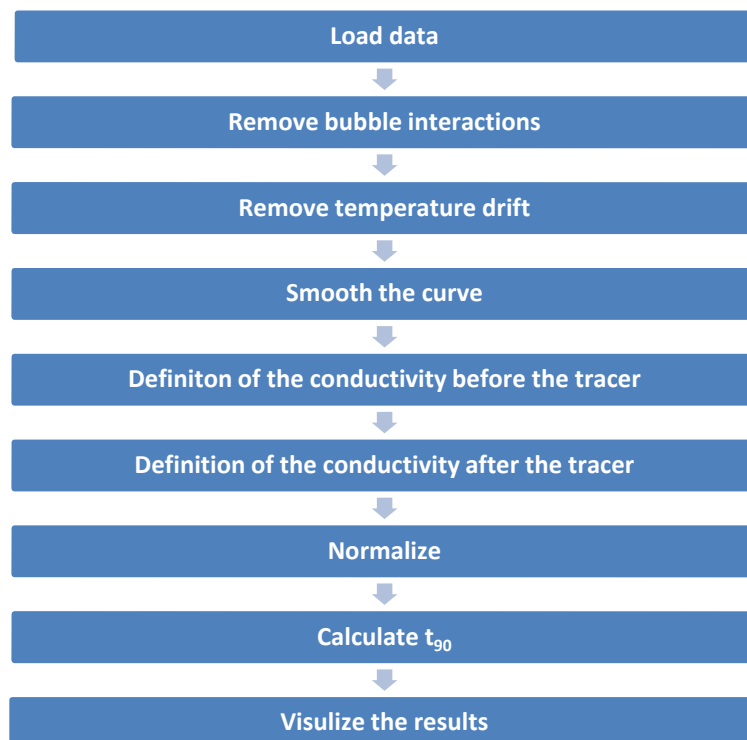


Figure 72: Workflow of the mixing time post processing algorithm

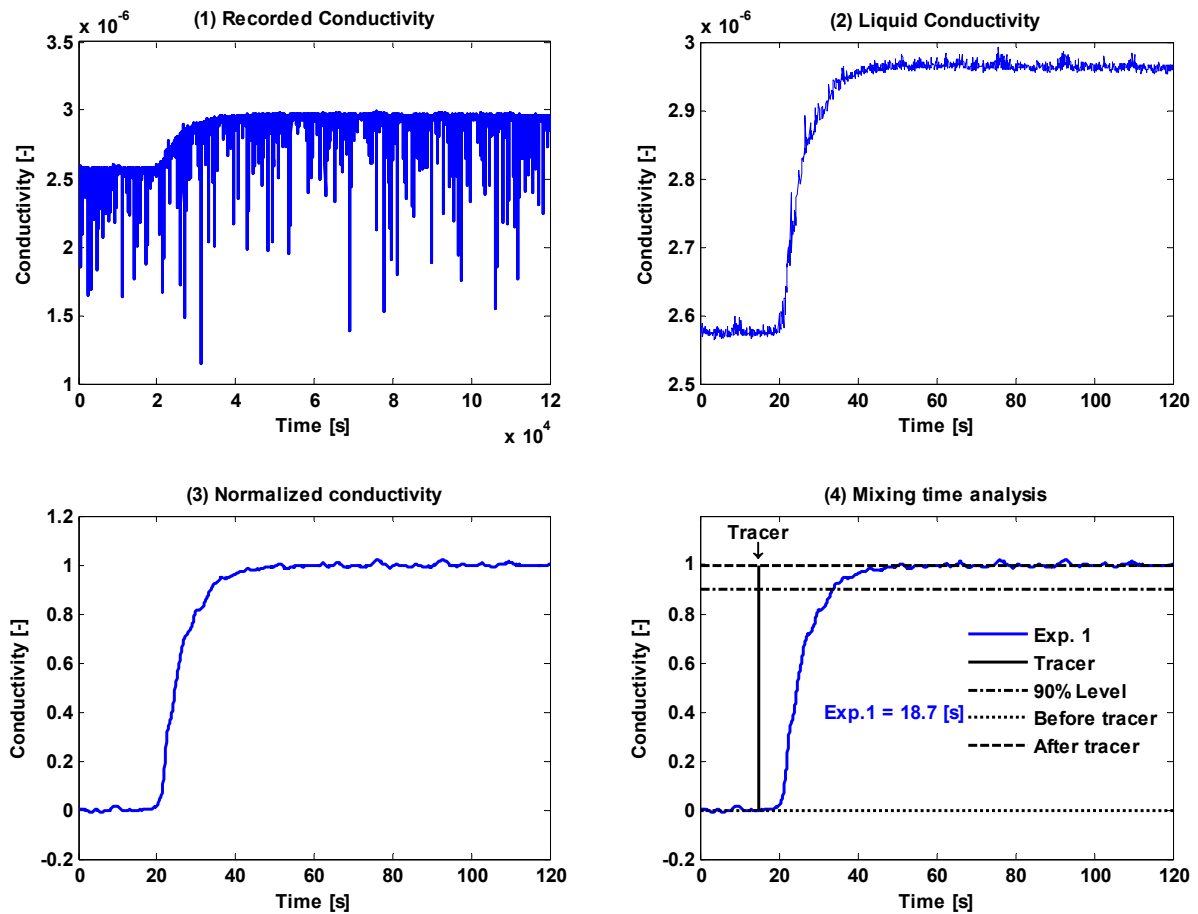


Figure 73: Illustration of the mixing post processing algorithm

5.2.2.2 Result

Figure 74 shows the result of the conductivity curves analysis obtained from the mixing experiments. The diagrams show the normalized conductivity changes of the continuous liquid phase. Table 9 shows the summary of the obtained results. The shortest mixing time was measured in flooding regime F6 with 16.7 [s]. In the flooding regime the liquid flow field develops one big loop in the reactor, see Figure 66. The total liquid of the reactor is moving with this loop and cause therefore a fast mixing. In the flow regime F1 to F5 flow compartments are developed as explained in the results of the gas hold-up experiments. This compartment interact slowly with each other, so that, a higher mixing time was measured. The mixing time in these regimes are strongly dependent on the Froude number and therewith the impeller rotational speed. F2 and F3 show a significant shorter mixing time compared to F1, F4 and F5.

Table 9: Summary of the mixing experiments

Flowmap	Fr [-]	Fl [-]	$t_{90,1}$ [s]	$t_{90,2}$ [s]	$t_{90,3}$ [s]	$t_{90,a}$ [s]	average deviation [s]
F1	0.15	0.02	18.7	25.2	26.1	23.3	3.1
F2	0.8	0.02	19.1	19.8	17.5	18.8	0.9
F3	1.1	0.05	18.1	18	19.9	18.7	0.8
F4	0.15	0.05	31.7	32.6	32.3	32.2	0.3
F5	0.5	0.12	27.8	28.9	31.6	29.4	1.4
F6	0.15	0.5	16.3	15.6	18.2	16.7	1.0

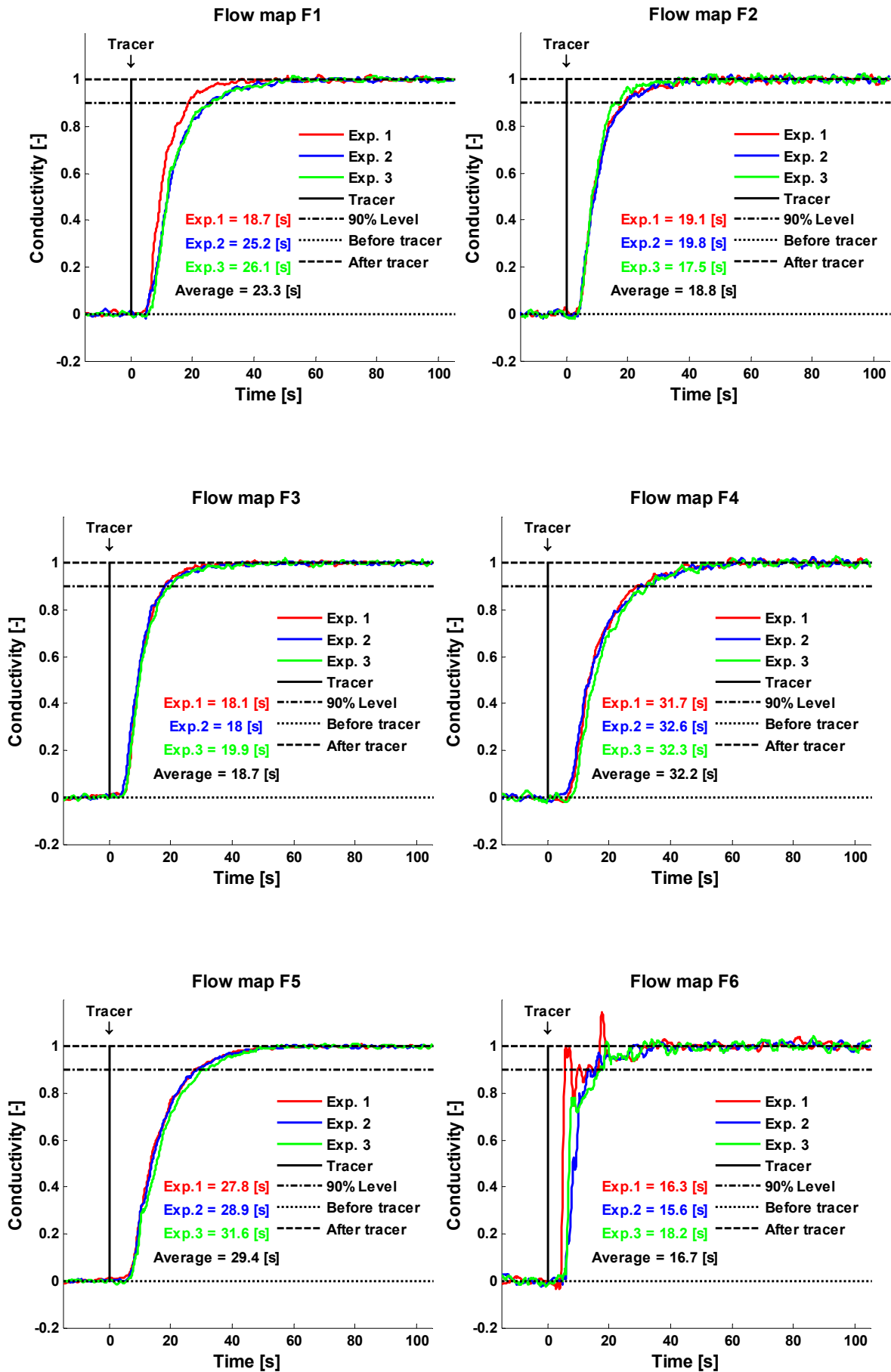


Figure 74: Analyzed data of the mixing experiments in the laboratory-scale reactor

5.2.3 Discussion

The experiments to determine the mixing time in the laboratory-scale reactor show good reproducibility. The averaged deviation to the averaged mixing time is 1.3 [s]. It has been shown that conductivity probes can be used to determine the mixing time in multiphase flow without shielding as recommended by Pinelli [7].

6 Conclusion

6.1 Summary

An electrical conductivity based gas hold-up and mixing time measurement system has been developed. It can be used to gain insight into gas hold-up distribution and mixing behaviour of multiphase flows. It is an intrusive measurement technique, in which a probe has to be placed inside the flow. The gas hold-up measurement principle is based on difference in conductivity between the phases, whereas the mixing measurement principle is based on conductivity change of the liquid phase by tracer concentration. The time resolution of the measurement system is 1 [ms]. The probe is designed as a single-tip needle probe with 300 [μm] tip diameter. This setup enables us to capture small gas bubbles and rapid changes in conductivity during a mixing experiment. The data are acquired with National Instruments hardware, subsequently analyzed and visualized with Matlab[®]. The measurement system was validated with a high-speed camera. It has been applied to measure the gas hold-up distribution and the mixing time in a multiphase stirred reactor. The multiphase reactor has been designed and set up during this work. It is built of Plexiglas[®], which enables us to visual observations of the flow pattern.

The reliability of the developed measurement system has been proven with an image analysis technique and experiments in a laboratory-scale reactor. Furthermore, the measured data showed good agreement with visual observation. Thus, the developed measurement system can be considered as a powerful tool to gain insight of a multiphase flow.

6.2 Outlook

The measurement system obtains good results in this setup, but there are ideas to improve it. Suggested improvement for the measurement systems are: a higher sampling frequency, further development of the GUI and software, and the redesign of the single tip conductivity probe. A multiple tip conductivity probe could deliver additional information such as bubble size and velocity. The laboratory reactor has been found as powerful a tool to investigate the multiphase flow in a stirred reactor. It can be equipped with different impeller and baffle combinations. Future experiments could be made with non-Newtonian liquids and compared to data presented in literature. Further suggestions for the laboratory-scale reactor are an automatic probe adjustment, a mass flow controller and a motor controller which are connected with a central control unit, such that gas hold-up profiles can be measured fully automatic.

7 Lists

7.1 List of literature

- [1]. **Bombac, A., et al.** Gas-Filled Cavity Structures and Local Void Fraction Distribution in Aerated Stirred Vessel. *AIChE Journal*. November, 1997, Vol. 43, 11.
- [2]. **Bombac, A. and Zun, Iztok.** Individual impeller flooding in aerated vessel stirred by multiple-Rushton impellers. *Chemical Engineering Journal*. 2006, 116.
- [3]. **Sanwani, E., et al.** *Comparison of gas hold-up distribution measurement in a flotation cell using capturing and conductivity techniques*. s.l. : Minerals Engineering, 2006. pp. 1362-1372.
- [4]. **Jose da Silva, M.** *Impedance Sensors for Fast Multiphase Flow Measurement and Imaging*. s.l. : Technische Universität Dresden, 2008.
- [5]. **Hampel, U.** *Measurement Techniques and Experimental Investigations for Multiphase Flows*. Dresden : ANSYS, 2010.
- [6]. **Shewale, S.D. and Pandit, A.B.** Studies in multiple impeller agitated gas-liquid contactors. *Chemical Engineering Science*. 2006, 61.
- [7]. **Pinelli, D., et al.** Comparison of Experimental Techniques for the Measurement of Mixing Time in Gas-Liquid Systems. *Chem. Eng. Technol.* 2001, 24.
- [8]. **Tropea, C., Yarin, A.L. and Foss, J.F.** *Handbook of Experimental Fluid Mechanics*. Berlin Heidelberg : Springer, 2007. 978-3-540-25141-5.
- [9]. **H.R. Langguth, R. Voigt.** *Hydrogeologische Methoden*. Berlin : Springer, 2004. 978-3540211266.
- [10]. **Flickinger, M.C. and Drew, S. W.** *Encyclopedia of Bioprocess Technology*. s.l. : Wiley-Interscience, 1999. 978-0471138228.
- [11]. **WTW GmbH.** *Leitfähigkeits-Fibel*. s.l. : Selbstverlag.
- [12]. **Sartorius.** www.sartorius.com. *Handbuch der Elektroanalytik - Teil 3 - Die elektrische Leitfähigkeit*. [Online] [Cited: 11 22, 2010.] www.sartorius.com.
- [13]. **Oertel, H.** *Prandtl-Essentials of Fluid Mechanics*. s.l. : Springer, 2010. 978-1-4419-1563-4.
- [14]. **Clift, R., Grace, J. and Weber, M.E.** *Bubbles, Drops, and Particles*. London : Dover Publ Inc, 2005. 978-0486445809.
- [15]. **Prince, M.J. and Blanch, H.W.** Bubble Coalescence and Break-Up in Air-Sparged Bubble Columns. *AIChE Journal*. 1990, Vol. 10, 36.

- [16]. **Paul, E.L., Atiemo-Obeng, V.A. and Kresta, S.M.** *Handbook of Industrial Mixing: Science and Practice*. New Jersey : John Wiley & Sons, 2003. ISBN 0-471-26919-0.
- [17]. **Gezork, K.M., et al.** Mass transfer and hold-up characteristics in a gassed, stirred vessel at intensified operating conditions. *Trans IChemE*. 2001, Vol. A, 79.
- [18]. —. The transition from homogeneous to heterogeneous flow in a gassed stirred vessel. *Chemical Engineering Research and Design*. 2000, Vol. 3, 78.
- [19]. **Evans, G. M. and S.A. Manning, G.J. Jameson.** Cavity Formation, Growth, and Dispersion behind Rotating Impeller Blades. *Ind. Eng. Chem. Res.* 2005, 44.
- [20]. **Paglianti, A., Pintus, S. and Giona, M.** Time-series analysis approach for the identification of flooding/loading in gas-liquid stirred tank reactor. *Chemical Engineering Science*. 2000, 55.
- [21]. **Treffer, D.** *Development of a conductivity based gas hold-up measurement system*. s.l. : Institute for Process and Particle Engineering, University of Technology, 2010.
- [22]. **Treffer, D., Sungkorn, R. and Khinast, J.G.** High Sensitivity Conductivity Probe for Measurement of Gas hold-up and Mixing Time. [ed.] *Processnet Jahrestagung der Fachausschüsse CFD und Mixing*. [Poster]. Dortmund, Germany : Institute for Process and Particle Engineering, University of Technology Graz, 2011.
- [23]. **Blumenthal, G., Linke, D. and Vieth, S.** *Chemie - Grundwissen für Ingenieure*. Wiesbaden : B.G. Teubner Verlag / GWV Fachverlage GmbH,, 2006. 978-3-519-03551-0.
- [24]. **Becker, S., Sokolichin, A. and Eigenberger, G.** Gas-liquid flow in bubble columns and loop reactors: Part II, Comparison of detailed experiments and flow simulations. *Chemical Engineering Science*. 1994, Vol. 49, 24B, pp. 5747-5762.
- [25]. **Pucher, H.** *Aufbau einer Blasensäule zur Untersuchung der Vermischung in Mehrphasensystemen*. Graz : Institut für Prozess- und Partikeltechnik, Technische Universität Graz, 2010.
- [26]. **Becker, S., Bie, H. De and Sweeney, J.** Dynamic flow behaviour in bubble columns. *Chemical Engineering Science*. 1999, 54, pp. 4929-4935.
- [27]. **Zahradnik, J., Fialova, M. and Linek, V.** The effect of surface-active additives on bubble coalescence in aqueous media. *Chemical Engineering Science*. 1999, 54, pp. 4757-4766.
- [28]. **Hudcova, V. and Machon, V.** Gas-Liquid Dispersion with Dual Rushton Turbine Impellers. *Biotechnology and Bioengineering*. 1989, 34.
- [29]. **Gogate, P. R., Beenackers, A. A.C.M and Pandit, Aniruddha B.** Multiple-impeller systems with a special emphasis on bioreactors: a critical review. *Biochemical Engineering Journal*. 2000, 6.

7.2 List of figures

Figure 1: Illustration of the gas hold-up (a) and mixing time (b) measurement principle	5
Figure 2: Illustration of a simple probe geometrie[11].....	6
Figure 3: Shear stress for Newtonian and non-Newtonian fluids [13]	7
Figure 4: Forces acting on a bubble	8
Figure 5: Terminal velocity for an air water system at 20°C [14]	8
Figure 6: Bubble shape depending on Eö-, Re and M-Number [14]	9
Figure 7: Illustration of multiple impeller multiphase reactor	10
Figure 8: Axial flow impellers (left), radial flow impellers (right) [16]	11
Figure 9: Hydrofoil impeller (left), high shear impeller (right) [16]	11
Figure 10: Liquid flow pattern in a stirred reactor; left: radial impeller, right: axial impeller [16]	11
Figure 11: Flow pattern as a function of the impeller spacing [28].....	12
Figure 12: Variation of unaerated power draw with impeller spacing[28] [29]	12
Figure 13: Illustration of homogeneous and heterogeneous distribution [17]	13
Figure 14: Flow patterns in a gas liquid stirred reactor [16].....	14
Figure 15: Cavity regimes in loading and flooding[20]	14
Figure 16: Cavity Structures behind a Rushton blade [16]	15
Figure 17: Flow map for single Rushton impeller [16]	15
Figure 18: Flow map for a triple Rushton Impeller reactor [16]	16
Figure 19: Flooding recognition with a resistivity probe: (a) raw signal; (b) frequency spectrum [2]	17
Figure 20: Illustration of the measurement principle [22]	18
Figure 21: 3D View of the conductivity probe	19
Figure 22: 3D view of the conductivity probe tip, highlighted in the ellipsoid in figure 21	20
Figure 23: Illustration of the needle probe in a water-filled vessel.....	20
Figure 24: Raw signal and filtered signal.....	21
Figure 25: Electrical circuit of the measurement system.....	21
Figure 26: Graphical user interface (GUI) of the measurement software in Matlab®	23
Figure 27: Illustration of the box for single bubble experiments	24
Figure 28: Illustration of the verification setup	24
Figure 29: Snapshots of a rising bubble with the M3 high-speed camera at 1000 [Hz]	25
Figure 30: Illustration of the Matlab® post processing for the image analysis	25
Figure 31: Snapshots of characteristic bubbles of the verification procedure.....	26
Figure 32: Conductivity curve obtained from the verification experiment with bubble size (a)	28
Figure 33: Zoom of the bubble interactions in Figure 32 (- threshold, -conductivity, -- reconstructed signal).....	28
Figure 34: Conductivity curve obtained from the verification experiment with bubble size (b)	29

Figure 35: Zoom of the bubble interactions in Figure 34 (- threshold, -conductivity, --reconstructed signal).....	29
Figure 36: Conductivity curve obtained from the verification experiment with bubble size (c)	30
Figure 37: Zoom of the bubble interactions in Figure 36 (- threshold, -conductivity, --reconstructed signal).....	30
Figure 38: Illustration of the laboratory stirred reactor	31
Figure 39: Visual observation in transparent vessels [16]	31
Figure 40: Photo and three dimensional view of the reactor in ProEngineer	32
Figure 41: Photograph (A) and three dimensional ProEngineer illustration (B) of the Rushton turbine	33
Figure 42: Three dimensional ProEngineer illustration of the ring sparger	33
Figure 43: Photograph of the probe holder	33
Figure 44: Illustration of the probe positions	34
Figure 45: Illustration of the bubble column	34
Figure 46: Compartment of the bubble column	35
Figure 47: Summary of the snapshots and gas hold-up profiles obtained of the bubble column experiments at different air flow rates (A: 1 [l/min], B: 5 [l/min], C: 10 l/min]) [22].	36
Figure 48: Illustration of the measurement levels.....	36
Figure 49: Flow map of the laboratory reactor [Internal report, R. Sungkorn]	37
Figure 50: Work flow of the gas hold-up measurement post processing.....	38
Figure 51: (F1) Snapshots and gas hold-up profile of the reactor & conductivity curve analysis at L1.4	43
Figure 52: (F1) Conductivity curve analysis at L2.4	44
Figure 53: (F1) Conductivity curve analysis at L3.4	44
Figure 54: (F2) Snapshots and gas hold-up profile of the reactor & conductivity curve analysis at L1.4	45
Figure 55: (F2) Conductivity curve analysis at L3.4	46
Figure 56: (F2) Conductivity curve analysis at L3.4	46
Figure 57: (F3) Snapshots and gas hold-up profile of the reactor & conductivity curve analysis at L1.4	47
Figure 58: (F3) Conductivity curve analysis at L2.4	48
Figure 59: (F3) Conductivity curve analysis at L3.4	48
Figure 60: (F4) Snapshots and gas hold-up profile of the reactor & conductivity curve analysis at L1.4	49
Figure 61: (F4) Conductivity curve analysis at L2.4	50
Figure 62: (F4) Conductivity curve analysis at L3.4	50
Figure 63: (F5) Snapshots and gas hold-up profile of the reactor & conductivity curve analysis at L1.4	51
Figure 64: (F5) Conductivity curve analysis at L2.4	52
Figure 65: (F5) Conductivity curve analysis at L3.4	52
Figure 66: (F6) Snapshots and gas hold-up profile of the reactor & conductivity curve analysis at L1.4	53

Figure 67: (F6) Conductivity curve analysis at L2.4.....	54
Figure 68: (F6) Conductivity curve analysis at L3.4.....	54
Figure 69: Comparison of the gas hold-up profiles.....	55
Figure 70: Comparison of the flow regime snapshots.....	56
Figure 71: Coalescence percentage in aqueous solutions of electrolytes[27]	57
Figure 72: Workflow of the mixing time post processing algorithm	58
Figure 73: Illustration of the mixing post processing algorithm	59
Figure 74: Analyzed data of the mixing experiments in the laboratory-scale reactor	60

7.3 List of equations

Equation 1: Ohm's law	6
Equation 2: Relation between resistance and conductivity	6
Equation 3: Conductivity	6
Equation 4: Cell constant	6
Equation 5: Temperature compensation for water systems [12].....	6
Equation 6: Reynolds number	7
Equation 7: Re – Reynolds number of a bubble.....	8
Equation 8: $Eö$ – Eötvös number of a bubble.....	9
Equation 9: M – Morton number of a bubble.....	9
Equation 10: v_{vm} Gas flow.....	12
Equation 11: Superficial gas velocity.....	12
Equation 12: Gas hold-up.....	13
Equation 13: Re – Reynolds number of an impeller	13
Equation 14: Fr - Froude number.....	13
Equation 15: Fl - Flow number	13
Equation 16: Electrolysis of water [23]	18
Equation 17: RMS of a set of data points.....	21
Equation 18: Correlation for the terminal velocity in pure water and $d_e > 1.3$ [mm] [14]	26

7.4 List of tables

Table 1: Standard electrode potentials of copper and gold [15].....	19
Table 2: Calculation of the theoretical contact time	26
Table 3: Comparison of the obtained intervals between image analysis and conductivity measurement (IA .. image analysis; CM .. conductivity measurement; Dev .. deviation).....	27
Table 4: Comparison of the contact times (IA .. image analysis; CM .. conductivity measurement; Dev .. deviation).....	27
Table 5: Impeller dimensions	33
Table 6: Operating conditions of the experiments	37
Table 7: Results of the flow regime experiments	55
Table 8: Basic tracer calculations	58
Table 9: Summary of the mixing experiments	59

8 Appendix

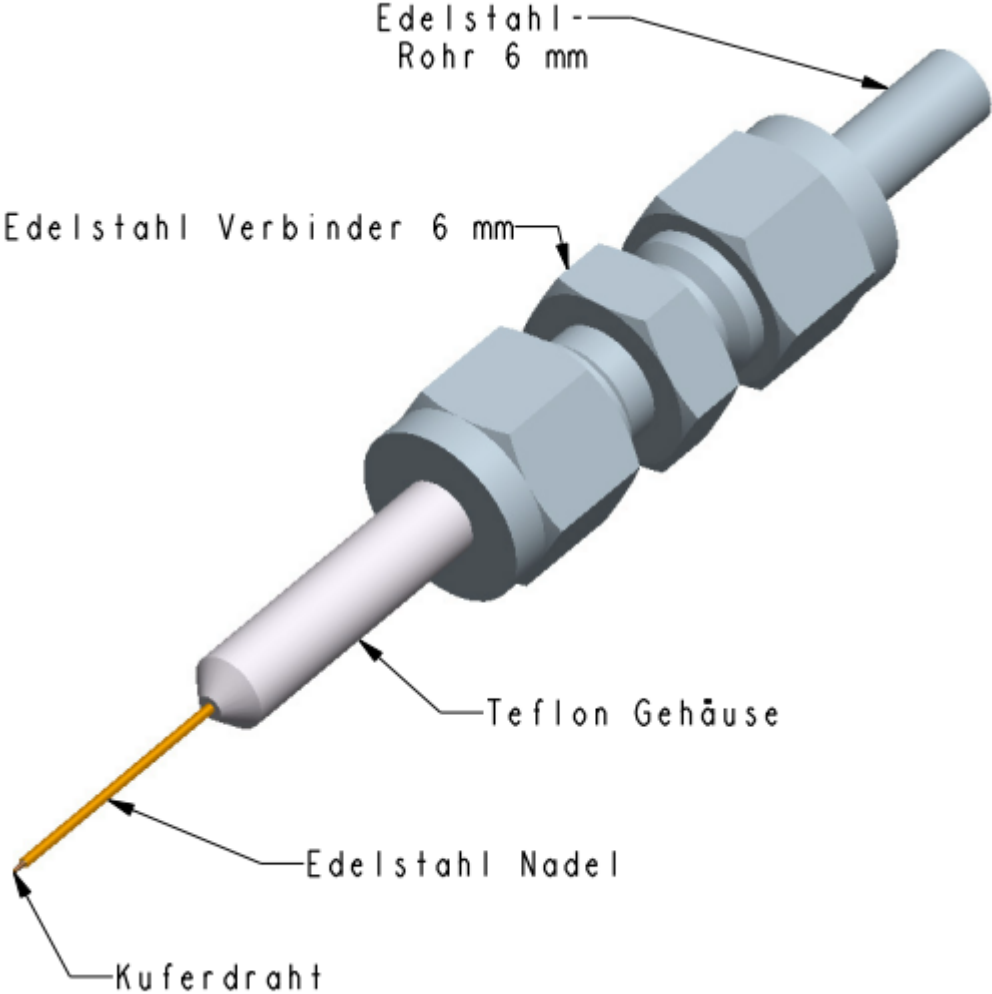
8.1 Nomenclature

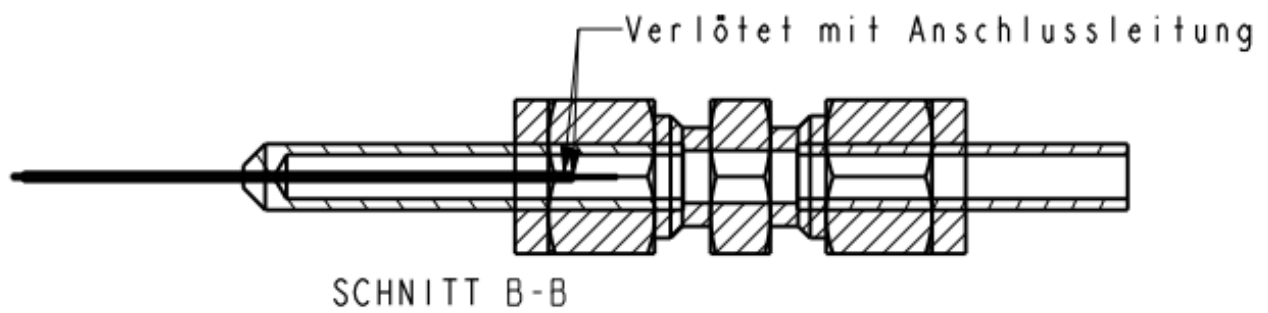
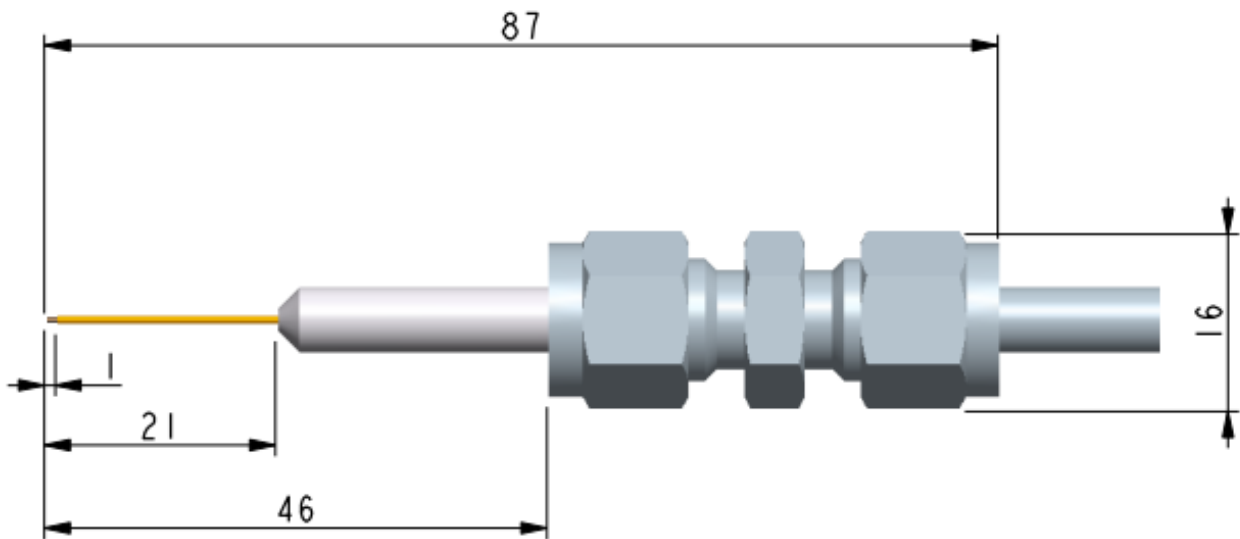
\dot{G}	[m ³ /s]	Gas flow rate
μ	[Pa s]	Viscosity
A	[m ²]	Screened area
A _R	[m ²]	Reactor cross sectional area
C	[1/m]	Cell constant
c _A	[mol/l]	Electrolyte concentration
c _D	[-]	Drag coefficient
CM	[-]	Conductivity measurement
C _T	[mm]	Impeller clearance
d	[mm]	Bubble diameter
D	[mm]	Impeller diameter
D _B	[mm]	Bubble column depth
d _e	[mm]	Equal diameter
Dev	[-]	Deviation
E ₀	[V]	Standard electrode potential
Eö	[-]	Eötvös number
F _B	[N]	Buoyancy force
f _b	[Hz]	Blade frequency
F _D	[N]	Drag force
F _G	[N]	Gravitational force
Fl	[-]	Flow number
Fr	[-]	Froude number
Fx	[-]	Flow regime x
g	[m/s ²]	Constant of gravity
H	[mm]	Plexiglas box height
h	[mm]	Bubble height
H _B	[mm]	Bubble column height
H _T	[mm]	Impeller spacing
I	[A]	Electrical current
IA	[-]	Image analysis
L	[mm]	Plexiglas box depth
L _x	[mm]	Measurement level x
L _{x.y}	[mm]	Measurement level x point y
M	[-]	Morton number

N	[1/s]	Impeller rotational speed
R	[Ω]	Resistance
Re	[-]	Reynolds number
Re _B	[-]	Reynolds number of a bubble
Re _{SR}	[-]	Impeller Reynolds number
S _T	[mm]	Sparger height
T	[°C]	Temperature
t	[s]	Time
Δt	[s]	Measurement time
Δt_{Gi}	[s]	Contact time with the dispersed phase
t _{cx}	[ms]	Contact time of bubble x
T _T	[mm]	Tank diameter
t _{xy}	[ms]	Time interval between bubbles x & y
U	[V]	Electrical voltage
U _S	[m/s]	Superficial gas velocity
u _T	[m/s]	Terminal velocity
V _C	[m ³]	Volume continuous phase
V _D	[m ³]	Volume dispersed phase
V _{eps}	[m ³]	Volume of a ellipsoid
vvm	[1/min]	Gas volume flow per liquid volume per minute
W _{PB}	[mm]	Plexiglas box width
W	[mm]	Bubble width
W _B	[mm]	Bubble column width
x _{RMS}	[-]	RMS value of a set of data points
α	[-]	Global gas hold-up
$\alpha(x)$	[-]	Local gas hold-up
ρ	[kg/m ³]	Density
ρ_b	[kg/m ³]	Bubble density
ρ_l	[kg/m ³]	Liquid density
σ	[S]	Conductivity
σ_{spec}	[S/m]	Specific conductivity
Ψ	[-]	Bubble coalescence percentage

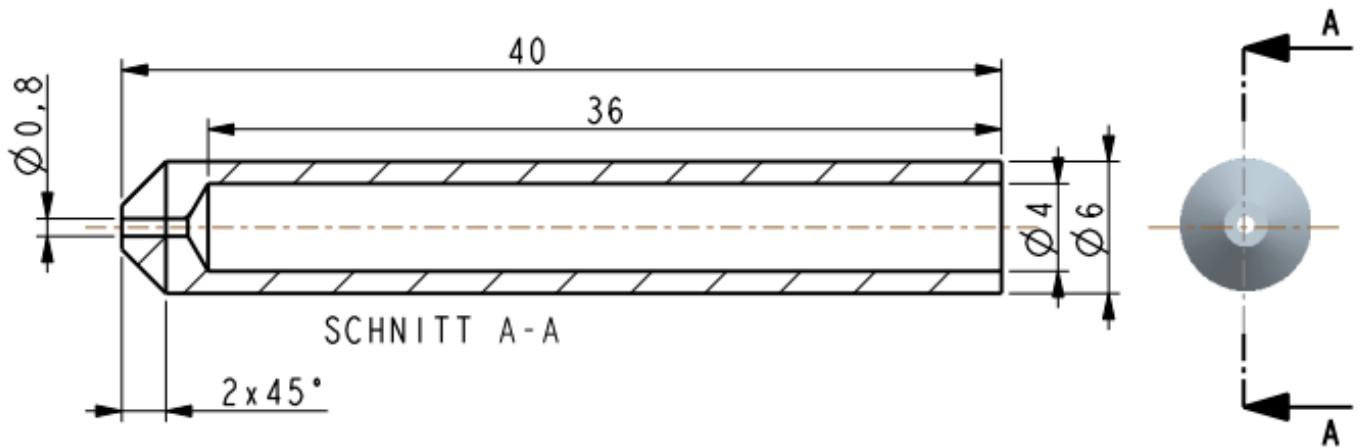
8.1.1 Design drawings

8.1.2 Single tip conductivity probe

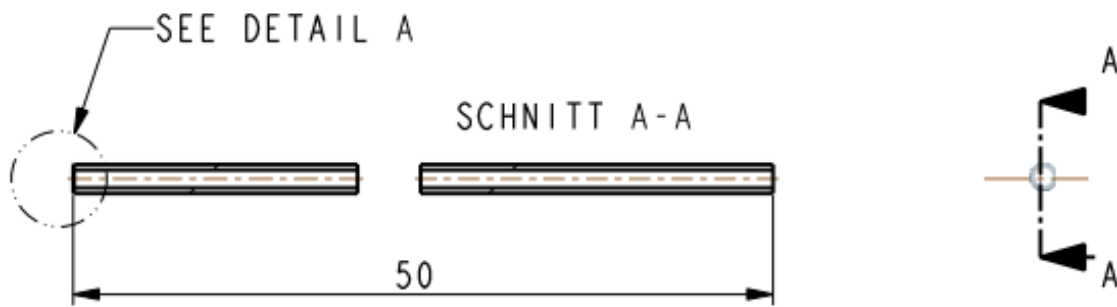




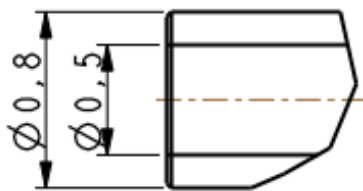
<i>Verwendungsbereich</i>				<i>Oberfläche</i>		<i>Maßstab 1,500</i>		<i>Gewicht</i>		
				<i>Allgemeintoleranz ISO 2768-mK</i>		<i>Werkstoff/Halbzeug</i>				
				<i>Datum</i>	<i>Name</i>	<i>Benennung</i> Zusammenstellungszeichnung				
				<i>Bearb.</i>	<i>13.10.2010</i>					<i>D. Treffer</i>
				<i>Gepr.</i>						
				<i>Norm</i>						
				<i>Komm.-Nr.:</i>						
				IPPT TU GRAZ		<i>Zeichnung/Sach-Nr.:</i>			<i>Blatt 2</i>	
									<i>Bl.</i>	
<i>Zust.</i>	<i>Änderung</i>	<i>Datum</i>	<i>Name</i>			<i>Ers.f.:</i>		<i>Ers.d.:</i>		



<i>Verwendungsbereich</i>				<i>Oberflaeche</i>		<i>Maßstab</i> 3,000		<i>Gewicht</i>	
				Allgemeintoleranz ISO 2768-mK		Werkstoff/Halbzeug Teflon			
				Datum		Name		Benennung Casing	
				Bearb. 13.10.2010		D. Treffer			
				Gepr.					
				Norm					
				Komm.-Nr.:					
				IPPT TU GRAZ		Zeichnung/Sach-Nr.:			Blatt 1
									Bl.
<i>Zust.</i>	<i>Aenderung</i>	<i>Datum</i>	<i>Name</i>	<i>Ers.f.:</i>			<i>Ers.d.:</i>		



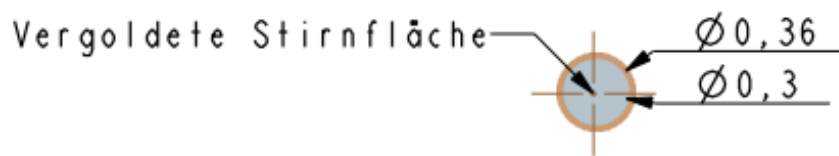
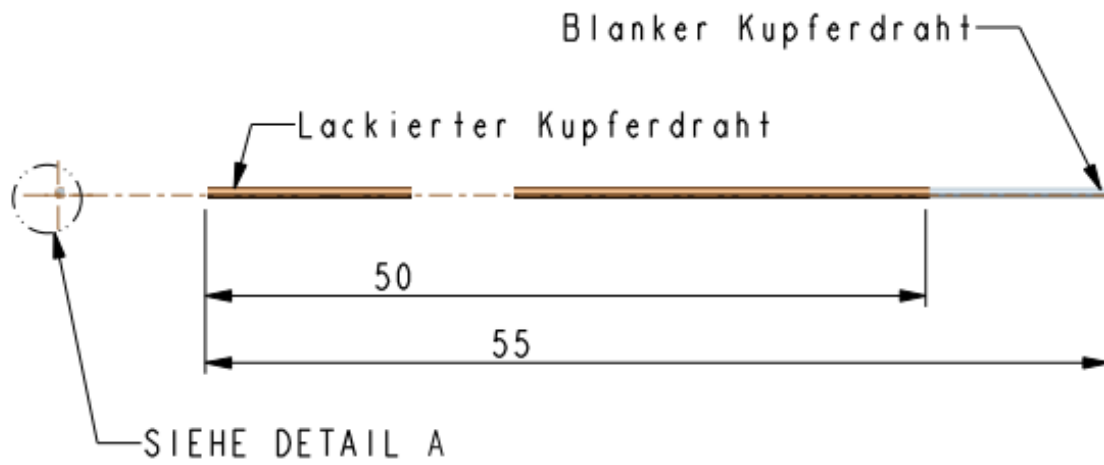
Kanten gebrochen &
Oberfläche vergoldet



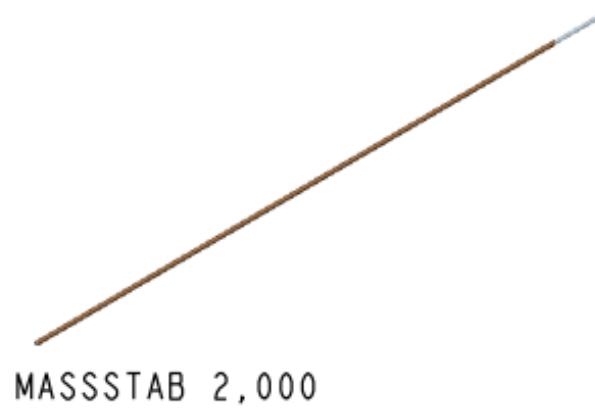
DETAIL A
SCALE 30,000



<i>Verwendungsbereich</i>				<i>Oberfläche</i>		<i>Maßstab</i> 5,000		<i>Gewicht</i>	
				<i>Allgemeintoleranz</i> ISO 2768-mK		<i>Werkstoff/Halbzeug</i> Edelstahl			
				<i>Datum</i>	<i>Name</i>	<i>Benennung</i> Needle			
				<i>Bearb.</i> 13.10.2010	<i>D. Treffer</i>				
				<i>Gepr.</i>					
				<i>Norm</i>					
				<i>Komm.-Nr.:</i>					
				IPPT TU GRAZ		<i>Zeichnung/Sach-Nr.:</i>			<i>Blatt</i> 1
									<i>Bl.</i>
<i>Zust.</i>	<i>Aenderung</i>	<i>Datum</i>	<i>Name</i>			<i>Ers.f.:</i>		<i>Ers.d.:</i>	

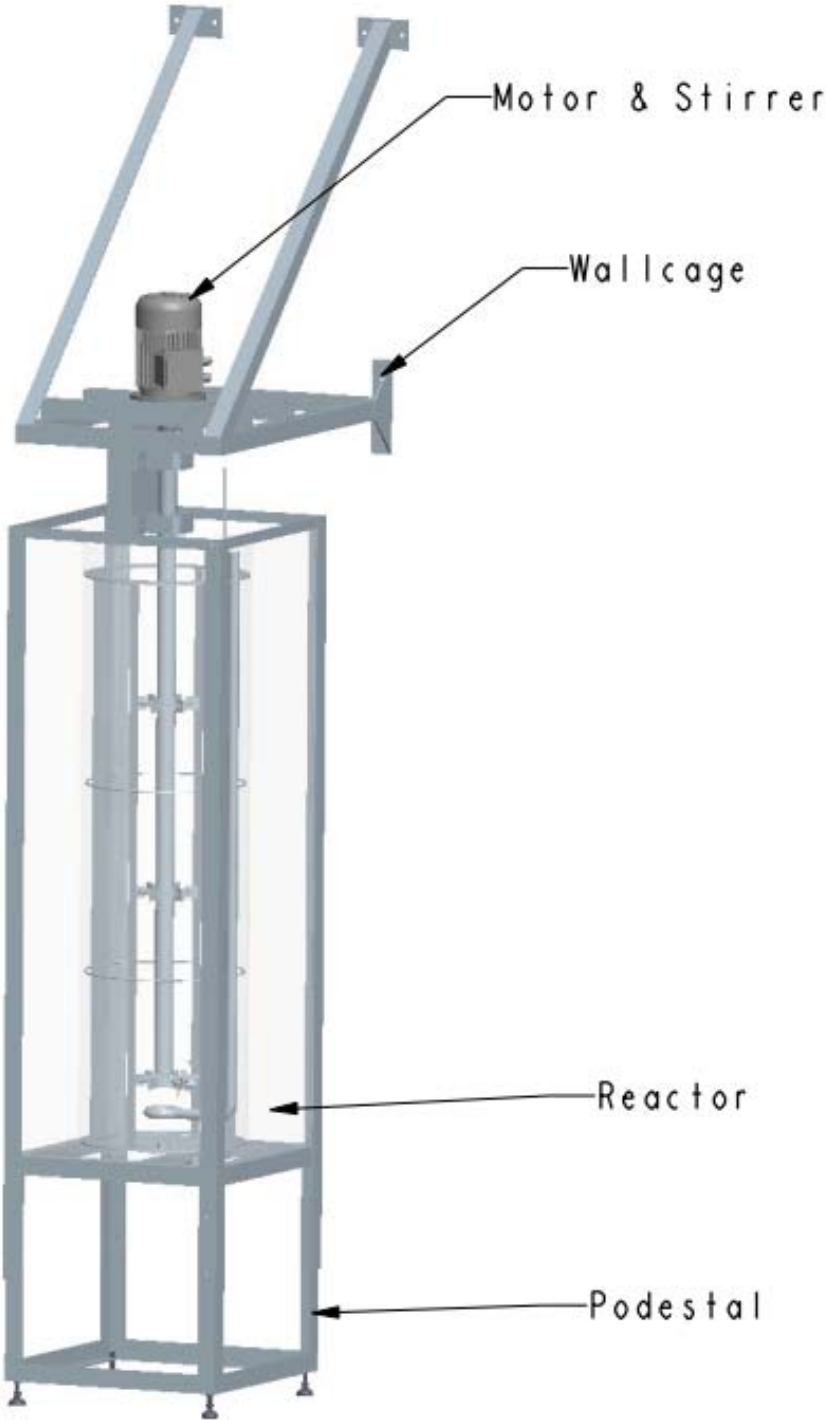


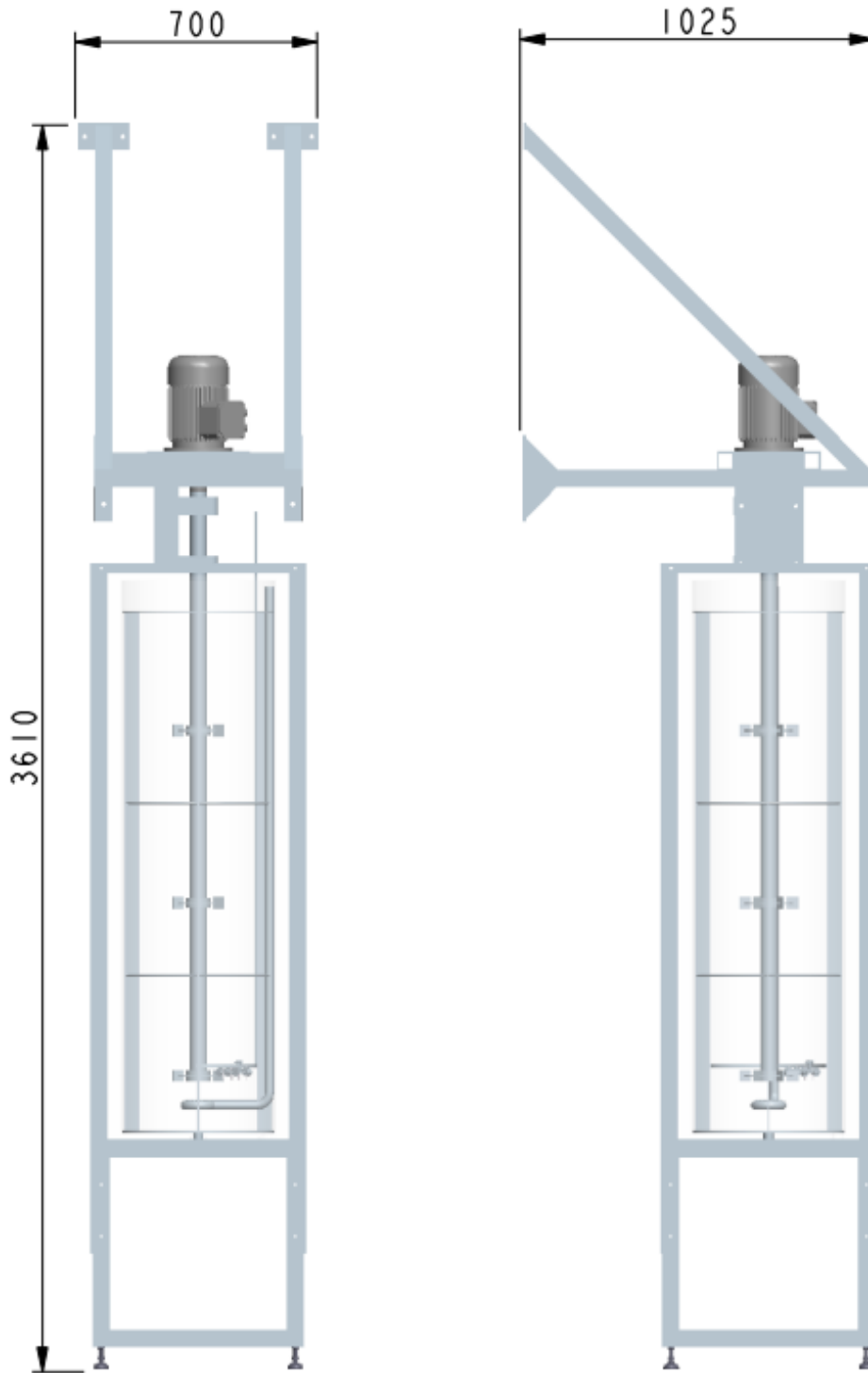
DETAIL A
MASSTAB 30,000



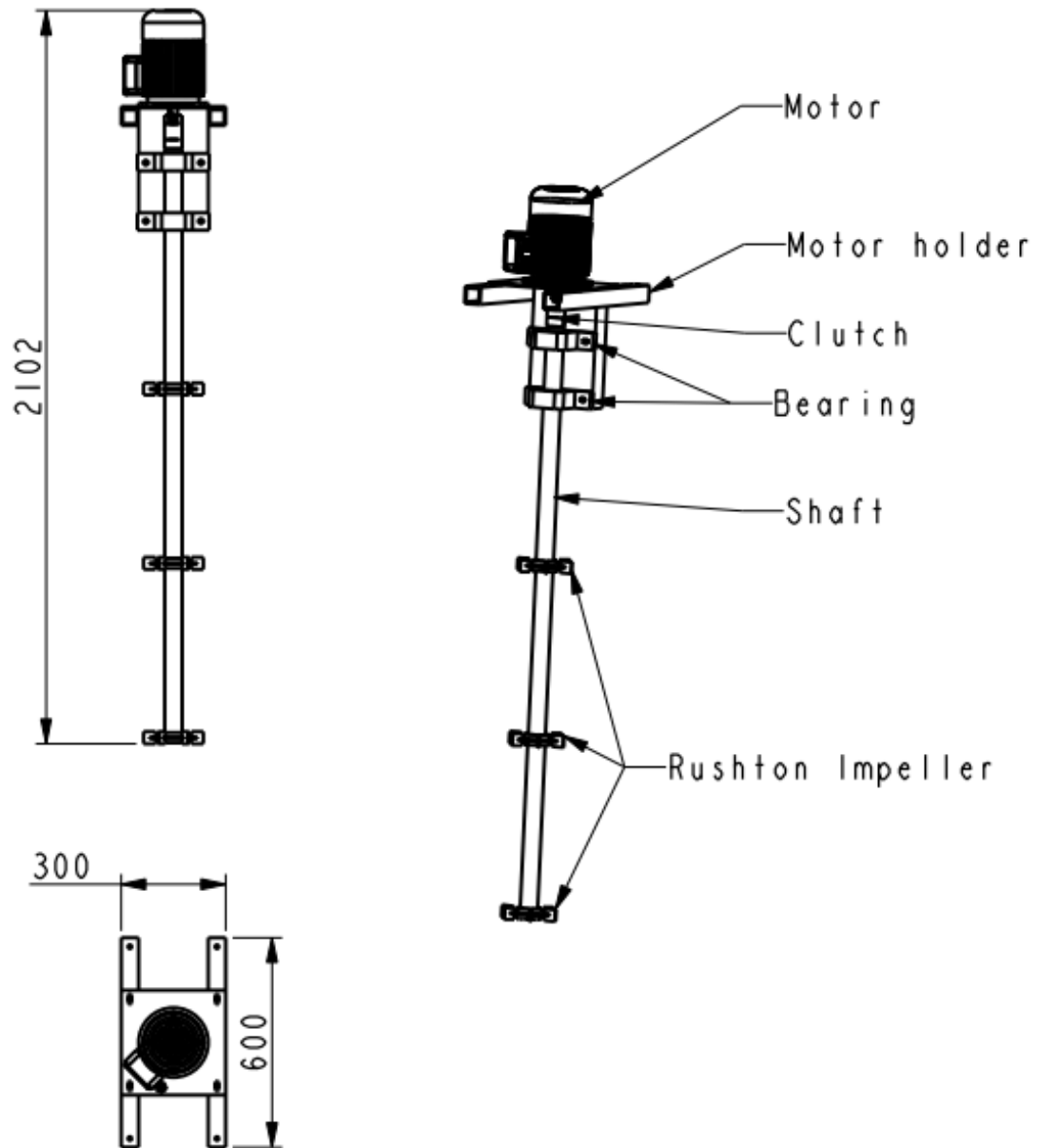
Verwendungsbereich				Oberfläche		Masstab 5,000		Gewicht	
				Allgemeintoleranz ISO 2768-mK				Werkstoff/Halbzeug Kupferlackdraht 0,3 mm	
				Datum		Name		Benennung Kupferdraht	
				Bearb.		20.04.2011 D. Treffer			
				Gepr.					
				Norm					
				Komm.-Nr.:					
IPPT TU GRAZ				Zeichnung/Sach-Nr.:				Blatt 1	
								Bl.	
				Ers.f.:				Ers.d.:	
Zust.	Aenderung	Datum	Name						

8.1.3 Reactor

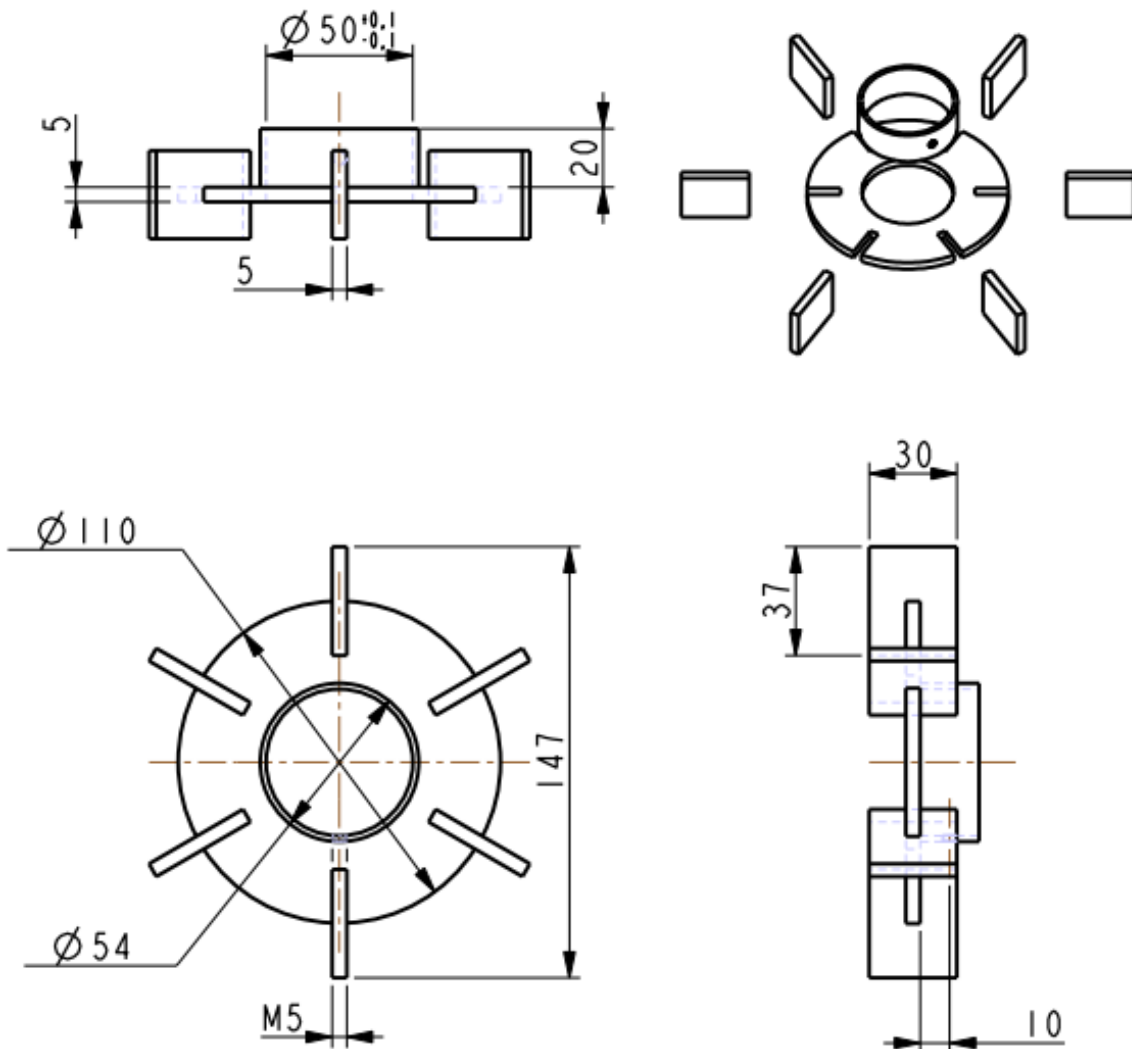




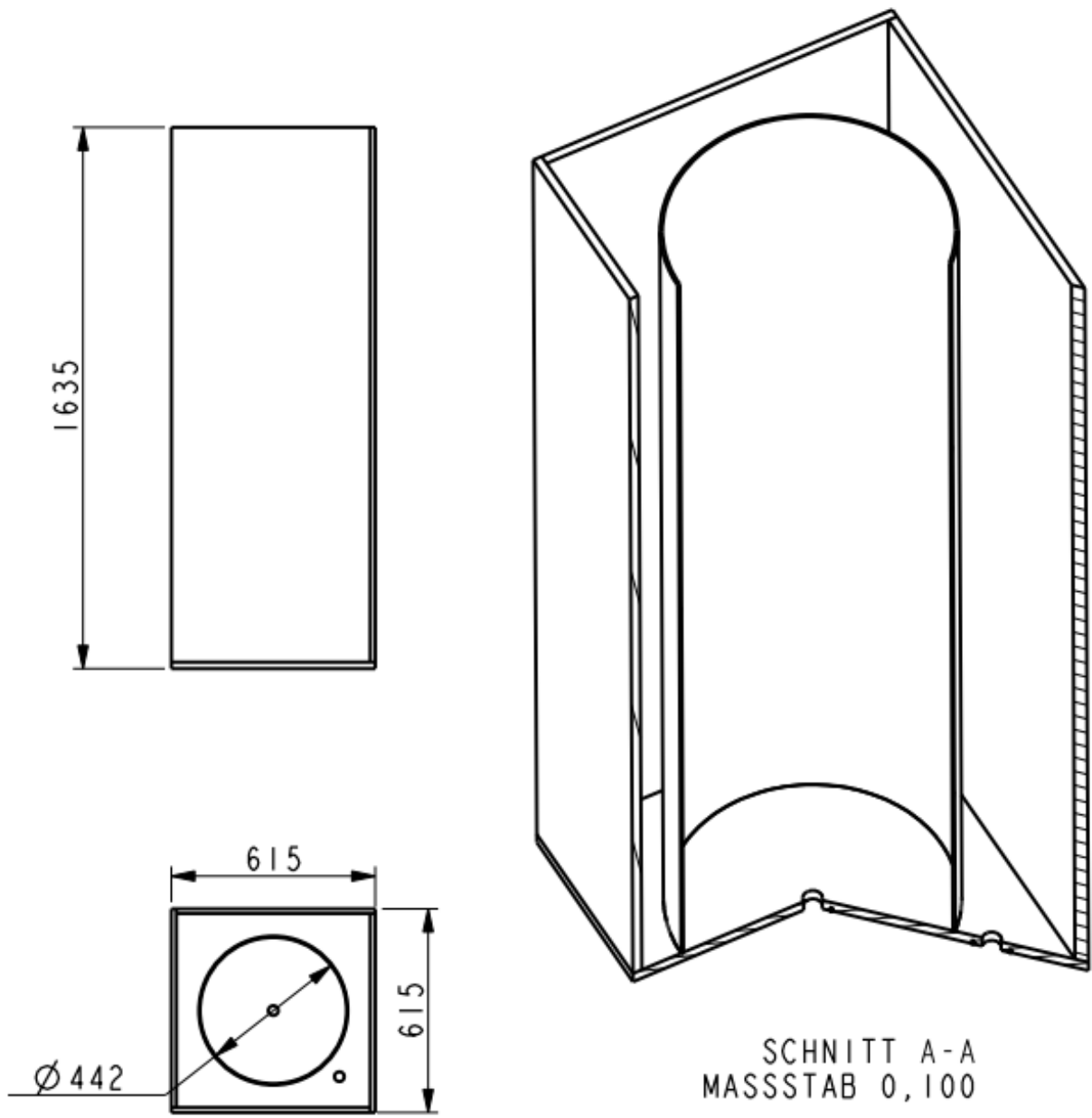
<i>Verwendungsbereich</i>				<i>Oberflaeche</i>		<i>Maßstab</i> 0,050		<i>Gewicht</i>		
				<i>Allgemeintoleranz ISO 2768-mK</i>		<i>Werkstoff/Halbzeug</i>				
				<i>Datum</i>	<i>Name</i>	<i>Benennung</i> Main dimensions				
				<i>Bearb.</i> 20.04.2011	<i>D. Treffer</i>					
				<i>Gepr.</i>						
				<i>Norm</i>						
				<i>Komm.-Nr.:</i>						
				IPPT TU GRAZ		<i>Zeichnung/Sach-Nr.:</i>			<i>Blatt</i> 1	
<i>Zust.</i>	<i>Aenderung</i>	<i>Datum</i>	<i>Name</i>			<i>Ers.f.:</i>		<i>Ers.d.:</i>		



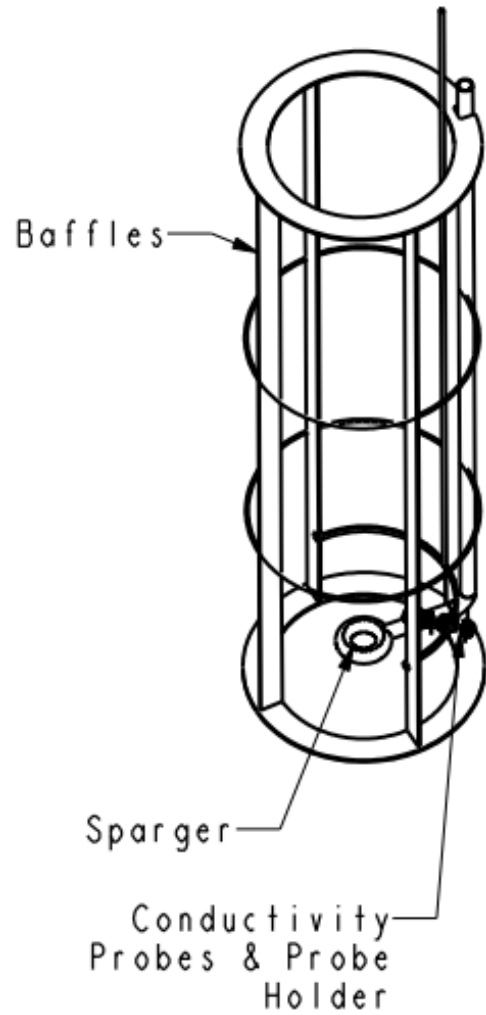
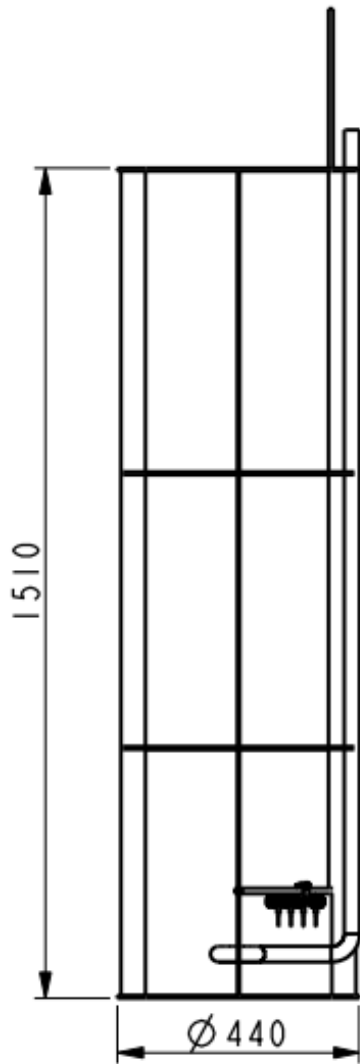
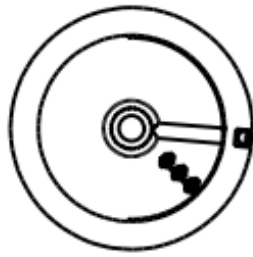
Verwendungsbereich				Oberflaeche		Masstab 0,050		Gewicht		
				Allgemeintoleranz ISO 2768-mK				Werkstoff/Halbzeug		
				Datum	Name	Benennung Motor & Stirrer				
				Bearb.	20.04.2011					D. Treffer
				Gepr.						
				Norm						
				Komm.-Nr.:						
				IPPT TU GRAZ		Zeichnung/Sach-Nr.:			Blatt 1	
									Bl.	
Zust.	Aenderung	Datum	Name			Ers.f.:	Ers.d.:			



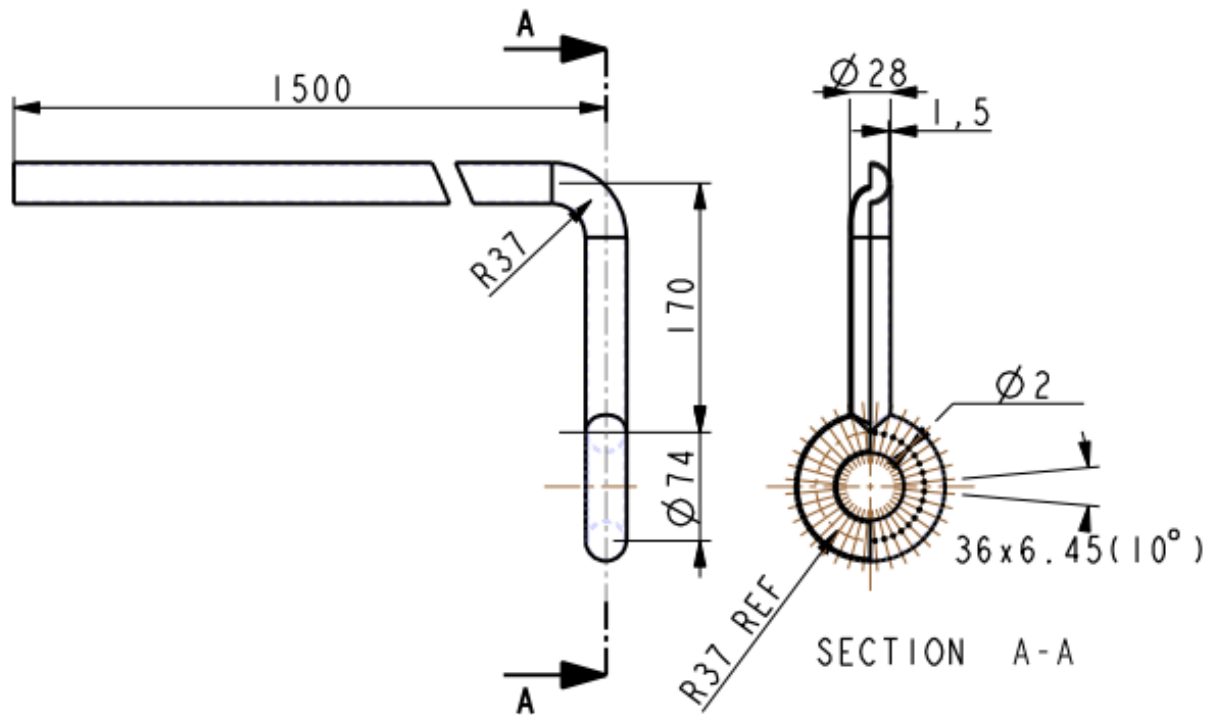
Verwendungsbereich				Oberflaeche		Masstab 0,200		Gewicht		
				Allgemeintoleranz ISO 2768-mK				Werkstoff/Halbzeug		
				Datum	Name	Benennung Impeller				
				Bearb.	20.04.2011					D. Treffer
				Gepr.						
				Norm						
				Komm.-Nr.:						
				IPPT TU GRAZ		Zeichnung/Sach-Nr.:			Blatt 1	
									Bl.	
Zust.	Aenderung	Datum	Name			Ers.f.:	Ers.d.:			



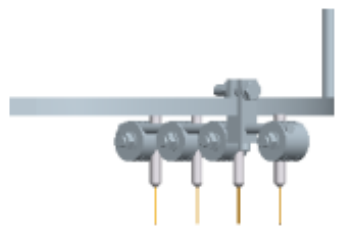
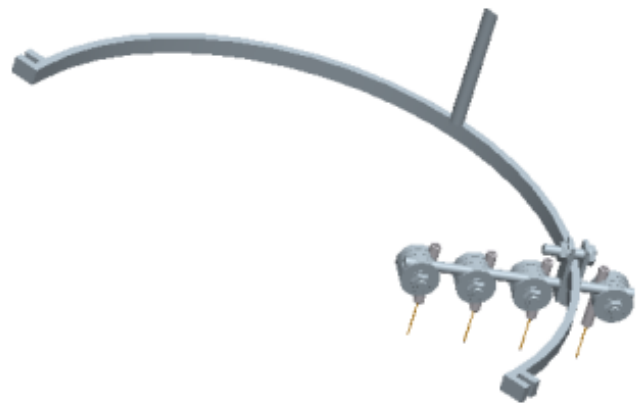
<i>Verwendungsbereich</i>				<i>Oberflaeche</i>		<i>Masstab 0,050</i>		<i>Gewicht</i>		
				<i>Allgemeintoleranz ISO 2768-mK</i>				<i>Werkstoff/Halbzeug</i>		
				<i>Datum</i>	<i>Name</i>	<i>Benennung</i> Plexiglas Reactor				
				<i>Bearb.</i>	20.04.2011					D. Treffer
				<i>Gepr.</i>						
				<i>Norm</i>						
				<i>Komm.-Nr.:</i>		<i>Zeichnung/Sach-Nr.:</i>				
				IPPT TU GRAZ						<i>Blatt</i>
<i>Zust.</i>	<i>Aenderung</i>	<i>Datum</i>	<i>Name</i>					<i>Ers.f.:</i>		<i>Ers.d.:</i>
								<i>Bl.</i>		



<i>Verwendungsbereich</i>				<i>Oberflaeche</i>		<i>Maßstab</i> 0,075		<i>Gewicht</i>	
				<i>Allgemeintoleranz ISO 2768-mK</i>				<i>Werkstoff/Halbzeug</i>	
				<i>Datum</i>	<i>Name</i>	<i>Benennung</i> Internals			
				<i>Bearb.</i> 20.04.2011	<i>D. Treffer</i>				
				<i>Gepr.</i>					
				<i>Norm</i>					
				<i>Komm.-Nr.:</i>					
				IPPT TU GRAZ		<i>Zeichnung/Sach-Nr.:</i>			<i>Blatt</i> 2
									<i>Bl.</i>
<i>Zust.</i>	<i>Aenderung</i>	<i>Datum</i>	<i>Name</i>				<i>Ers.f.:</i>	<i>Ers.d.:</i>	



Verwendungsbereich				Oberflaeche		Masstab 0,045		Gewicht	
				Allgemeintoleranz ISO 2768-mK				Werkstoff/Halbzeug	
				Datum		Name		Benennung Sparger	
				Bearb. 20.04.2011		D. Treffer			
				Gepr.					
				Norm					
				Komm.-Nr.:					
IPPT TU GRAZ				Zeichnung/Sach-Nr.:				Blatt 1	
								Bl.	
				Ers.f.:				Ers.d.:	
Zust.	Aenderung	Datum	Name						



<i>Verwendungsbereich</i>				<i>Oberflaeche</i>		<i>Maßstab</i> 0,250		<i>Gewicht</i>	
				<i>Allgemeintoleranz ISO 2768-mK</i>				<i>Werkstoff/Halbzeug</i>	
				<i>Datum</i>	<i>Name</i>	<i>Benennung</i> Probe Holder			
				<i>Bearb.</i> 20.04.2011	<i>D. Treffer</i>				
				<i>Gepr.</i>					
				<i>Norm</i>					
				<i>Komm.-Nr.:</i>					
				IPPT TU GRAZ		<i>Zeichnung/Sach-Nr.:</i>			<i>Blatt</i> 2
									<i>Bl.</i>
						<i>Ers.f.:</i>			<i>Ers.d.:</i>
<i>Zust.</i>	<i>Aenderung</i>	<i>Datum</i>	<i>Name</i>						

8.2 Hardware

8.2.1 M3 - Highspeed camera

Type:	M3
Resolution:	1280x1024
Framerate:	62.5-32.000
Memory:	1.3 GB



8.2.2 National Instruments NI 9203 - analog input module

Type:	NI 9203
Range:	+/- 20 [mA]
Channels:	8
Resolution:	16 [bit]
Sampling rate:	200 [kS/s] for all channels



8.2.3 National Instruments NI 9263 - analog input module

Type:	NI 9263
Range:	+/- 10 [V]
Channels:	4
Resolution:	16 [bit]
Sampling rate:	100 [kS/s] per channel



8.3 Matlab® codes

The printed Matlab® source code files can be found on the DVD on the last page.

8.3.1 Image analysis post processing

```
function Y=imageanalysis(S,RL)

N=normalize(S);

X=reconstruct(N,RL);

ghr = X(X < 1);

Y=bubblecount(X);
figure

% === PLOT ====
%Plot normalized data
subplot(2,1,1)
plot(N(:,1),N(:,2),[0 max(N(:,1))],[RL/100 RL/100], 'r')
axis([0 max(N(:,1)) -0.1 1.1])
title(['Normalized Signal'],'FontSize',24,'Fontweight','bold')
xlabel('Time [ms]','FontSize',16)
ylabel('Conductivity [-]','FontSize',16)

%Plot reconstructed signal

subplot(2,1,2)
plot(X(:,1),X(:,2))
axis([0 max(X(:,1)) -0.1 1.1])
title(['Reconstructed Signal - Gas hold-up = ', ...
      num2str(size(ghr,1)/size(X,1))],'FontSize',24,'Fontweight','bold')
xlabel('Time [ms]','FontSize',16)
ylabel('Conductivity [-]','FontSize',16)

%Plot bubble interaction
fighandle = figure;
set(fighandle, 'Position', [50, 50, 950 , 950]);
size(Y,1)
if size(Y,1)<=20
    np=size(Y,1);
else
    np=20;
end
for i=1:np
    if Y(i,2)>20
        subplot(5,3,i)
        plot(N(Y(i,2)-20:Y(i,3)+20,1),N(Y(i,2)-20:Y(i,3)+20,2), 'LineWidth',2)
        hold on
        plot([N(Y(i,2)-20) N(Y(i,3)+20)],[RL/100 RL/100], 'r', 'LineWidth',2)
        plot(X(Y(i,2)-20:Y(i,3)+20,1),X(Y(i,2)-
20:Y(i,3)+20,2), 'black', 'LineWidth',2, 'LineStyle', ':')
        title(['Bubble ', num2str(i)], 'FontSize',12, 'Fontweight', 'bold')
        axis([N(Y(i,2)-20) N(Y(i,3)+20) -0.1 1.1])
        set(gca, 'FontWeight', 'bold')
    end
end
end
function binf=bubblecount(X)
counter=0;
binf=[];
```

```

for i=2:size(X,1)
    if X(i-1,2)==1
        if X(i,2)==0
            counter=counter+1;
            binf(counter,1)=counter;
            binf(counter,2)=X(i,1);
        end
    else
        if X(i,2)==1
            if counter==0
                counter=1
            end
            binf(counter,3)=X(i,1);
            binf(counter,4)=binf(counter,3)-binf(counter,2);
        end
    end
end
binf(1:end-1,5)=binf(1:end-1,2)-binf(2:end,2);
end

function N=normalize(S)
minrms=min(S(:,2));
S(:,2)=S(:,2)-minrms;
[histx histy]=hist(S(:,2),1000);
[xv mv]=max(histx);
S(:,2)=S(:,2)/histy(mv);
N=S;
end

function R=reconstruct(S,RL)
Z=zeros(size(S,1),2);
Z(:,1)=S(:,1);
ind=find(abs(S(:,2))<RL/100);
S(ind,2)=0;
ind=find(abs(S(:,2))>=RL/100);
S(ind,2)=1;
R=S;
end

```

8.3.2 Gas hold-up post processing

```
function gh=postprocess(RL,S,CF,P,fb)
if nargin<5
    fb=0;
end

%check if there was some bubble interaction
if min(S(:,2))/max(S(:,2))<.9

%Remove drift
S=pofit(S,P);

%Normalize the signal
minrms=min(S(:,2));
S(:,2)=S(:,2)-minrms;
S(:,2)=S(:,2)/max(S(:,2));

%Create Histogram data
[histx histy]=hist(S(:,2),1000);
[xv mv]=max(histx);

%Normalize to liquid conductivity
S(:,2)=S(:,2)/histy(mv);

[histx histy]=hist(S(:,2),1000);
[xv mv]=max(histx);

%Calculate Threshold
RLmed=histy(mv)*RL/100;
rmsdata=S(:,2);

below = rmsdata(rmsdata <= RLmed);
gh=size(below,1)/size(S,1)/CF*100;

%Calculate the reconstructed signal
R=reconstruct(S,RL);

%Frequency spectrum
f=frespe(R);

if P==1

% histogram plot
fighandle = figure;
set(fighandle, 'Position', [50, 50, 950 , 675]);
subplot(3,2,5)
hold on
plot(histy,histx)

title(['5. Normalized Histogram'],'FontSize',12,'Fontweight','bold')
plot([RL/100 RL/100],[0 xv],'r','Linewidth',2)
axis([0 1.1 0 max(histx)*1.1])
xlabel('Conductivity [-'],'FontSize',10,'Fontweight','bold')
ylabel('Time [ms]','FontSize',10,'Fontweight','bold')
set(gca,'FontWeight','bold')

% Plot
subplot(3,2,1)
title(['1. Conductivity curve of 180
[s]'],'FontSize',12,'Fontweight','bold')
```

```

hold on
plot(S(:,1),S(:,2))
plot([0,S(end,1)],[RLmed,RLmed], 'r', 'Linewidth',2)
axis([0,S(end,1) 0 1.1])
xlabel('Time [ms]', 'FontSize',10, 'Fontweight', 'bold')
ylabel('Conductivity [-]', 'FontSize',10, 'Fontweight', 'bold')
set(gca, 'FontWeight', 'bold')

subplot(3,2,2)
hold on
title(['2. Conductivity curve section of 5
[s]'], 'FontSize',12, 'Fontweight', 'bold')
plot(S(1:5000,1),S(1:5000,2))
plot([0,S(5000,1)],[RLmed,RLmed], 'r', 'Linewidth',2)
axis([0,S(5000,1) 0 1.1])
xlabel('Time [ms]', 'FontSize',10, 'Fontweight', 'bold')
ylabel('Conductivity [-]', 'FontSize',10, 'Fontweight', 'bold')
set(gca, 'FontWeight', 'bold')

subplot(3,2,3)
hold on
title(['3. Conductivity curve section of 1
[s]'], 'FontSize',12, 'Fontweight', 'bold')
plot(S(1:1000,1),S(1:1000,2))
plot([0,S(1000,1)],[RLmed,RLmed], 'r', 'Linewidth',2)
axis([0,S(1000,1) 0 1.1])
xlabel('Time [ms]', 'FontSize',10, 'Fontweight', 'bold')
ylabel('Conductivity [-]', 'FontSize',10, 'Fontweight', 'bold')
set(gca, 'FontWeight', 'bold')
hold off

subplot(3,2,4)
hold on
title(['4. Reconst. cond. curve section of 1
[s]'], 'FontSize',12, 'Fontweight', 'bold')
plot(R(1:1000,1),R(1:1000,2))
axis([0,S(1000,1) -.1 1.1])
xlabel('Time [ms]', 'FontSize',10, 'Fontweight', 'bold')
ylabel('Conductivity [-]', 'FontSize',10, 'Fontweight', 'bold')
set(gca, 'FontWeight', 'bold')
hold off

subplot(3,2,6)
hold on
title(['6. Frequency spectrum'], 'FontSize',12, 'Fontweight', 'bold')
plot(f(:,1),f(:,2), 'blue', [fb fb], [0 max(f(100:end,2))], 'green')
axis([10 100 0 max(f(100:end,2))*1.1])
xlabel('Frequency [Hz]', 'FontSize',10, 'Fontweight', 'bold')
ylabel('[-]', 'FontSize',10, 'Fontweight', 'bold')
set(gca, 'FontWeight', 'bold')
hold off
pause()
close
end
else
    gh=0;
end

```

```

function S=pofit(S,P)

x=S(:,1);
y=S(:,2);

P1 = polyfit(x,y,1);

yhat = polyval(P1,x);
Sn=y-yhat+yhat(end);
S(:,2)=Sn;

if P==1
subplot(2,1,1)
plot(x,y,x,yhat,'r-')
hold on
plot([min(x) max(x)],[max(y) max(y)])
plot([min(x) max(x)],[min(y) min(y)])
hold off
subplot(2,1,2)

plot(x,Sn)
hold on
plot([min(x) max(x)],[max(Sn) max(Sn)])
plot([min(x) max(x)],[min(Sn) min(Sn)])
xlabel X
ylabel Y
grid on
title 'Linear polynomial fit'
hold off
pause()
close
end
end

function R=reconstruct(S,RL)

Z=zeros(size(S,1),2);
Z(:,1)=S(:,1);

ind=find(abs(S(:,2))<RL/100);
S(ind,2)=0;

ind=find(abs(S(:,2))>=RL/100);
S(ind,2)=1;

R=S;
end

function f=frespe(S)

Fs = 1000; % Sampling frequency
L = size(S,1); % Length of signal

NFFT = 2^nextpow2(L); % Next power of 2 from length of y
Y = fft(S(:,2),NFFT)/L;
f = Fs/2*linspace(0,1,NFFT/2+1);

f=f';
f(:,2)=2*abs(Y(1:NFFT/2+1))';

```

8.3.3 Mixing post processing

```
function mixing(flowmap)

cd(num2str(flowmap))
cd('mix')
list = dir('*.mat');

average=100;
t=zeros(numel(list),1);

fighandle = figure;
set(fighandle, 'Position', [100, 50, 423 , 100]);

for i=1:numel(list)
    load(list(i).name);
    S(:,1)=S(:,1)/1000;
    ss=size(S,1);
    color(1)='r'; %red
    color(2)='b'; %blue
    color(3)='g'; %green
    color(4)='c'; %cyan
    color(5)='y'; %yellow
    color(6)='m'; %magenta

    Sa=zeros(ss/average,2);
    for j=1:ss/average
        Sa(j,2)=max(S(1+(j-1)*average:j*average,2));
        Sa(j,1)=j*average/1000;
    end

    ss=size(Sa,1);

    y=Sa(round(ss*0.6):ss,2);
    x=Sa(round(ss*0.6):ss,1);
    P1 = polyfit(x,y,1);
    yhat = polyval(P1,Sa(:,1));

    Sa(:,2)=Sa(:,2)-yhat;
    Sa(:,2)=Sa(:,2)-mean(Sa(1:150,2));
    Sa(:,2)=Sa(:,2)/mean(Sa(ss-150:ss,2));

    size(Sa)

    yy = smooth(Sa(:,2),25,'sgolay',2)';
    Sa(:,2)=yy';

    for k=1:size(Sa,1)
        if Sa(k,2)>=0.9
            t(i)=k*average;
            break
        end
    end
    hold on
    plot(Sa(:,1),Sa(:,2),color(i),'LineWidth', 2)
end

plot([15 15],[0,1],'black','LineWidth',2)
text(15,1.08,'\downarrow','FontSize',10,'Fontweight','bold'...
    ,'HorizontalAlignment','Center')
text(15,1.15,'Tracer','FontSize',10,'Fontweight','bold'...
    ,'HorizontalAlignment','Center')
```

```

plot([0 S(end,1)], [0.90 0.90], 'black', 'LineWidth', 2, 'LineStyle', '-.')
plot([0 S(end,1)], [0 0], 'black', 'LineStyle', ':', 'LineWidth', 2)
plot([0 S(end,1)], [1 1], 'black', 'LineStyle', '- -', 'LineWidth', 2)
text(S(end,1)*0.41, 0.4, ['Exp.1 = ', num2str(t(1)/1000-15), ' [s]'], ...
    'FontSize', 10, 'Fontweight', 'bold', 'Color', 'red', ...
    'HorizontalAlignment', 'Center')
text(S(end,1)*0.41, 0.3, ['Exp.2 = ', num2str(t(2)/1000-15), ' [s]'], ...
    'FontSize', 10, 'Fontweight', 'bold', 'Color', 'blue', ...
    'HorizontalAlignment', 'Center')
text(S(end,1)*0.41, 0.2, ['Exp.3 = ', num2str(t(3)/1000-15), ' [s]'], ...
    'FontSize', 10, 'Fontweight', 'bold', 'Color', 'green', ...
    'HorizontalAlignment', 'Center')
text(S(end,1)*0.41, 0.1, ['Average = ', ...
    num2str(round(mean(t/1000-15)*10)/10), ' [s]'], 'FontSize', 10, ...
    'Fontweight', 'bold', 'HorizontalAlignment', 'Center')
axis([0 120 -0.2 1.2])
title(['Flowmap P', num2str(flowmap)], 'FontSize', 12, 'Fontweight', 'bold')
xlabel('Time [s]', 'FontSize', 12, 'Fontweight', 'bold')
ylabel('Conductivity [-]', 'FontSize', 12, 'Fontweight', 'bold')

set(gca, 'FontWeight', 'bold')

legend('Exp. 1', 'Exp. 2', 'Exp. 3', 'Tracer', '90% Level', ...
    'Before tracer', 'After tracer', 'Location', 'East')
legend('boxoff')

cd ..
cd ..

end

```